NOVEL STRATEGIES FOR VALIDATING METABOLIC NETWORK MODELS USING STABLE ISOTOPE TRACERS

by

Jennifer Au

A dissertation submitted to the Faculty of the University of Delaware in partial fulfillment of the requirements for the degree of Doctor of Philosophy in Chemical Engineering

Summer 2016

NOVEL STRATEGIES FOR VALIDATING METABOLIC NETWORK MODELS USING STABLE ISOTOPE TRACERS

by

Jennifer Au

Approved: _____
Abraham M. Lenhoff, Ph.D.
Chair of the Department of Chemical & Biomolecular Engineering

Approved: _____
Babatunde A. Ogunnaike, Ph.D.
Dean of the College of Engineering

Approved: _____
Ann L. Ardis, Ph.D.
Senior Vice Provost for Graduate and Professional Education

I certify that I have read this dissertation and that in my opinion it meets the academic and professional standard required by the University as a dissertation for the degree of Doctor of Philosophy.

Signed: _____

Maciek R. Antoniewicz, Ph.D.
Professor in charge of dissertation

I certify that I have read this dissertation and that in my opinion it meets the academic and professional standard required by the University as a dissertation for the degree of Doctor of Philosophy.

Signed: _____

Eleftherios T. Papoutsakis, Ph.D.
Member of dissertation committee

I certify that I have read this dissertation and that in my opinion it meets the academic and professional standard required by the University as a dissertation for the degree of Doctor of Philosophy.

Signed: _____

Wilfred Chen, Ph.D.
Member of dissertation committee

I certify that I have read this dissertation and that in my opinion it meets the academic and professional standard required by the University as a dissertation for the degree of Doctor of Philosophy.

Signed: _____

Bryan P. Tracy, Ph.D.
Member of dissertation committee

ACKNOWLEDGMENTS

This dissertation would not have been possible without many people, and I am grateful for their influence and support. First and foremost, I would like to thank my advisor, Maciek Antoniewicz. His insight and mentorship helped bring this work to fruition, and his curiosity and enthusiasm continues to inspire me to be a better scientist. I am incredibly grateful to have had the opportunity to work with and learn from him. I would also like to thank my committee, Terry Papoutsakis, Wilfred Chen, and Bryan Tracy, for their valuable feedback on my work. I would also like to extend a special thanks to Shawn Jones and Keerthi Venkataramanan, both of whom graciously lent their time to help prepare my *C. acetobutylicum* cultures and run my samples on the HPLC. I also thank Jongyoun Baik for helping me with my initial CHO cell cultures.

My experience at UD would be incomplete without my fellow grad students. I have been incredibly fortunate to have the support of the Antoniewicz group members, both past and present. I could not have asked for a better group of people to work alongside. I especially want to thank Nikodimos Gebreselassie and Chris Long, with whom most of my tenure here was spent. Our scientific and non-scientific discussions have helped keep day-to-day life both enlightening and enjoyable. I would also like to thank my friends, especially Lisa, Annie, Scott, and Stephen, who helped me make the most of living in Delaware.

I also thank my parents for always stressing the importance of my education and supporting me through my career goals. Their encouragement means more to me

than they know. Finally, I could not have completed this dissertation without the support of my fiancé, Max. Your love and patience has helped carry me through the most challenging times of my Ph.D. I can’t wait to spend the rest of my life with you, and I love you.

TABLE OF CONTENTS

LIST OF TABLES

LIST OF FIGURES

ABSTRACT

^{13}C-Metabolic flux analysis (^{13}C-MFA) has developed into a powerful tool for characterizing the structure of metabolic networks and determining detailed flux distributions in living cells. Fluxes provide a quantitative understanding of metabolism that can be applied to areas such as metabolic engineering, systems biology, and biomedical research. The accuracy and precision of flux estimates from ^{13}C-MFA are strongly influenced by the design of the ^{13}C labeling experiment. There are three major decision points in designing ^{13}C labeling experiments: (1) experimental layout (i.e. single or parallel labeling experiments); (2) ^{13}C tracer selection; and (3) selection of isotopic measurements. Recent advances in each of these areas have enabled higher quality flux estimates. In this dissertation, we highlight the applicability of these new approaches in validating metabolic network models and estimating metabolic fluxes for several biological systems.

First, we describe an application of parallel labeling experiments for characterizing the metabolism of *Clostridium acetobutylicum*, an important anaerobe for biofuel production. We present a systematic approach based on statistical analysis to establish a metabolic network model that fit all experimental data from several parallel cultures. The flux results provided valuable insights into the metabolism of *C. acetobutylicum*; specifically, we conclusively determined the structure of the TCA cycle. Furthermore, we describe the use of ^{13}C labeling experiments for characterizing

the metabolic stress response of *C. acetobutylicum* to butanol and butyric acid, two industrially-important, but toxic fermentation products.

Second, we describe two examples of how ^{13}C amino acid tracers can be used to validate metabolic network models and characterize metabolism. The first example tests a common assumption in ^{13}C-MFA, namely that no carbon flows from secondary pathways (such as amino acid metabolism) back to central metabolism. Using multiple ^{13}C amino acid tracers, we determined there is an active metabolic cycle in *C. acetobutylicum* that runs from aspartate to pyruvate. In the second example, we applied ^{13}C alanine tracers and knockout strains to quantify flux from pyruvate to phosphoenolpyruvate (PEP) in *E. coli* under gluconeogenic and glycolytic growth. Contrary to current understanding of the phosphoenolpyruvate-carbohydrate phosphotransferase system (PTS) system, we found there is a significant *in vivo* flux from pyruvate to PEP under glycolytic growth.

Lastly, we demonstrate the value of glycogen and RNA labeling measurements for ^{13}C-MFA. We present a GC-MS based method for measuring multiple fragments of the glucose and ribose moieties of glycogen and RNA, respectively. We demonstrate the practical importance of these measurements in two biological systems: *E. coli* as a model microbial system and CHO cells as a model mammalian system. Overall, these measurements improved the precision of ^{13}C-MFA flux estimates.

Chapter 1

INTRODUCTION

1.1 Toward a Comprehensive Understanding of Metabolism

Cells have evolved complex metabolic pathways to allow them to thrive in their natural environments. Taking advantage of this machinery and recombinant DNA technology, the field of metabolic engineering emerged to modify the biochemical reactions and regulatory processes of cells for desired products (Bailey, 1991; Stephanopoulos et al., 1998). Metabolic engineering has sought to address the need for renewable fuels (S. K. Lee et al., 2008) and pharmaceuticals (Wurm, 2004) by improving the production of an organism's native products, diversifying an organism's substrate utilization range, designing pathways for chemical degradation, introducing pathways for new products, and modifying cellular properties (Cameron and Tong, 1993). While metabolism has long been an active area of research, the need to more rationally engineer organisms has led to the development of quantitative tools for studying metabolism (Toya and Shimizu, 2013). These tools are becoming increasingly important in biomedical research as the role of altered metabolism in cancer, diabetes, and other diseases becomes apparent (Hiller and Metallo, 2013; Keibler et al., 2012).

Properties of metabolism can be described through the large-scale profiling of an organism's genes, transcripts, proteins, metabolites, and metabolic rates. Of these "omics" technologies, fluxomics provides the most physiologically relevant description of metabolism in the form of metabolic fluxes (Tang et al., 2009a). Fluxes

describe the rates of metabolite conversion through metabolic pathways and represent the integrated output of the underlying cellular processes described by other omics. Flux quantification has provided valuable insights into the intracellular metabolism of biological systems such as *E. coli* (Toya and Shimizu, 2013), yeast (Niklas et al., 2010), plants (Junker, 2014), and mammalian cells (Quek et al., 2010).

Early approaches to flux quantification were based on stoichiometric metabolic flux analysis (MFA), which relies on the stoichiometry of a metabolic network (Antoniewicz, 2015a; Wiechert, 2001). Assuming a pseudo-steady state, the resulting metabolite balances, coupled with extracellular measurements (e.g. growth rate, substrate uptake rates), can be computationally solved to obtain fluxes. For many biological systems, however, the number of stoichiometric constraints and extracellular measurements are insufficient to observe all important pathways. Importantly, the fluxes of parallel pathways, cyclic pathways, and reversible reactions cannot be calculated. In these cases, the use of stable isotope tracers can provide the necessary constraints to estimate all fluxes of interest.

1.2 Role of Stable Isotope Tracers

Stable isotope tracers are molecules in which a specific atom, or atoms, has been replaced with a non-radioactive isotope (e.g. ^{13}C, ^{2}H, ^{15}N, ^{18}O) (Crown and Antoniewicz, 2013a). In a tracer experiment, a specifically-labeled substrate is fed to a biological system, which metabolizes the tracer and incorporates the isotopes into its metabolites. After a sufficient incubation time, the intracellular and extracellular metabolites can be isolated, and the isotopic enrichment of the metabolites is measured via nuclear magnetic resonance (NMR), mass spectrometry (MS), or tandem mass spectrometry (MS/MS). The resulting labeling data can be analyzed in the context of

the known or predicted biochemistry of the biological system. This so-called qualitative analysis of tracer experiments has proven to be tremendously useful in determining the existence of metabolic pathways, the relative activities of pathways, the stereochemistry of specific reactions, the contribution of nutrients to different metabolites, and the structure of pathways (Buescher et al., 2015; Crown and Antoniewicz, 2013a). The remainder of this introduction focuses on the use of ^{13}C tracers specifically.

In labeling experiments, ^{13}C atoms are distributed into metabolites based on the structure of the metabolic network and the relative distribution of fluxes. Thus, ^{13}C labeling data can provide additional constraints in flux estimation, a method termed ^{13}C metabolic flux analysis (^{13}C-MFA) (Antoniewicz, 2015a; Wiechert, 2001). ^{13}C-MFA uses non-linear least squares regression to find a set of fluxes that minimizes the differences between the experimental ^{13}C labeling measurements and those simulated within a metabolic network model. Following flux estimation, confidence intervals are calculated to determine the precision of the flux estimates (Antoniewicz et al., 2006). While ^{13}C-MFA requires more experimental and computational effort and resources than stoichiometric MFA, it has become the primary approach for quantifying *in vivo* fluxes (Zamboni, 2011).

1.3 Considerations for Designing ^{13}C Tracer Experiments

The success of a ^{13}C labeling experiment and ^{13}C-MFA is dependent on numerous factors, some of which can be controlled by the investigator. The following subsections discuss in detail three major decision points in designing ^{13}C tracer experiments.

1.3.1 Tracer Selection

A wide variety of tracers exist for ^{13}C labeling experiments. Among ^{13}C glucose tracers alone, there are 32 (2^6) uniquely labeled tracers. Some are readily available at ~$100/g, while others must be custom synthesized at ≥$3000/g (Antoniewicz, 2013a). Given the costs and wide selection, tracers must be carefully evaluated and chosen based on the information to be gained.

For qualitative analyses where ^{13}C labeling data are directly interpreted without formal flux analysis, tracers are primarily selected based on the specific pathway(s) of interest and prior knowledge of the organism's metabolism. Observability of a specific pathway is highly dependent on the structure of the metabolic network, as this dictates the distribution of the ^{13}C atoms in metabolism, as well as the resultant labeling patterns observed in measured metabolites. ^{13}C labeling studies aimed at probing specific pathways have utilized common substrates such as glucose (Crown et al., 2011), and various amino acids (Amador-Noguez et al., 2010).

For ^{13}C-MFA, the ability to produce precise flux estimates must also be considered. Flux confidence intervals are determined by the sensitivities of the ^{13}C labeling data to flux changes (Antoniewicz et al., 2006). These sensitivities are directly related to the specific tracer used. Although many ^{13}C-MFA studies have utilized conventional tracers such as [1-^{13}C]glucose and [U-^{13}C]glucose, other studies have focused on identifying optimal tracers for flux resolution. For example, Metallo et al. (Metallo et al., 2009) identified [U-^{13}C]glutamine as an effective tracer for resolving TCA cycle fluxes in a mammalian system, and Nargund and Sriram (Nargund and Sriram, 2013) identified [3,4,5,6-^{13}C]glucose as the optimal tracer for resolving PPP fluxes in plants. More rigorous methodologies for identifying optimal

tracers have also been developed (Crown and Antoniewicz, 2012; Walther et al., 2012).

1.3.2 Measurement Selection

^{13}C labeling experiments typically produce labeled biomass macromolecules such as proteins, intracellular metabolites, and excreted metabolites. Although the specific labeling measurements should be chosen to complement the chosen tracer(s) (and vice versa), the actual measurements used for qualitative analyses or flux estimation are often limited by the available resources. At present, the techniques for measuring ^{13}C enrichment include NMR (Masakapalli et al., 2013; Truong et al., 2014), MS (Antoniewicz et al., 2007a), or tandem MS (Choi and Antoniewicz, 2011; Jeffrey et al., 2002). While NMR can provide positional labeling information, MS-based techniques such as gas chromatography-mass spectrometry (GC-MS) and liquid chromatography-mass spectrometry (LC-MS) are typically favored due to their sensitivity, accessibility, and relatively low cost (Antoniewicz, 2013a).

Of the labeled metabolites produced in a ^{13}C labeling experiment, biomass amino acids are among the most commonly measured due to their relative abundance in cells and the wealth of pathway information that can be inferred from their labeling patterns. Despite their overall usefulness, in some cases, biomass amino acids alone cannot fully resolve all metabolic pathways. For example, flux analysis of the pentose phosphate pathway (PPP) mainly relies on labeling data of a single amino acid, phenylalanine, which is derived from erythrose-4-phosphate (E4P) and phosphoenolpyruvate (PEP). Mammalian systems do not synthesize phenylalanine (as it is an essential amino acid) and thus, flux analysis in those systems relies on labeling measurements of intracellular metabolites such as 3-phosphoglycerate (3PG) or PEP

(Ahn and Antoniewicz, 2013; Templeton et al., 2014). Accurate measurement of these intracellular metabolites requires laborious quenching and extraction procedures, as well large sample volumes to compensate for the low concentration of intracellular metabolites within the cells. The lack of relevant metabolite measurements and the relative difficulty in measuring some metabolites ultimately contribute to decreased observability and precision of flux estimates throughout central carbon metabolism.

1.3.3 Parallel Labeling Experiments

Though many ^{13}C-MFA studies have been successfully conducted using a single labeling experiment, an increasing number of studies are employing parallel labeling experiments (Antoniewicz, 2015b; Crown and Antoniewicz, 2013a). In this approach, two or more cultures are grown simultaneously, each with a different isotopic tracer. The cultures are initiated from the same inoculum to minimize errors arising from any biological variability. Labeling data from the parallel experiments are then qualitatively analyzed together or integrated into ^{13}C-MFA. In integrated ^{13}C-MFA, measurements from all experiments are simultaneously fitted to a single metabolic network model, producing a single set of fluxes that fits all of the provided measurements. Parallel labeling experiments have been applied to study many organisms, including *E. coli* (Crown et al., 2015), *Geobacillus* (Cordova and Antoniewicz, 2016), *C. glutamicum* (Kind et al., 2013), acetic acid bacteria (Adler et al., 2014), CHO cells (Ahn and Antoniewicz, 2013; Sheikholeslami et al., 2014), and plants (Masakapalli et al., 2014b; Nargund et al., 2014).

A key advantage of the parallel labeling approach is the potential to precisely resolve all relevant fluxes of interest. Given the complexity of metabolism in most organisms, no single tracer is optimal for achieving good flux observability in all

central metabolic pathways (Crown and Antoniewicz, 2012; Schellenberger et al., 2012). As detailed in Section 1.3.1, different tracers have been found to be optimal for observing different pathways in different organisms. With the parallel labeling approach, the labeling data from each of these tracers can be combined to provide complementary pathway information and to increase the number of labeling measurements, both of which contribute to increased flux precision. Parallel labeling experiments have also proven to be useful in overcoming slow labeling dynamics (and thereby reducing the length of the experiment) (Ahn and Antoniewicz, 2013), and in validating metabolic network models (Leighty and Antoniewicz, 2012).

1.4 Aims and Outline of Thesis

Although ^{13}C-MFA is a well-established technique for quantifying cellular metabolism, the power of recent advances in the design of ^{13}C labeling experiments are only just being realized. The goal of this dissertation was to apply these novel strategies to validate metabolic network models, elucidate previously unexplored parts of metabolism, and increase the quality of flux estimates. Specifically, we highlight the use of parallel labeling experiments and ^{13}C amino acid tracers for validating the network model of *Clostridium acetobutylicum*, an important anaerobe for biofuel applications. Additionally, we introduce RNA and glycogen labeling measurements as important components for more precise ^{13}C-MFA. Stable isotope tracers were also used to characterize two areas of high interest within the metabolic engineering community: stress metabolism and the phosphoenolpyruvate-carbohydrate phosphotransferase system (PTS). The main findings of this work are outlined as follows:

- **Chapter 2** describes the application of parallel labeling experiments and ^{13}C-MFA to flux quantification in *C. acetobutylicum*. We present a systematic approach based on statistical analysis to establish a metabolic network model that fit all experimental data from several parallel cultures. The flux results provided valuable insights into the metabolism of *C. acetobutylicum*; specifically, we found that the TCA cycle is incomplete with no measurable flux between α-ketoglutarate and succinyl-CoA, succinate and fumarate, and malate and oxaloacetate. Additionally, we experimentally validated specific aspects of the metabolic network model using several follow-up tracer experiments.

- **Chapter 3** describes an example of how multiple ^{13}C amino acid tracers can be used to validate metabolic network models. This work tests a common assumption in ^{13}C-MFA, namely that no carbon flows from secondary pathways (such as amino acid metabolism) back to central metabolism. [1-^{13}C]Aspartate, [4-^{13}C]aspartate, and [1-^{13}C]serine tracers were applied to *C. acetobutylicum* and *E. coli* to identify metabolic cycles between central carbon metabolism and amino acid metabolism. Importantly, I demonstrate that *C. acetobutylicum* has an active metabolic cycle where carbon atoms flow from aspartate to threonine, serine, pyruvate, oxaloacetate and back to aspartate.

- **Chapter 4** describes the characterization of butanol and butyric acid stresses on *C. acetobutylicum* metabolism. Butanol and butyric acid are important, yet toxic metabolites of *C. acetobutylicum* fermentations. To better understand the metabolite stress response, ^{13}C labeling experiments and mass isotopomer analysis were used to characterize changes to metabolism under butanol and butyric acid stresses. In contrast to previously published transcriptomic studies, I show that the relative flux distributions remain unchanged during stress despite suboptimal growth.

- **Chapter 5** describes the quantification of the flux from pyruvate to phosphoenolpyruvate (PEP) in *E. coli* using ^{13}C alanine tracers and knockout strains. This work was performed in collaboration with another student in the Antoniewicz Lab, Christopher Long. First, we determined the contributions of phosphoenolpyruvate synthetase (pps) and Enzyme I (EI), the terminal phosphotransferase of the PTS, to this flux during gluconeogenic growth. Second, we investigated the roles and contributions of these enzymes and other components of the PTS to the back flux during growth on glycolytic substrates.

- **Chapter 6** presents a GC-MS based method for measuring the isotopic labeling of glycogen and RNA, and demonstrates the efficacy of these measurements for ^{13}C-MFA. This work was performed in collaboration with another student in the Antoniewicz Lab, Christopher Long. The

developed method provides labeling information on the glucose moiety of glycogen and the ribose moiety of RNA. Compared to alternative methods, this approach uses a relatively small amount of biomass and avoids the pitfalls of LC-MS and LC-MS/MS based techniques. Using *E. coli* as a model microbial system and CHO cells as a model mammalian system, we demonstrated the applicability of these measurements to ^{13}C-MFA of the pentose phosphate pathway and upper glycolysis. Overall, glycogen and RNA measurements allowed for more precise flux estimation of these pathways.

- **Chapter 7** summarizes the main findings of this dissertation and highlights their applicability in metabolic engineering and systems biology. Areas of future work are also addressed.

Chapter 2

PARALLEL LABELING EXPERIMENTS VALIDATE *CLOSTRIDIUM ACETOBUTYLICUM* METABOLIC NETWORK MODEL FOR ^{13}C METABOLIC FLUX ANALYSIS

Reproduced with permission from Au, J., Choi, J., Jones, S.W., Venkataramanan, K.P., Antoniewicz, M.R., 2014. Parallel labeling experiments validate *Clostridium acetobutylicum* metabolic network model for ^{13}C metabolic flux analysis. Metab. Eng. 26, 23–33.

2.1 Introduction

In recent decades, fluctuating oil prices, diminishing fossil fuel supplies, and concerns about climate change have prompted demand for alternative energy sources (Stephanopoulos, 2008). Considerable effort has gone into research and development of microbial biofuel production from biomass (Stephanopoulos, 2007). Due to their wide substrate range, solventogenic clostridia are seen as a promising class of organisms for biofuel production (Tracy et al., 2012). *Clostridium acetobutylicum*, in particular, was historically used for industrial-scale acetone-butanol-ethanol (ABE) fermentation and may potentially play a role in butanol production today (Dürre, 1998). Research on the genetics and metabolic engineering of this model organism may also lead to its use in new industrial processes for the production of butyric acid, butanediol, propanol, acetoin, and biohydrogen (Papoutsakis, 2008; Tracy et al., 2012).

Although the biochemistry of *C. acetobutylicum* has been extensively reviewed (Nolling et al., 2001; Papoutsakis, 1984; Paredes et al., 2005), the central metabolic pathways remain only partially resolved for this organism (Crown et al., 2011). As an example, two recent reconstructions of genome-scale models for *C. acetobutylicum* (J. Lee et al., 2008; Senger and Papoutsakis, 2008) have proposed different mechanisms for the biosynthesis of α-ketoglutarate, the precursor for glutamate, glutamine and proline. One model posed the production of glutamate via the urea cycle and arginine biosynthesis pathway operating in the reverse direction (Senger and Papoutsakis, 2008), while the other suggested a reductive TCA cycle operating in the direction from oxaloacetate to fumarate and to α-ketoglutarate (J. Lee et al., 2008). Recently, stable-isotope labeling experiments and qualitative ^{13}C-isotopomer analysis have lent new insights into *C. acetobutylicum* metabolism. Two studies supported the idea of an incomplete TCA cycle and suggested a *Re*-stereospecificity for the citrate synthase reaction (Amador-Noguez et al., 2010; Crown et al., 2011). Another study suggested that the TCA cycle was bifurcated with an oxidative and reductive branch resulting in the excretion of succinate as a dead-end product (Amador-Noguez et al., 2011).

In this work, we have quantitatively elucidated the central metabolism of *C. acetobutylicum* using ^{13}C-metabolic flux analysis (^{13}C-MFA), a powerful method for determining intracellular metabolic fluxes in living cells (Antoniewicz, 2013b; Crown and Antoniewicz, 2013a). In contrast with previous qualitative studies, here we used the power of parallel labeling experiments and rigorous statistical analysis (Antoniewicz, 2013a) to conclusively establish the structure of central metabolic pathways and the direction of carbon flow in the TCA cycle and through amino acid biosynthesis pathways in *C. acetobutylicum*. Contrary to previously proposed

hypotheses, we find that while the TCA cycle runs in the oxidative direction, there is no significant flux between α-ketoglutarate and succinyl-CoA or succinate and fumarate, and that the conversion of succinyl-CoA to succinate proceeds independently of the TCA cycle. Notably, we also show that there is no flux between malate and oxaloacetate. Additionally, we identified a pyruvate-to-fumarate pathway that proceeds via aspartate. Finally, we identified a putative citramalate synthase gene that is the first step in the biosynthesis of isoleucine in *C. acetobutylicum*. This work illustrates the power of ^{13}C-MFA and parallel labeling experiments in validating metabolic network models and quantifying accurate metabolic fluxes. The systematic approach employed here can be easily applied to elucidate the metabolism of other poorly understood organisms (Swarup et al., 2014; Tang et al., 2012, 2009b).

2.2 Materials and Methods

2.2.1 Materials

Media and chemicals were purchased from Sigma-Aldrich (St. Louis, MO). [1-^{13}C]Glucose (99.5% ^{13}C) and [U-^{13}C]glucose (99.2% ^{13}C) (Antoniewicz et al., 2011) were purchased from Cambridge Isotope Laboratories (Andover, MA). [4-^{13}C]Asparate (99% ^{13}C), [U-^{13}C]fumarate (99% ^{13}C) and [1-^{13}C]serine (99.0% ^{13}C) were purchased from Isotec (St. Louis, MO). The defined clostridial growth medium (CGM) contained per liter of medium: 0.75 g KH_2PO_4, 0.98 g K_2HPO_4•$3H_2O$, 1.0 g NaCl, 3.3 g ammonium acetate, 0.05 g $CaCl_2$•$2H_2O$, 0.35 g $MgSO_4$, 0.01 $MnSO_4$•H_2O, 0.01 g $FeSO_4$•$7H_2O$, 0.004 g PABA, 0.00001 g biotin, and 20 to 40 g glucose.

2.2.2 Strains and Growth Conditions

C. acetobutylicum ATCC 824 (American Type Culture Collection, Manassas, VA) was stored at -85°C in CGM medium containing 15% glycerol. For the pre-culture, a single colony of *C. acetobutylicum* from CGM agar plate was inoculated into a culture tube containing 10 mL of CGM. Cells were then grown anaerobically at 37°C in an anaerobic chamber (Forma, Thermo Scientific) to an optical density (OD_{600}) of 0.5-1.0. About 0.5 mL of this culture was then used to inoculate 10 mL of fresh CGM with 20 g/L glucose, i.e. 5% (v/v) inoculum fraction. Four cultures were inoculated at the same time, which were then transferred to mini-bioreactors that were custom-constructed using 15-mL anaerobic Hungate tubes (Bellco Glass Cat. No. 2047-16125). Each culture tube had a screw cap with a rubber septum that was pierced by three needles for: (1) supply of filter-sterilized N_2 (injected into the head space at 5 mL/min to maintain anaerobic growth conditions); (2) sampling of the cell culture; and (3) venting of off-gasses. The mini-bioreactors were autoclaved prior to inoculation. Gas flow rates were monitored by a digital flowmeter (Supelco, Veri-Flow 500). The temperature of cultures was maintained at 37°C by placing the tubes in a heating block (J-KEM Parallel Bioreactor System, PRS-120R), and mixing in the mini-bioreactors was achieved using a magnetic stirring bar.

After inoculation, the four parallel cultures were grown for 6.5 h, when a bolus of [U-^{13}C]glucose (20 wt% solution) was added to two of the cultures, and a bolus of [1-^{13}C]glucose (20 wt% solution) was added to the other two cultures. The resulting concentration of ^{13}C-labeled glucose in each culture vessel was approximately 20 g/L (i.e. ~50% unlabeled glucose and ~50% ^{13}C-labeled glucose). The cultures were then grown for another 3 h. At 9.5 h, cells were harvested by centrifugation and used for subsequent GC-MS analysis. In the follow-up tracer experiments with [U-

^{13}C]fumarate and [1-^{13}C]serine, cells were first grown on medium without ^{13}C-tracers until early exponential growth phase. Next, a bolus of [U-^{13}C]fumarate or [1-^{13}C]serine was added to a final concentration of 4 mM [U-^{13}C]fumarate or 2 mM [1-^{13}C]serine. The cells were then grown for another 8 h, at which point cellular metabolism was quenched by placing the culture tubes in -20 °C freezer for 10 minutes, and cells intracellular metabolites were extracted. In the follow-up tracer experiment with [4-^{13}C]aspartate cells inoculated into medium that contained 6 mM of [4-^{13}C]aspartate in addition to glucose. After an overnight incubation, metabolism was quenched at -20 °C and cells were harvested by centrifugation and used for subsequent intracellular metabolite extraction (Amador-Noguez et al., 2010) and GC-MS analysis.

2.2.3 Analytical Methods

Medium samples were collected at multiple time points during the culture to monitor cell growth, glucose consumption, and product accumulation. Optical density at 600 nm (OD_{600}) was measured using a spectrophotometer (Eppendorf BioPhotometer). The OD_{600} values were converted to cell dry weight concentrations using a pre-determined OD_{600}-dry cell weight relationship (1.0 OD_{600} = 0.26 g_{DW}/L). After centrifugation, the supernatant was separated from the biomass pellet and glucose concentration in the supernatant was determined by YSI 2700 biochemistry analyzer (YSI, Yellow Springs, OH). Concentrations of acetate, butyrate, acetoin, acetone, butanol, and ethanol in the supernatant were determined using an Agilent 1200 Series HPLC (Tomas et al., 2003).

2.2.4 Gas Chromatography-Mass Spectrometry

GC-MS analysis of ^{13}C-labeling was performed on an Agilent 7890A GC system equipped with a DB-5MS capillary column (30 m, 0.25 mm i.d., 0.25 µm-phase thickness; Agilent J&W Scientific), connected to a Waters Quattro Micro Tandem Mass Spectrometer (GC-MS/MS) operating under ionization by electron impact (EI) at 70 eV. GC-MS analysis of *tert*-butyldimethylsilyl (TBDMS) derivatized proteinogenic amino acids was performed as described by (Leighty and Antoniewicz, 2012) GC-MS analysis of TBDMS derivatized intracellular metabolites was performed as described by (Ahn and Antoniewicz, 2011). Mass isotopomer distributions were obtained by integration (Antoniewicz et al., 2007a) and corrected for natural isotope abundances (Fernandez et al., 1996).

2.2.5 Metabolic Network Model

An initial metabolic network model of *C. acetobutylicum* metabolism was constructed for ^{13}C-MFA based on available genome scale models (J. Lee et al., 2008; Senger and Papoutsakis, 2008) and annotated metabolic pathway databases (Caspi et al., 2012; Kanehisa and Goto, 2000; Kanehisa et al., 2012). In addition, an extended network model was constructed that included additional reactions that were found to improve the fits of ^{13}C-labeling data. Finally, a minimal network model was constructed after removing all reactions from the extended model that were determined to carry no measurable flux. The minimal model was confirmed to produce a statistically acceptable fit of all ^{13}C-labeling data in this study. All three models are provided in Table A.1 in Appendix A.

2.2.6 ^{13}C-Metabolic Flux Analysis

^{13}C-MFA was performed using the Metran software (Yoo et al., 2008), which is based on the elementary metabolite units (EMU) framework (Antoniewicz et al., 2007b; Young et al., 2008). Fluxes were estimated by minimizing the variance-weighted sum of squared residuals (SSR) between the experimentally measured and model predicted metabolite yields for acetate, butyrate, acetoin, acetone, butanol, ethanol, and biomass, and mass isotopomer distributions of protein-bound amino acids using non-linear least-squares regression (Antoniewicz et al., 2006). Metabolite yields were expressed as mol product produced / 100 mol glucose consumed, and glucose uptake was fixed at 100 (Crown and Antoniewicz, 2013b). For combined analysis of parallel labeling experiments, multiple data sets were fitted simultaneously to a single flux model, as described previously (Leighty and Antoniewicz, 2012). In all cases, flux estimation was repeated at least 10 times starting with random initial values for all fluxes to find a global solution. At convergence, accurate 95% confidence intervals were computed for all estimated fluxes by evaluating the sensitivity of the minimized SSR to flux variations (Antoniewicz et al., 2006). Precision of estimated fluxes was determined as follows (Antoniewicz et al., 2006):

$$\text{Flux precision (stdev)} = [(\text{flux}_{\text{upper bound 95\%}}) - (\text{flux}_{\text{lower bound 95\%}})] / 4 \qquad (2.1)$$

To model fractional labeling of glucose in the medium (i.e. only about 50% of glucose in the medium was ^{13}C-labeled), a D-value parameter was included in ^{13}C-MFA (Antoniewicz et al., 2007c). To model fractional labeling of biomass amino acids, G-value parameters were also included in ^{13}C-MFA (Antoniewicz et al., 2007c). As described previously, a G-value represents the fraction of a metabolite pool that is

produced during the labeling period (i.e. in this case between 6.5 h and 9.5 h), while 1-G represents the fraction of naturally labeled biomass that was present prior to the addition of tracers. One G-value parameter was included for each measured amino acid in each data set (Antoniewicz et al., 2007c; Leighty and Antoniewicz, 2012). Reversible reactions were modeled as separate forward and backward fluxes. Net and exchange fluxes were determined as follows: $v_{net} = v_f - v_b$; $v_{exch} = \min(v_f, v_b)$.

2.2.7 Goodness-of-Fit Analysis

To determine the goodness-of-fit, ^{13}C-MFA fitting results were subjected to a χ^2-statistical test. In short, assuming the network model is correct and data are without gross measurement errors, the minimized SSR is a stochastic variable with a χ^2-distribution. The number of degrees of freedom is equal to the number of fitted measurements *n* minus the number of estimated independent parameters *p*. The acceptable range of SSR values is between $\chi^2_{\alpha/2}(n-p)$ and $\chi^2_{1-\alpha/2}(n-p)$, where α is a certain chosen threshold value, for example 0.05 for 95% confidence interval (Antoniewicz et al., 2006). Fits with a minimized SSR above the threshold value were considered statistically not acceptable.

2.3 Results and Discussion

2.3.1 Parallel Labeling Experiments

C. acetobutylicum ATCC 824 was grown anaerobically in four parallel cultures at 37°C on defined medium with 20 g/L glucose and 40 mM acetate. Acetate served here as a buffer to prevent large pH drops that would inhibit cell growth. Cells were inoculated at an optical density (OD_{600}) of approximately 0.05. After 6.5 h, a bolus of ^{13}C-labeled glucose was added. Two cultures received a bolus of 20 g/L [U-

^{13}C]glucose, and two cultures received a bolus of 20 g/L [1-^{13}C]glucose. The cells were then grown for an additional 3 h in the presence of the ^{13}C-tracers, and at 9.5 h the cells were harvested by centrifugation for subsequent GC-MS analysis. The final OD_{600} of the parallel cultures was 1.5 ± 0.3. Over the course of the experiment the cells produced about 4 mM acetic acid and 9 mM butyric acid. Only very low concentrations of solvents were detected by HPLC (acetoin, acetone, butanol, and ethanol were less than 1 mM), indicating that the cells were still in the acetogenic growth phase. Detailed growth data are given in Table A.3 in Appendix A.

2.3.2 Gas Chromatograph-Mass Spectrometry Analysis

Isotopic labeling of biomass amino acids was determined by GC-MS for ^{13}C-MFA, after hydrolysis of biomass and TBDMS derivatization of the amino acids. There was good agreement between the measured mass isotopomer distributions (MIDs) for the two biological replicates for each isotopic tracer. The average difference between the measured mass isotopomer abundances for [U-^{13}C]glucose experiments was 0.15 mol%, and the average difference for [1-^{13}C]glucose experiments was 0.14 mol%. This good agreement confirms that biological variability between the four labeling experiments was small, which is important since good biological reproducibility is a strict requirement for combined flux analysis of parallel labeling experiments (Crown and Antoniewicz, 2013a; Leighty and Antoniewicz, 2013).

2.3.3 ^{13}C-Metabolic Flux Analysis and Network Model Validation

A detailed metabolic network model of *C. acetobutylicum* metabolism was constructed for ^{13}C-MFA based on two available genome-scale models and reactions

annotated in KEGG and BioCyc databases. The base model (86 reactions, Table A.1 in Appendix A) included all major metabolic pathways of central carbon metabolism, lumped amino acid biosynthesis pathways, and a lumped reaction for cell growth. When ^{13}C-MFA was performed with this base model, however, we did not obtain statistically acceptable fits for the [U-^{13}C]glucose data, [1-^{13}C]glucose data, and combined analysis of all four parallel labeling experiments. The weighted sum of squared residuals (SSR) values were more than 10-fold higher than statistically acceptable given the number of redundant measurements (Table 2.1).

Table 2.1: Goodness-of-fit analysis for different metabolic network models of *C. acetobutylicum*

		[U]Gluc		**[1]Gluc**		**[U]Gluc & [1]Gluc**	
No. of fitted data sets		2		2		4	
No. of fitted labeling measurements*		202		138		340	
No. of redundant measurements**		178		114		292	
Acceptable SSR values (95% Conf.)**		[143, 217]		[86, 145]		[246,341]	
Network model***	**No. of reactions**	**SSR**	**Accepted**	**SSR**	**Accepted**	**SSR**	**Accepted**
Base	86	3706	No	489	No	6789	No
Base +Ac	87	917	No	355	No	4342	No
Base +Ac +Ile	89	419	No	103	Yes	3373	No
Base +Ac +Ile +PFOR	90	220	No	98	Yes	672	No
Base +Ac +Ile +PFOR +CO_2	91	201	Yes	92	Yes	312	Yes
Minimal model	81	208	Yes	92	Yes	320	Yes

* Number of fitted measurements includes only mass isotopomers that were non-zero after correction for natural isotope abundances.

** Number of redundant measurements and acceptable range of SSR values for the minimal model.

*** The following reactions were subsequently added to the base model: +Ac = dilution of intracellular AcCoA by external acetate (v_{91}); +Ile = two alternative isoleucine biosynthesis pathways (v_{64} and v_{66}); +PFOR = reversible PFOR reaction (v_{21}); +CO2 = dilution of intracellular CO_2 by unlabeled CO_2 sources (v_{90}).

Inspection of the residuals between the measured and predicted mass isotopomers revealed that the largest residuals were due to poor fits of leucine and isoleucine mass isotopomers, which are produced from acetyl-CoA and pyruvate. To improve the fits of leucine, we added a reaction to the model that accounted for dilution of intracellular acetyl-CoA pool by extracellular unlabeled acetate (v_{91}). It was previously reported that extracellular acetate can dilute the labeling of intracellular acetyl-CoA pool by up to 20% (Amador-Noguez et al., 2010). Indeed, we found that the addition of this flux significantly improved the fits of leucine labeling data; however, isoleucine mass isotopomers still contributed to large SSR values. In the base model, isoleucine was produced from aspartate as proposed by Senger and Papoutsakis (Senger and Papoutsakis, 2008). However, there are two alternative pathways for isoleucine biosynthesis known: one from threonine and a second from pyruvate and acetyl-CoA via citramalate synthase (Wu et al., 2010). Both pathways were added to the model (lumped reactions v_{64} and v_{66}). The addition of these reactions resulted in significant improvements in the fits of isoleucine labeling data.

With this updated model, [1-^{13}C]glucose data was fitted adequately (Table 2.1). However, the model still did not produce acceptable fits for [U-^{13}C]glucose data, and for combined analysis of all four data sets. Inspection of the residuals revealed that the largest residuals were now due to poor fits of alanine and valine mass isotopomers in the [U-^{13}C]glucose data sets. This indicated that pyruvate labeling was not correctly described by the model. Specifically, the relatively high abundances of M+1 and M+2 isotopomers of alanine were unexpected. Previously, Amador-Noguez et al.(Amador-Noguez et al., 2010) identified a similar discrepancy in their data, which was resolved by assuming a reversible pyruvate ferredoxin oxidoreductase

(PFOR) reaction. It was proposed that the PFOR reaction should be modeled as a two-step process, consisting of a first reversible step that exchanges C1-atom of pyruvate with intracellular CO_2, and a second irreversible step that produces acetyl-CoA. Similar mechanism was also proposed for the PFOR reaction in the related organism *Clostridium thermoaceticum* (Furdui and Ragsdale, 2000). When we added this two-step PFOR reaction to our model (v_{21}), the fits were indeed significantly improved, especially for [U-^{13}C]glucose data; however, combined analysis of all four data sets still did not produce a statistically acceptable fit (Table 2.1). Now, the largest residuals were due to aspartate, threonine, and glutamate mass isotopomers. Previously, we observed a similar discrepancy in these amino acids when validating the metabolic network model for *E. coli* (Leighty and Antoniewicz, 2013, 2012). In that case, the discrepancy was resolved by adding a dilution flux for intracellular CO_2 pool from unlabeled CO_2 sources. To test if a similar dilution of intracellular CO_2 could be occurring in *C. acetobutylicum*, we added the same CO_2 dilution reaction to the model (v_{90}). With this extended model we finally obtained a statistically acceptable fit of all data, including combined analysis of all four data sets (Table 2.1).

2.3.4 Minimal Network Model

Next, we set out to establish a minimal network model of *C. acetobutylicum* metabolism that could still produce an acceptable fit of all ^{13}C-labeling data. A validated minimal model of *C. acetobutylicum* would be a valuable resource for future ^{13}C-MFA studies. For this purpose, we evaluated the 95% confidence intervals of the estimated metabolic fluxes in the extended model. We identified 12 fluxes that were determined to carry no flux, defined here as fluxes for which the 95% confidence interval included zero flux value. The following fluxes were identified as insignificant:

oxidative pentose phosphate pathway fluxes (v_9, v_{10} = 0.00 ± 0.04); Entner-Doudoroff pathway fluxes (v_{18}, v_{19} = 0.00 ± 0.05); flux from α-ketoglutarate to succinyl-CoA (v_{26} = 0.0 ± 0.1); flux from succinate to fumarate (v_{28} = 0.0 ± 0.1); flux from malate to oxaloacetate (v_{30f} = 0.00 ± 0.01); net and exchange fluxes between glycine and CO_2 + 5,10-methylene-THF (v_{55f} = 0.0 ± 0.3; v_{55b} = 0.0 ± 0.1); flux from glycine and acetaldehyde to threonine (v_{56b} = 0.08 ± 0.03); and fluxes from aspartate and threonine to isoleucine (v_{64}, v_{65} = 0.00 ± 0.01). All of these reactions were then removed from the model. The resulting minimal model consisted of 81 reactions (Table A.1 in Appendix A).

^{13}C-MFA performed with this minimal model produced statistically acceptable fits for all data sets, including combined flux analysis (Table 2.2). The minimized SSR values for the minimal model were similar to the SSR values obtained with the extended model (Table 2.1), thus confirming that the excluded reactions were not necessary to reproduce the measured mass isotopomer distributions. The estimated metabolic fluxes for *C. acetobutylicum* determined with the minimal model are shown schematically in Figure 2.1. The complete flux results are given in Table A.2 in Appendix A.

Table 2.2: Fitting of single and multiple labeling experiments with ^{13}C-MFA*

[U]Gluc Repl. 1	**[U]Gluc Repl. 2**	**[1]Gluc Repl. 1**	**[1]Gluc Repl. 2**	**No. of fitted labeling measurements****	**No. of redundant measurements**	**SSR**
X				101	89	108
	X			101	89	85
		X		69	57	47
			X	69	57	43
X	X			202	178	208
		X	X	138	114	92
X	X	X	X	340	292	320

* Minimal model was used for ^{13}C-MFA

** Number of fitted measurements includes only mass isotopomers that were non-zero after correction for natural isotope abundances.

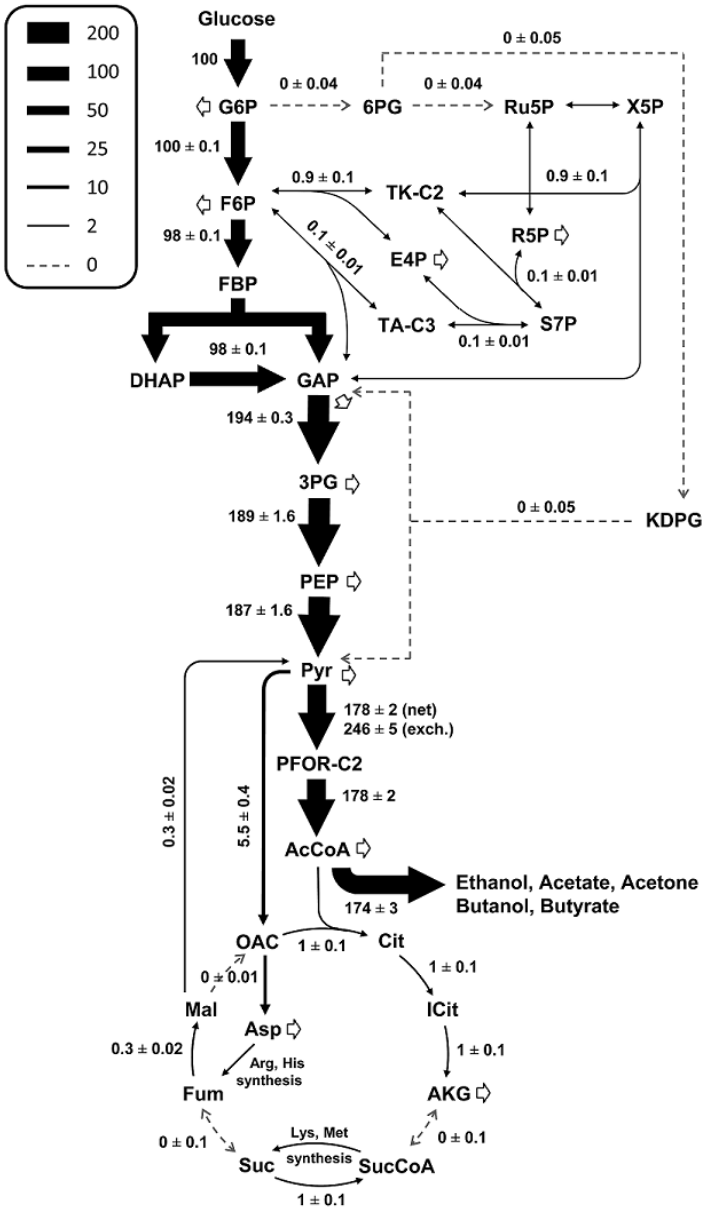

Figure 2.1: Metabolic flux map of central carbon metabolism for *C. acetobutylicum* grown anaerobically in batch culture with glucose as the main carbon substrate (estimated flux ± stdev). Fluxes were estimated using ^{13}C-MFA with the minimal network model for *C. acetobutylicum* (see section 2.3.4) by simultaneously fitting all four labeling data sets (i.e. from [U-^{13}C]glucose and [1-^{13}C]glucose tracer experiments) to a single flux model. Fluxes shown with dotted lines were determined to carry no flux in the extended model and were therefore not present in the minimal model.

2.3.5 An Active Pathway from Pyruvate to Fumarate via Aspartate

As described above, three fluxes in the TCA cycle were shown to carry no significant flux. In particular, the experiment with [1-^{13}C]glucose provided strong evidence that there was no flux from malate to oxaloacetate. As shown in Figure 2.2, [1-^{13}C]glucose was first converted to [3-^{13}C]pyruvate through glycolysis and then to [3-^{13}C]aspartate. Given that fumarate is a rotationally symmetric molecule, [3-^{13}C]aspartate then produced 50% [3-^{13}C]fumarate and 50% [2-^{13}C]fumarate. The fact that we did not observe any labeling in the first two carbon atoms of aspartate, i.e. *m/z* 302 fragment of aspartate was unlabeled (Figure 2.2), clearly indicated that fumarate and malate were not converted to oxaloacetate.

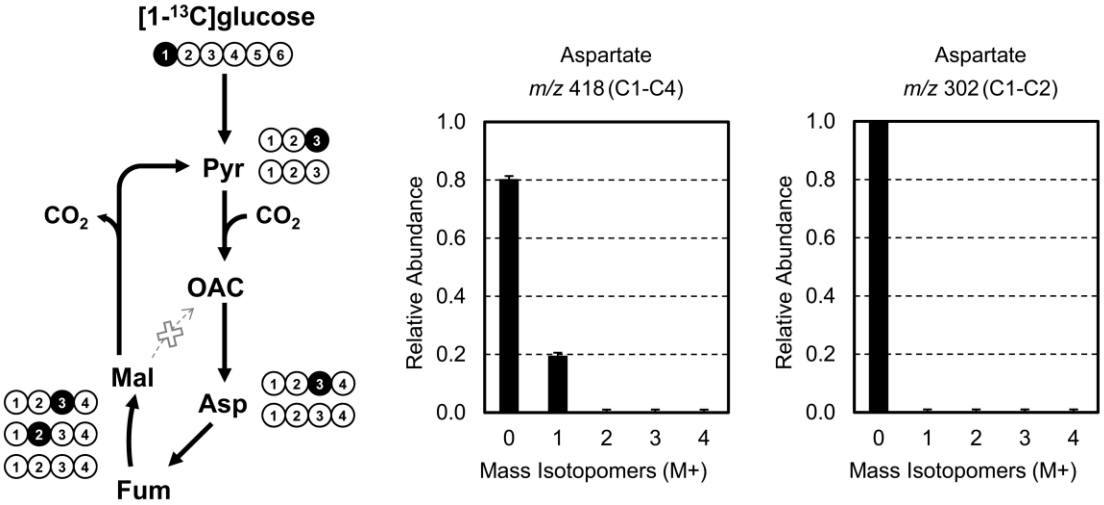

Figure 2.2: Pyruvate to fumarate pathway in *C. acetobutylicum* elucidated with isotopic tracer experiments and ^{13}C-MFA. Experiments with [1-^{13}C]glucose provided evidence that malate was not converted to oxaloacetate, since aspartate was not labeled at the first two carbon positions (*m/z* 302 fragment, C1-C2), but was labeled at the last two carbon positions (*m/z* 418 fragment, C1-C4).

The net result of this incomplete TCA cycle was the formation of the following pathway from pyruvate to fumarate in *C. acetobutylicum*: pyruvate → oxaloacetate → aspartate → fumarate (Figure 2.2 and 2.3A). The driving force for this pathway is the growth-associated conversion of aspartate to fumarate as part of the biosynthesis of arginine and histidine. Our flux results suggested that fumarate was converted to malate, which could potentially be recycled back to pyruvate via malic enzyme. To provide additional support for this result, we performed follow-up labeling experiments with [4-^{13}C]aspartate and [U-^{13}C]fumarate. Figure 2.3 shows the measured ^{13}C-labeling of intracellular aspartate, glutamate, fumarate, malate and alanine. [4-^{13}C]Aspartate labeled intracellular glutamate (92% M+1), fumarate (86% M+1), and malate (67% M+1). These data support the notion that carbon flows from aspartate to fumarate and then to malate. [U-^{13}C]Fumarate on the other hand only labeled intracellular malate (58% M+4), which also confirms that fumarate was converted to malate but malate was not converted to oxaloacetate.

2.3.6 Succinate and Succinyl-Coa are Disconnected from TCA Cycle

Our flux analysis results revealed that there was no measurable flux between α-ketoglutarate and succinyl-CoA, and between succinate and fumarate. The net effect of the absence of these fluxes is that succinate and succinyl-CoA effectively become disconnected from the TCA cycle. During cell growth, however, succinyl-CoA is converted to succinate as part of biosynthesis of lysine and methionine. If succinate is not recycled back to succinyl-CoA, succinate will become a dead-end product in the model. In fact, Amador-Noguez et al. (Amador-Noguez et al., 2010) did observe some succinate accumulation in the medium. However, inspection of their data reveals that succinate excretion rate was about 1000-fold smaller than excretion rates of other

products, thus suggesting that succinate must be largely recycled back to succinyl-CoA via a CoA transferase, as was also initially suggested by Senger and Papoutsakis (Senger and Papoutsakis, 2008). Although several CoA transferase genes have been identified in the genome of *C. acetobutylicum*, it is still unclear which CoA transferase is responsible for this activity.

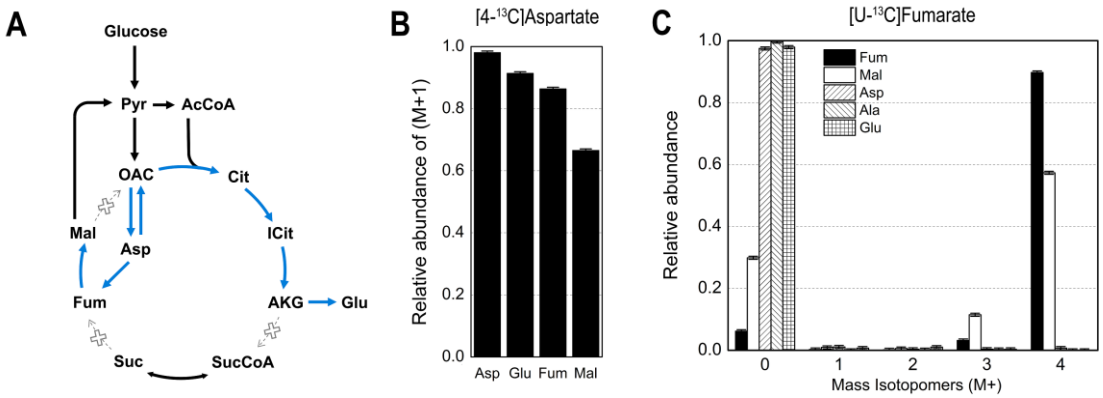

Figure 2.3: (A) Aspartate metabolism in *C. acetobutylicum* (highlighted with blue arrows) revealed by isotopic tracer experiments. (B) Relative abundances of M+1 mass isotopomer in intracellular metabolites from labeling experiment with [4-^{13}C]aspartate as tracer. (C) Mass isotopomer distributions of intracellular metabolites from labeling experiment with [U-^{13}C]fumarate as tracer.

Unfortunately, our flux analysis results did not provide a clear answer to the question: how are succinate or succinyl-CoA produced in the first place? Amador-Noguez et al. (Amador-Noguez et al., 2010) demonstrated experimentally that ^{13}C-aspartate and ^{13}C-glutamate could both produce ^{13}C-labeled succinate. The conversion of α-ketoglutarate to succinyl-CoA can be catalyzed by 2-oxoglutarate synthase (1.2.7.3, CAC2458 and CAC2459) (Crown et al., 2011), which would explain the

conversion of ^{13}C-glutamate to succinate. Senger and Papoutsakis (Senger and Papoutsakis, 2008) also proposed that fumarate could be converted to succinate during nucleotide biosynthesis via L-aspartate oxidase (1.4.3.16, CAC1024), which would explain the conversion of ^{13}C-aspartate to succinate. In our minimal network model neither of these reactions were required, thus suggesting that both of these fluxes are negligible in the overall carbon metabolism of *C. acetobutylicum*, i.e. the minimal model without these reactions still produced a statistically acceptable fit of all ^{13}C-labeling data with 292 redundant measurements. Taken together, these results clearly demonstrate the power of parallel labeling experiments, ^{13}C-MFA, and statistical analysis in identifying significant and insignificant metabolic fluxes in the context of the overall metabolism.

2.3.7 Isoleucine is Exclusively Produced via Citramalate Synthase

The flux results also suggested that isoleucine was not produced from aspartate or from threonine (Figure 2.4), but instead that isoleucine was produced exclusively from pyruvate and acetyl-CoA via citramalate synthase. This route of biosynthesis was previously proposed based on qualitative mass isotopomer analysis (Amador-Noguez et al., 2010). Until now, no citramalate synthase gene has been reported for *C. acetobutylicum*. To identify a putative citramalate synthase gene we performed BLASTp analysis. Several known citramalate synthases showed high homology with the CAC3174 gene, which is currently annotated as an α-isopropylmalate synthase. BLASTp of CAC3174 against the protein database also pulled up several known citramalate synthases as top hits. These results suggested that CAC3174 could code for the citramalate synthase activity that was identified here by ^{13}C-MFA. CAC3174 is the first gene of the operon CAC3174-3173-3172-3171-3170-3169. The other five

genes in this operon code for enzymes that catalyze sequential reactions in the proposed isoleucine biosynthesis pathway shown in Figure 2.4. Taken together, these results provide strong evidence that CAC3174 codes for citramalate synthase, which is the first reaction of the proposed isoleucine biosynthesis pathway in *C. acetobutylicum*.

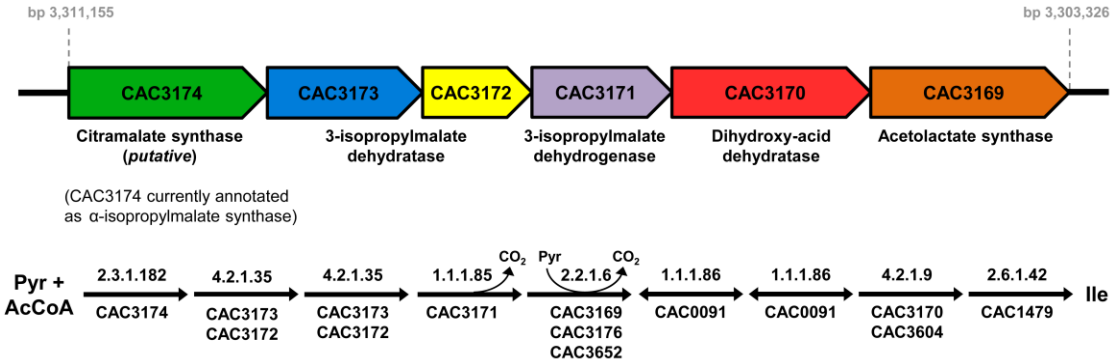

Figure 2.4: Putative citramalate synthase in *C. acetobutylicum* ATCC 824. Citramalate synthase (EC 2.3.1.182) is putatively coded by CAC3174, which is part of the operon CAC3174-3173-3172-3171-3170-3169. The other five genes in this operon code for enzymes that catalyze sequential reactions in the proposed isoleucine biosynthesis pathway.

2.3.8 One-Carbon Metabolism

Finally, our flux analysis results provided valuable insights into one-carbon metabolism in *C. acetobutylicum*. As shown in Figure 2.5A, C_1 units (which are needed for biosynthesis of methionine, purines and thymidine) were almost exclusively synthesized from pyruvate via pyruvate formate lyase and formate-tetrahydrofolate ligase. The conversion of serine to glycine did not contribute significantly to C_1 production. As discussed already in section 2.3.4, there was also no

significant flux from glycine to CO_2 + 5,10-methylene-THF. Thus, we determined that almost all of the C_1 units are derived from pyruvate in *C. acetobutylicum*. These findings are consistent with previously published results on one-carbon metabolism (Amador-Noguez et al., 2010). To further validate fluxes in this part of metabolism, we performed a follow-up labeling experiment with [1-^{13}C]serine. [1-^{13}C]Serine labeled glycine (58% M+1), alanine (11% M+1) and aspartate (8% M+1) (Figure 2.5B), thus supporting the notion that carbon flows from serine to glycine and from serine to alanine via the conversion of serine to pyruvate.

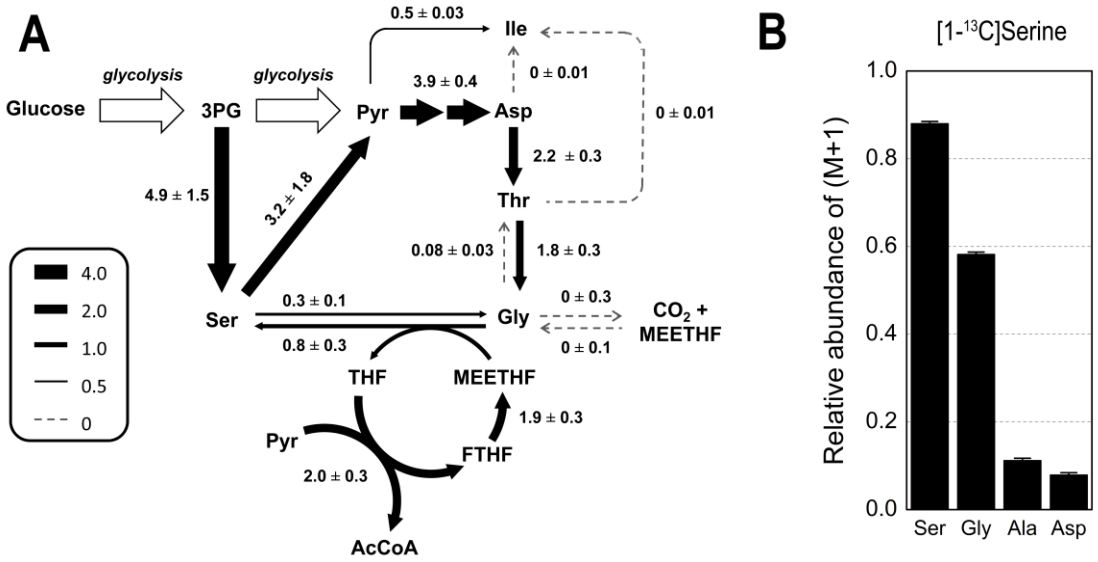

Figure 2.5: (A) Metabolic flux map of one-carbon metabolism and isoleucine biosynthesis in *C. acetobutylicum* (estimated flux ± stdev). Fluxes were estimated using ^{13}C-MFA and the minimal network model. Fluxes shown with dotted lines were determined to carry no flux in the extended model and were therefore not present in the minimal model. (B) Relative abundances of M+1 mass isotopomer in intracellular metabolites from labeling experiment with [1-^{13}C]serine as tracer.

2.3.9 Revised Model of *C. acetobutylicum* Metabolism

This work corroborates specific findings from previously published tracer studies (Amador-Noguez et al., 2010; Crown et al., 2011), and has provided several new insights into the metabolism of *C. acetobutylicum* that can have consequences for further efforts aimed at metabolic engineering of this organism for biofuels production, e.g. by engineering of redox and energy metabolism (Papoutsakis, 2008; Wang et al., 2013). As was described before (Amador-Noguez et al., 2010; Crown et al., 2011), *C. acetobutylicum* catabolizes glucose exclusively through glycolysis. Neither the oxidative pentose phosphate pathway, nor the Entner-Doudoroff pathway are active in *C. acetobutylicum*. The vast majority (about 90%) of pyruvate formed via glycolysis is converted to acetic and butyric acid during the growth phase. Consistent with findings by (Amador-Noguez et al., 2010), ^{13}C-MFA demonstrated that the decarboxylation step of the PFOR reaction is reversible, isoleucine is exclusively synthesized via citramalate synthase, and C_1 units are primarily derived from pyruvate.

In this study, we established for the first time quantitatively using ^{13}C-MFA that the TCA cycle runs in the oxidative direction and is incomplete, with no flux between α-ketoglutarate and succinyl-CoA, succinate and fumarate, and malate and oxaloacetate. These findings are consistent with the conclusions presented by (Crown et al., 2011), who demonstrated no carbon flow from α-ketoglutarate to fumarate, or from fumarate to α-ketoglutarate. The net result of this TCA cycle connectivity is that the remaining reactions exist primarily for amino acid biosynthesis. Additionally, we determined that the net carbon flow is from pyruvate to aspartate to fumarate, which is then further converted to malate (Figure 2.3). Previously, Amador-Noguez et al. (Amador-Noguez et al., 2011) noted that during growth on ^{13}C-glucose, ^{13}C-labeled malate and fumarate were produced; however, during the stationary phase the same

tracer did not label either of these metabolites. This previous unexpected observation can now be easily explained by the presence of the growth-associated pyruvate-to-fumarate pathway that was elucidated in this study.

2.4 Conclusions

This study clearly demonstrates the power of parallel labeling experiments, combined with ^{13}C-MFA and statistical analysis, to elucidate and quantitatively validate metabolic network models (Ahn and Antoniewicz, 2013; Crown and Antoniewicz, 2013a). Here, four isotopic labeling experiments were successfully integrated for ^{13}C-MFA. For the first time, we provide quantitative metabolic fluxes for *C. acetobutylicum* with narrow confidence intervals. Since combined analysis of parallel labeling experiments can provide a large number of redundant measurements (here, 292 redundant measurements), it can serve as a valuable tool for validating metabolic network models. Although our initial metabolic model did not produce statistically acceptable fits, we were able to resolve all inconsistencies using a step-by-step process by inspecting residuals and proposing and testing updated network models. The final extended model was then trimmed to a minimal model that could still produce an acceptable fit of all data. We believe that this systematic procedure is a powerful and unbiased approach to network model validation and flux analysis.

Taken together, this study has provided new and important insights into the metabolism of *C. acetobutylicum* and has resolved a number of inconsistencies in previous models. The fluxes in the TCA cycle were resolved for the first time with high precision. Furthermore, we validated the structure of amino acid biosynthesis pathways. In particular, we identified that *C. acetobutylicum* produces isoleucine exclusively via citramalate synthase, which is likely encoded by the CAC3174 gene.

In future work, we plan to focus on further elucidating the regulation of the pyruvate-to-fumarate pathway using new analytical techniques, recently developed in our lab, based on tandem mass spectrometry (Antoniewicz, 2013c; Choi and Antoniewicz, 2011), which can allow complete resolution of aspartate labeling (Choi et al., 2012), and using new dynamic metabolic flux analysis approaches (Antoniewicz, 2013d; Leighty and Antoniewicz, 2011).

Chapter 3

INVESTIGATION OF METABOLIC CYCLES IN *C. ACETOBUTYLICUM* AND *E. COLI*

3.1 Introduction

^{13}C Metabolic flux analysis (^{13}C-MFA) is a widely used method in metabolic engineering to elucidate metabolic pathway activities and identify bottlenecks in metabolism. ^{13}C-MFA offers significant advantages over alternative flux analysis approaches such as stoichiometric MFA (i.e. without isotopic tracers) and flux balance analysis (FBA), which rely on several questionable assumptions such as co-factor balancing and optimal organization of cellular metabolism for cell growth (Matsuoka and Shimizu, 2010). A key advantage of ^{13}C-MFA is that it allows quantification of fluxes of cyclic pathways, parallel pathways, and reversible reactions, which cannot be estimated with MFA and FBA (Wiechert, 2001). However, ^{13}C-MFA is not completely devoid of assumptions. Key assumptions of ^{13}C-MFA include: 1) the biological system studied is at metabolic steady state (i.e. constant intracellular fluxes); 2) enzymes do not discriminate between ^{12}C and ^{13}C atoms (i.e. no kinetic isotope effect); and 3) isotopic steady state is reached. The first assumption can be justified to a degree by demonstrating that external rates, such as substrate uptake, cell growth, and product formation, are constant during an experiment (Buescher et al., 2015). While there is some debate about the second assumption, in most cases the kinetic isotope effect is expected to be insignificant for ^{13}C-tracers (Leighty and Antoniewicz, 2012; Sandberg et al., 2016). Recent advances in flux modeling have

produced computational methods that permit flux estimation from transient ^{13}C-labeling data (Young et al., 2008), so the third assumption has also been addressed.

A fourth, yet unaddressed assumption in ^{13}C-MFA studies is that there is no carbon exchange between amino acid metabolism and central carbon metabolism. In almost all ^{13}C-MFA studies to date, amino acid metabolism is simply modeled as a set of lumped reactions that drain metabolic precursors from central carbon metabolism (Antoniewicz, 2013a). In other words, it is assumed that no carbon flows back into central carbon metabolism from secondary pathways. This assumption has been made in large part due to the difficulty in measuring any such potential metabolic exchange using ^{13}C-glucose tracers that are commonly used in ^{13}C-MFA. However, the absence of these cycles has not been properly validated for many biological systems.

In this work, we have tested this assumption in two model organisms, *E. coli* and *Clostridium acetobutylicum*. While *E. coli* metabolism has been extensively studied with ^{13}C tracers, there is still no consensus different metabolic network model for ^{13}C-MFA (Crown and Antoniewicz, 2013b). In *C. acetobutylicum,* the structure of the central metabolic pathways was only recently resolved using parallel labeling experiments and various ^{13}C-tracers (Au et al., 2014). Here, we have applied multiple ^{13}C-labeled amino acid tracers to detect additional pathways in both organisms that should be considered in ^{13}C-MFA studies. We specifically focused on cycling between amino acid metabolism and central carbon metabolism. In *E. coli,* we demonstrate that the conversion of serine to pyruvate is active in wild-type cells and should be included in ^{13}C-MFA studies. In *C. acetobutylicum,* we provide the first conclusive evidence that a metabolic cycle is active where carbon atoms flow from aspartate to threonine, to serine, to pyruvate, to oxaloacetate, and back to aspartate. Moreover, we

demonstrate reversibility of at least two reactions in this cycle. This study serves as an example of how multiple ^{13}C-labeled amino acid tracers can be applied to investigate metabolic network models in more detail to validate assumptions of ^{13}C-MFA and identify metabolic cycles that can be difficult to detect using traditional ^{13}C-glucose tracers.

3.2 Materials and Methods

3.2.1 Materials

Chemicals were purchased from Sigma-Aldrich (St. Louis, MO). [1-^{13}C]Aspartate (99.0% ^{13}C), [4-^{13}C]aspartate (99.0% ^{13}C), and [1-^{13}C]serine (99.0% ^{13}C), were purchased from Isotec (St. Louis, MO). For *E. coli* experiments, M9 minimal medium was used. For *C. acetobutylicum* experiments, a defined clostridial growth medium (CGM) was used that contained per liter of medium: 0.75 g KH_2PO_4, 0.98 g K_2HPO_4•$3H_2O$, 1.0 g NaCl, 3.3 g ammonium acetate, 0.05 g $CaCl_2$•$2H_2O$, 0.35 g $MgSO_4$, 0.01 $MnSO_4$•H_2O, 0.01 g $FeSO_4$•$7H_2O$, 0.004 g PABA, 0.00001 g biotin, and 40 g glucose.

3.2.2 Strains and Growth Conditions

E. coli K-12 MG1655 (ATCC 700926, Manassas, VA) and *C. acetobutylicum* ATCC 824 (Manassas, VA) were used in this study. For *E. coli* cultures, cells were grown aerobically in M9 minimal medium at 37°C in mini-bioreactors with 10 mL working volume as described previously (Crown et al., 2015). Parallel cultures were inoculated at an OD_{600} of 0.2. For *C. acetobutylicum* cultures, cells were grown anaerobically in mini-bioreactors with a working volume of 10 mL as described previously (Au et al., 2014). In short, for the pre-culture, a single colony from CGM

agar plate was grown in CGM medium at 37°C in an anaerobic chamber (Forma, Thermo Scientific) to an optical density (OD_{600}) of 0.5-1.0. About 0.5 mL of this culture was then used to inoculate 10 mL of fresh CGM medium. Parallel cultures were inoculated at the same time, which were then transferred to the mini-bioreactors. Anaerobic conditions were maintained in the mini-bioreactors by flowing nitrogen gas into the headspace at a rate of 5 mL/min. The temperature was maintained at 37°C by placing the mini-bioreactors in a heating block (J-KEM Parallel Bioreactor System, PRS-120R), and mixing was achieved using a magnetic stirring bar.

For both *E. coli* and *C. acetobutylicum* cultures, a bolus of either [1-^{13}C]aspartate (2 mL of 30 mM solution), [4-^{13}C]aspartate (2 mL of 30 mM solution), or [1-^{13}C]serine (0.2 mL of 450 mM solution) was added to each culture at an OD_{600} of 0.5. The resulting concentration of ^{13}C-aspartate was approximately 6 mM, and the concentration of ^{13}C-serine was approximately 10 mM. All cultures were then grown to an OD_{600} of 1.5, at which point cellular metabolism was quenched at -20 °C. The cells were harvested by centrifugation and used for subsequent intracellular metabolite extraction and GC-MS analysis.

3.2.3 Analytical Methods and Intracellular Metabolite Extraction

Medium samples were collected at multiple time points during the cultures to monitor cell growth. Optical density at 600 nm (OD_{600}) was measured using a spectrophotometer (Eppendorf BioPhotometer). After centrifugation, the supernatant was separated from the biomass pellet and glucose concentration in the supernatant was determined by YSI 2700 biochemistry analyzer (YSI, Yellow Springs, OH). Extraction of intracellular metabolites was carried out for *C. acetobutylicum* based on previously published protocols (Amador-Noguez et al., 2010). A mixture of

acetonitrile-methanol-water (40:20:20) was cooled to -20 °C and added to each sample of harvested cells. The samples were vortexed and allowed to incubate for 60 minutes. Following the incubation, the samples were centrifuged, and the supernatant was collected and dried under nitrogen flow at 45 °C for subsequent *tert*-butyldimethylsilyl (TBDMS) derivatization.

3.2.4 Gas Chromatography-Mass Spectrometry

For GC-MS analysis of TBDMS-derivatized metabolites from *E. coli*, the analysis was performed on an Agilent 7890B GC system equipped with a DB-5MS capillary column (30 m, 0.25 mm i.d., 0.25 µm-phase thickness; Agilent J&W Scientific), connected to an Agilent 5977A Mass Spectrometer operating under ionization by electron impact (EI) at 70 eV. Helium flow was maintained at 1 mL/min. The source temperature was maintained at 230°C, the MS quad temperature at 150°C, the interface temperature at 280°C, and the inlet temperature at 250 °C. GC-MS analysis of tert-butyldimethylsilyl (TBDMS) derivatized proteinogenic acids was performed as previously described (Leighty and Antoniewicz, 2013).

For GC-MS analysis of TBDMS-derivatized metabolites from *C. acetobutylicum*, the analysis of ^{13}C-labeling was performed on an Agilent 7890A GC system equipped with a DB-5MS capillary column (30 m, 0.25 mm i.d., 0.25 µm-phase thickness; Agilent J&W Scientific), connected to a Waters Quattro Micro Tandem Mass Spectrometer (GC-MS/MS) operating under ionization by electron impact (EI) at 70 eV. GC-MS analysis of TBDMS-derivatized proteinogenic amino acids and intracellular metabolites was performed as described previously (Ahn and Antoniewicz, 2013; Antoniewicz et al., 2007a). Mass isotopomer distributions of

selected fragments were obtained by integration (Antoniewicz et al., 2007a) and corrected for natural isotope abundances (Fernandez et al., 1996).

3.3 Results and Discussion

3.3.1 Conversion of Serine to Pyruvate in *E. coli*

Most metabolic network models for ^{13}C-MFA of *E. coli* include a consistent set of central metabolic pathways (including e.g. glycolysis, pentose phosphate pathway, and the TCA cycle); however, the coverage of secondary pathway reactions is less uniform. For example, *E. coli* is known to contain genes for threonine aldolase, which catalyzes the conversion of threonine to glycine, and serine dehydratase, which catalyzes the conversion of serine to pyruvate (Caspi et al., 2012). It is also known that serine hydroxymethyltransferase catalyzes the reversible conversion of serine to glycine (Schirch et al., 1985). However, as shown in Table 3.1, these reactions are not always included in metabolic network models for ^{13}C-MFA. Exclusion of these reactions effectively predefines these fluxes as insignificant, which may not be a valid assumption under all conditions. Additionally, the combined activity of all of these reactions would produce a potential metabolic cycle in *E. coli* connecting central carbon metabolism and amino acid metabolism as shown in Figure 3.1A. To our knowledge, the activity of this metabolic cycle has not been measured before.

Table 3.1: Secondary reactions included in *E. coli* metabolic network models

^{13}C-MFA Study	Includes Thr → Gly	Reversible Ser ↔ Gly	Includes Ser → Pyr
Crown et al., 2015	Yes	Yes	No
Fu et al., 2015	Yes	Yes	No
Gopalakrishnan and Maranas, 2015	Yes	Yes	Yes
Okahashi et al., 2014	No	Yes	No
Arifin et al., 2014	Yes	Yes	No
Ranganathan et al., 2012	Yes	No	Yes
Chen et al., 2011	Yes	No	No

To probe the activity of reactions in this potential metabolic cycle in *E. coli*, wild-type *E. coli* was grown in three parallel cultures on glucose to an OD_{600} = 0.5, at which point a bolus of either [1-^{13}C]aspartate, [4-^{13}C]aspartate, or [1-^{13}C]serine was added. The cells were then grown in the presence of the specific ^{13}C-tracer to an OD_{600} of 1.5. Cells were harvested for subsequent biomass hydrolysis and GC-MS analysis.

The labeling data are summarized in Figure 3.1. Both aspartate tracers, [1-^{13}C]aspartate and [4-^{13}C]aspartate, produced a similar degree of labeling in threonine, consistent with the known pathway for threonine biosynthesis from aspartate in *E. coli*. [4-^{13}C]Aspartate did not label glycine, as was also expected based on the known atom transitions for the threonine aldolase reaction, i.e. carbon atoms 1-2 of threonine are transferred to glycine. The small amount of labeling in glycine from [1-^{13}C]aspartate (2% M+1) suggests that glycine was mainly generated via the traditional pathway from serine, rather than from threonine. This was further supported by the labeling data from [1-^{13}C]serine labeling experiment, where [1-^{13}C]serine produced significantly labeled glycine (60% M+1). More surprisingly, however, was the fact that [1-^{13}C]serine also labeled alanine to a significant degree (15% M+1). Since alanine is generated from pyruvate, this result suggests that serine is converted to

pyruvate in *E. coli*, demonstrating that this often omitted reaction in ^{13}C-MFA studies is in fact active in *E. coli*.

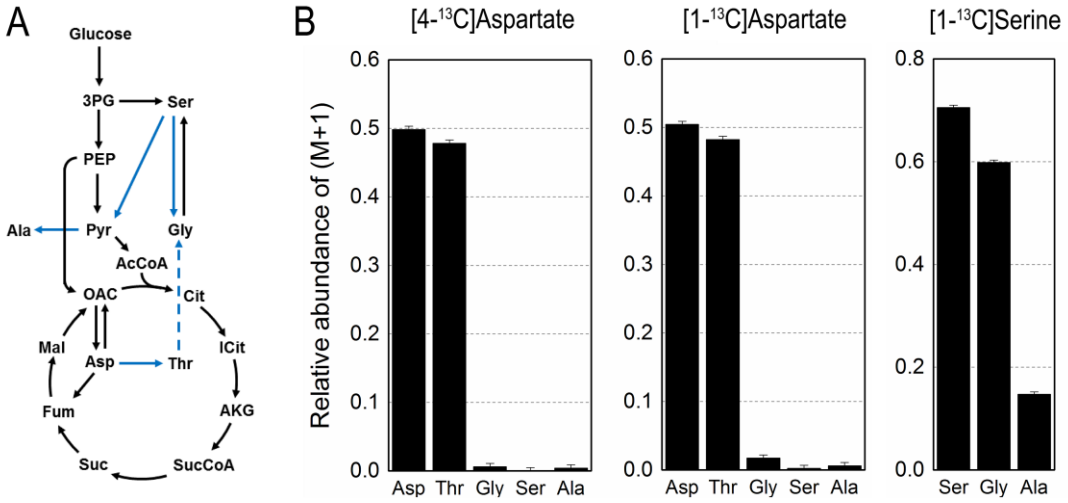

Figure 3.1: Secondary reactions in *E. coli* metabolism (A) Schematic diagram of the probed reactions, which are highlighted in blue. (B) Relative abundances of M+1 mass isotopomers in biomass amino acids from three parallel labeling experiments with [4-^{13}C]aspartate, [1-^{13}C]aspartate, and [1-^{13}C]serine. Mass isotopomers shown here were corrected for natural isotope abundances.

3.3.2 Conversion of Aspartate to Pyruvate is Observed in *C. acetobutylicum*

Next, we sought to characterize the activity of the same set of reactions in the model anaerobic organism *C. acetobutylicum*. Similar to the *E. coli* experiments, *C. acetobutylicum* was grown in three parallel cultures on defined medium containing 40 g/L glucose as the main carbon source. At OD_{600} = 0.5, a bolus of either [1-^{13}C]aspartate, [4-^{13}C]aspartate, or [1-^{13}C]serine was added to each culture. At OD_{600} = 1.5, metabolism was quenched and the cells were harvested for subsequent intracellular metabolite extraction and GC-MS analysis.

Figure 3.2B shows the relative degree of ^{13}C-labeling in the measured intracellular metabolites. [4-^{13}C]Aspartate labeled glutamate, fumarate, and malate, but did not label glycine, serine, or alanine, which is consistent with the known atom transitions for glycine biosynthesis from threonine. During the conversion of threonine to glycine, the fourth carbon of threonine (which is also the fourth carbon of aspartate) is converted to acetaldehyde. The amount of labeling in glutamate (82% M+1) relative to fumarate (85% M+1) and malate (74% M+1) suggested that the conversion of oxaloacetate to aspartate was reversible and α-ketoglutarate was primarily produced via the TCA cycle running in the oxidative direction. If α-ketoglutarate had been produced via malate or via fumarate with a reductive TCA cycle, then the relative abundance of the M+1 mass isotopomer of glutamate would have been significantly lower than that of fumarate or malate. Taken together, these findings are consistent with previous flux analysis results indicating an oxidative TCA cycle and no carbon flow between α-ketoglutarate and succinyl-CoA, succinate and fumarate, and malate and oxaloacetate.

To further examine amino acid metabolism, we also analyzed intracellular metabolite labeling from [1-^{13}C]aspartate and [1-^{13}C]serine experiments (Fig 3.2B). [1-^{13}C]Aspartate labeled fumarate, malate, glycine, serine, and alanine. The absence of labeling in glutamate is consistent with the stereochemistry of *Re*-citrate synthase. The presence of significant labeling in glycine (64% M+1) and serine (42% M+1) was the result of the successive conversions of aspartate to threonine, to glycine, and to serine. [1-^{13}C]Serine also labeled glycine (34% M+1), demonstrating the reversibility of the reaction between serine and glycine. Labeling in alanine was apparent in both experiments (7% M+1 in [1-^{13}C]aspartate experiment, and 14% M+1 in [1-^{13}C]serine

experiment), suggesting that serine was converted to pyruvate, which was then further converted to alanine. Overall, these results demonstrate an active metabolic pathway from aspartate to threonine, to glycine, to serine, and to pyruvate.

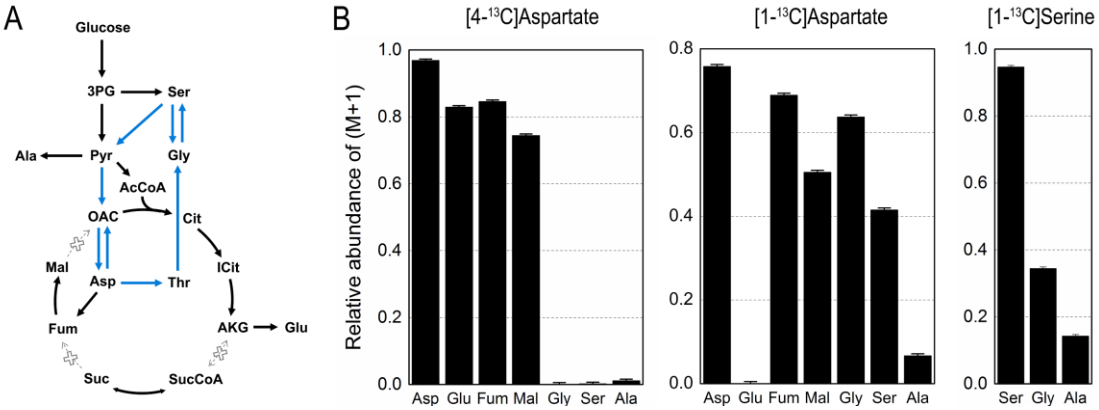

Figure 3.2: Metabolic cycle between central carbon metabolism and amino acid metabolism elucidated in *Clostridium acetobutylicum* using ^{13}C-labeling experiments. (A) Schematic diagram of the metabolic cycle, which is highlighted in blue. (B) Relative abundances of M+1 mass isotopomers in extracted intracellular metabolites from three parallel labeling experiments with [4-^{13}C]aspartate, [1-^{13}C]aspartate, and [1-^{13}C]serine. Mass isotopomers shown here were corrected for natural isotope abundances.

3.3.3 An Unexpected Metabolic Cycle Characterized in *C. acetobutylicum*

In addition to analyzing intracellular metabolite labeling, ^{13}C-labeling of biomass amino acids was also determined by GC-MS. The labeling data provided additional evidence for the findings described above based on intracellular metabolite data analysis. For example, as shown in Figure 3.3, [4-^{13}C]aspartate produced high degrees of M+1 labeling in glutamate (69% M+1) and threonine (70% M+1); while

[1-^{13}C]aspartate produced significantly labeled threonine (59% M+1), glycine (51% M+1), serine (11% M+1), and alanine (5% M+1).

Biomass amino acid labeling from the [1-^{13}C]serine experiment (Fig. 3.3C) also indicated the presence of an active metabolic cycle between amino acid metabolism and central carbon metabolism. As demonstrated by the labeling in the intracellular metabolites, carbon was flowing from aspartate to threonine, to glycine, to serine, and to pyruvate. Further evidence for the conversion of serine to pyruvate can be found in the labeling of Ala-260 fragment (carbon atoms 2-3) and Val-288 fragment (carbon atoms 2-5). Both of these amino acids show significant labeling and both are derived from pyruvate. The metabolic cycle is completed with reactions from pyruvate to oxaloacetate, and to aspartate. The deamination of [1-^{13}C]serine produces [1-^{13}C]pyruvate. When [1-^{13}C]pyruvate is converted to acetyl-CoA via pyruvate ferredoxin oxidoreductase (PFOR), this produces labeled CO_2. Labeled CO_2, along with [1-^{13}C]pyruvate, produces [1-^{13}C]oxaloacetate and [4-^{13}C]oxaloacetate via pyruvate carboxylase, and these metabolites are further converted to [1-^{13}C]aspartate and [4-^{13}C]aspartate. This is clearly reflected in the labeling of Asp-390 (carbons 2-4 of aspartate; 6% M+1) and Asp-302 (carbons 1-2; 6% M+1). The relative abundance of the M+1 mass isotopomer of Asp-418 (full molecule of aspartate; 10% M+1) is approximately the sum of the relative abundances of Asp-390 and Asp-302. Similar logic also applies to Thr-376 (carbons 2-4 of threonine; 4% M+1) and Thr-404 (full molecule of threonine; 10% M+1), since threonine is directly derived from aspartate. The relative abundance of Glu-330 (carbons 2-5 of glutamate) and Glu-432 (full molecule of glutamate) M+1 mass isotopomer is approximately half the abundance of

Asp-418 M+1 mass isotopomer because the labeled carbon of [1-^{13}C]oxaloacetate is lost as CO_2 given the stereochemistry of *Re*-citrate synthase.

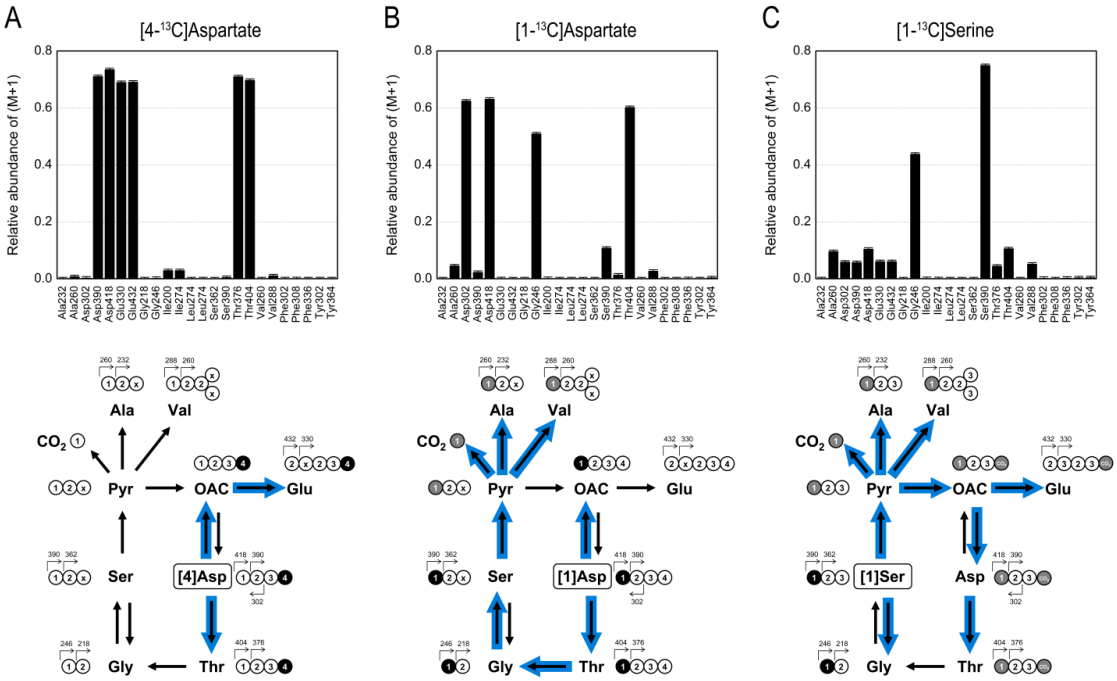

Figure 3.3: Relative abundances of M+1 mass isotopomers in biomass amino acids from three *C. acetobutylicum* parallel labeling experiments with [4-^{13}C]aspartate (A), [1-^{13}C]aspartate (B), and [1-^{13}C]serine (C). Blue arrows in the diagrams show the flow of ^{13}C-atoms, i.e. from the ^{13}C-tracer to the respective measured biomass amino acids. Numbers in the spheres refer to origin of the carbon atom, i.e. referring to the numbering of carbon atoms in the ^{13}C-tracer. Mass isotopomers of TBDMS-derivatized amino acids shown here were obtained by GC-MS and corrected for natural isotope abundances.

3.3.4 Implications of Metabolic Cycling in *C. acetobutylicum*

Taken together, we provide strong evidence of an active metabolic cycle between amino acid metabolism and central carbon metabolism in *C. acetobutylicum*.

Evidence for this cycle came from intracellular metabolite labeling data and biomass amino acid labeling data from tracer experiments with [1-^{13}C]aspartate, [4-^{13}C]aspartate, and [1-^{13}C]serine . While more research is required to completely elucidate the exact purpose of this cycle, one hypothesis is that this metabolic cycle allows *C. acetobutylicum* to efficiently interconvert several metabolites needed for cell growth and maintenance. For example, deamination of serine of pyruvate will produce ammonium, which may act as a nitrogen source for the cells under certain conditions. The cycle also connects several amino acids to intermediates of glycolysis and TCA cycle, which may allow *C. acetobutylicum* to rapidly interconvert several amino acids that are needed at a specific ratio for cell growth.

In terms of metabolic cost of this cycle, the net effect of this cycle is the consumption of 3 ATP and conversion of 2 NADPH to 2 NADH. Based on previous flux calculations for central carbon metabolism the net flux through this cycle is estimated to be roughly 0.5 mol per 100 mol of glucose consumed. This means that the net amount of ATP and NADPH consumed by this cycle is relatively small compared to the overall amount of ATP generated (~200 mol ATP produced per 100 mol glucose consumed) and NADPH generated (~100 mol NADPH produced per 100 mol glucose consumed). In short, this cycle permits *C. acetobutylicum* more flexibility to produce several key metabolites without greatly affecting the overall energy and redox balance.

3.4 Conclusions

In this work, we have demonstrated how multiple ^{13}C-labeled amino acid tracers can be used to probe specific reactions and cycles in central carbon metabolism and amino acid metabolism that are difficult to detect using traditional ^{13}C-glucose

tracers. Using [1-^{13}C]aspartate, [4-^{13}C]aspartate, and [1-^{13}C]serine labeling experiments and mass isotopomer analysis, we have identified a active metabolic cycle in *C. acetobutylicum* that involves two key metabolic intermediates in central carbon metabolism (puruvate and oxaloacetate) and four amino acids (aspartate, threonine, glycine, and serine). For this cycle, we demonstrated the reversibility of reactions, i.e. between oxaloacetate and aspartate, and between glycine and serine.

Additionally, we have conclusively validated that serine is actively converted to pyruvate in *E. coli*, demonstrating the importance of considering additional reactions for ^{13}C-MFA, even in well-studied organisms such as *E. coli*. The importance of using more complete models for ^{13}C-MFA may be of particular significance in the study of strains with altered phenotypes (Long and Antoniewicz, 2014a). In general, this study shows that amino acid tracers, along with parallel labeling experiments, can be used to validate metabolic network models and lay the foundation for unbiased flux measurements using ^{13}C-MFA.

Chapter 4

QUALITATIVE ^{13}C-ISOTOPOMER ANALYSIS CHARACTERIZES SHORT TERM AND LONG TERM EFFECTS OF BUTANOL AND BUTYRIC ACID STRESS ON THE METABOLISM OF *CLOSTRIDIUM ACETOBUTYLICUM*

4.1 Introduction

Clostridia are anaerobic, Gram-positive, endospore-forming bacteria that are important in areas such as human and animal physiology, bioremediation, and biotechnology (Tracy et al., 2012). Their ability to utilize a wide range of substrates (e.g. simple carbohydrates, gases, and cellulosic material) and produce a wide range of products (e.g. various carboxylic acids and alcohols) make them attractive platform organisms for chemical and fuel production (Papoutsakis, 2008). *Clostridium acetobutylicum* is of particular importance as a model organism and for its history with industrial-scale acetone-butanol-ethanol (ABE) fermentation (Jones and Woods, 1986; Moon et al., 2016). Given the growing concerns about climate change and the volatility of oil prices, there is renewed interest to develop *C. acetobutylicum* and other *Clostridia* for industrial-scale production of added-value compounds such as butanol and butyric acid.

Despite being natural fermentation products, butanol and butyric acid are toxic to *Clostridia* (Nicolaou et al., 2010; Peabody and Kao, 2016), with butanol reported as one of the most toxic solvents (Huffer et al., 2011). Accumulation of butanol and butyric acid often leads to reduced cell growth and premature cell death, impacting product yields, final titers, and the overall process productivity of *Clostridium*

cultures. For clostridial platforms to be economically viable, they must be engineered to be more tolerant to the fermentation products.

Butanol and butyric acid are known to induce a metabolite stress response, which is a complex, mulitgenic trait affecting many cellular processes. In *Clostridia*, this response includes the differential expression of genes related to heat shock proteins, amino acid and nucleic acid synthesis pathways, fatty acid biosynthesis, motility, and chemotaxis (Alsaker et al., 2010). There is also evidence that the metabolite stress response is connected to tolerance (Alsaker et al., 2010, 2004; Borden and Papoutsakis, 2007; Borden et al., 2010; Tomas et al., 2003, 2004). For example, heat shock proteins have been implicated for their role in the stress responses of many cellular systems (Guisbert et al., 2008). Tomas et al. (Tomas et al., 2003) demonstrated that overexpression of the *groESL* operon genes, which encode for Class I heat shock proteins, allows *C. acetobutylicum* to withstand more butanol than a control strain and produce ≥40% more butanol than the wild type. Thus, promising strategies for engineering more tolerant strains may be gained through a more comprehensive understanding of the metabolite stress response.

Omics tools have enabled numerous insights into understanding stress response and tolerance. Previous work has focused on the transcriptomic (Alsaker et al., 2010, 2004; Hönicke et al., 2012; Janssen et al., 2012; Schwarz et al., 2012; Tomas et al., 2004; Venkataramanan et al., 2013; Wang et al., 2013) and proteomic responses (Hou et al., 2013; Mao et al., 2011, 2010; Venkataramanan et al., 2015) to butanol and butyric acid stress in *Clostridia*. However, as of today, no studies have directly investigated the effects of these toxic metabolites on metabolic fluxes and metabolic pathways. Here, we have applied ^{13}C tracers and mass isotopomer analysis to elucidate

the short term and long term effects of butanol and butyric acid stress on central carbon metabolism and amino acid metabolism in *C. acetobutylicum*. This information on the metabolic responses to stress contributes to our current understanding of the metabolite stress response and may lead to better strategies for rationally engineering *C. acetobutylicum* for the production of these inherently toxic compounds.

4.2 Materials and Methods

4.2.1 Materials

Media and chemicals were purchased from Sigma-Aldrich (St. Louis, MO). n-Butanol and butyric acid were purchased from Fisher Scientific (Hampton, NH). For the butyric acid stress experiments, 1 M butyric acid solution was prepared and the pH was adjusted to pH 5 using 1 N KOH, resulting in a 0.63 M butyric acid solution. [1-^{13}C]Aspartate (99% ^{13}C) was purchased from Isotec (St. Louis, MO), and [U-^{13}C]glucose (99.2% ^{13}C) was purchased from Cambridge Isotope Laboratories (Andover, MA). The composition of the defined clostridial growth medium (CGM) was previously described in (Au et al., 2014).

4.2.2 Strain and Inoculum

C. acetobutylicum ATCC 824 (American Type Culture Collection, Manassas, VA) was stored at -85°C in CGM medium containing 15% glycerol. For all pre-cultures, a single colony of *C. acetobutylicum* from CGM agar plate was inoculated into a culture tube containing 10 mL of CGM. Cells were then grown anaerobically at 37°C in an anaerobic chamber (Forma, Thermo Scientific) to an optical density (OD_{600}) of 0.5-1.0. In each culture, about 0.5 mL of this pre-culture was used to inoculate 10 mL of fresh CGM with 40 g/L glucose, i.e. 5% (v/v) inoculum fraction.

4.2.3 Analysis of Stress on Cell Growth by On-Line Mass Spectrometer

For each stressor studied, four 10 mL cultures were inoculated at the same time from the same pre-culture and grown in previously described mini-bioreactors (Au et al., 2014) that were modified with a pH probe and a needle for delivery of 1 N NaOH. During the culture, the pH was maintained at pH 5 using a custom-constructed pH controller (J-KEM Scientific Inc.). Gas flow rates were maintained at 10 mL/min N_2 and were monitored by a digital flowmeter (Supelco, Veri-Flow 500). The temperature of cultures was maintained at 37°C by placing the tubes in a heating block (J-KEM Parallel Bioreactor System, PRS-120R), and mixing in the mini-bioreactors was achieved using a magnetic stirring bar. Molar percentages of hydrogen (H_2, *m/z* 2), nitrogen (N_2, *m/z* 28), and carbon dioxide (CO_2, *m/z* 44) in the off-gases of the mini-bioreactors were monitored in real-time by an on-line mass spectrometer for off-gas analysis (Ametek Proline, Berwyn, PA). The CO_2 production rates (mmol/h) were calculated from off-gas analysis data as previously described (Antoniewicz et al., 2007c).

When the cultures reached an OD_{600} of 1, either no stress, low, medium, or high stress levels were introduced. For the butanol stress experiments, the low, medium, and high levels of stress were achieved by adding a bolus of 1 M butanol to resulting concentrations of 30 mM, 60 mM, and 90 mM of butanol, respectively. For the butyric acid stress experiments, the low, medium, and high levels of stress were achieved by adding a bolus of 0.63 M butyric acid to resulting concentrations of 30 mM, 40 mM, and 50 mM of butyric acid, respectively.

4.2.4 Short Term Stress Experiments

For each stressor studied, eight 10 mL cultures were inoculated at the same time and grown in previously described mini-bioreactors (Au et al., 2014). Gas flow rates, temperature, and mixing were maintained as described in Section 4.2.3. When the cultures reached an OD_{600} of 1, a bolus of stress (either 1 M butanol or 0.63 M butyric acid), tracer (either 30 mM [1-^{13}C]aspartate or 2 M [U-^{13}C]glucose), and 2 M unlabeled glucose, or 30 mM unlabeled aspartate was added to achieve the resulting concentrations described in Tables 4.1 and 4.2. At three time points (0.5, 1, and 2 h) after the stress and tracers were introduced, cells were harvested by centrifugation and stored in -20 °C freezer for subsequent biomass hydrolysis.

Table 4.1: Concentrations of stress, [1-^{13}C]aspartate, and glucose introduced at OD_{600}=1 for short term stress experiments.

Culture	No Stress [1-^{13}C]Asp + glucose	Low Stress [1-^{13}C]Asp + glucose	Medium Stress [1-^{13}C]Asp + glucose	High Stress [1-^{13}C]Asp + glucose
Stress (mM)*	0	30 mM BuOH or 30 mM BA	60 mM BuOH or 40 mM BA	90 mM BuOH or 50 mM BA
[1-^{13}C]Asp (mM)	1.5 mM	1.5 mM	1.5 mM	1.5 mM
Glucose (mM)**	100 mM	100 mM	100 mM	100 mM

* Does not include butyric acid already present at OD_{600}=1
**Does not include unlabeled glucose already present at OD_{600}=1
BuOH = butanol; BA = butyric acid

Table 4.2: Concentrations of stress, [U-^{13}C]glucose, and aspartate introduced at OD_{600}=1 for short term stress experiments.

Culture	No Stress [U-^{13}C]Gluc + aspartate	Low Stress [U-^{13}C]Gluc + aspartate	Medium Stress [U-^{13}C]Gluc + aspartate	High Stress [U-^{13}C]Gluc + aspartate
Stress (mM)*	0	30 mM BuOH or 30 mM BA	60 mM BuOH or 40 mM BA	90 mM BuOH or 50 mM BA
[U-^{13}C]Gluc (mM)	100 mM	100 mM	100 mM	100 mM
Aspartate (mM)	1.5 mM	1.5 mM	1.5 mM	1.5 mM

* Does not include butyric acid already present at OD_{600}=1
BuOH = butanol; BA = butyric acid

4.2.5 Long Term Stress Experiments

For each stressor studied, four 10 mL cultures were inoculated at the same time and grown in previously described mini-bioreactors (Au et al., 2014). Gas flow rates, temperature, and mixing were maintained as described in Section 4.2.3. When the cultures reached an OD_{600} of 1, a bolus of stress (either 1 M butanol or 0.63 M butyric acid) and tracer (either 30 mM aspartate or 2 M [U-^{13}C]glucose) was added to achieve the resulting concentrations described in Table 4.3. Two replicates for each level of stress and tracer combination were studied. At four time points (2, 4, 6, 8 h) after the stress and tracers were introduced, cells were harvested by centrifugation and stored in -20 °C freezer for subsequent biomass hydrolysis.

Table 4.3: Concentrations of stress and tracer introduced at OD_{600}=1 for long term stress experiments

Culture	No Stress [U-^{13}C]Gluc	High Stress [U-^{13}C]Gluc	No Stress [1-^{13}C]Asp	High Stress [1-^{13}C]Asp
Stress (mM)*	0	90 mM BuOH or 50 mM BA	0	90 mM BuOH or 50 mM BA
[U-^{13}C]Gluc (mM)	100 mM	100 mM	n/a	n/a
[1-^{13}C]Asp (mM)	n/a	n/a	1.2 mM	1.2 mM

* Does not include butyric acid already present at OD_{600}=1
BuOH = butanol; BA = butyric acid

4.2.6 Analytical Methods

Medium samples were collected at multiple time points during the culture to monitor cell growth, glucose consumption, and product accumulation. Optical density at 600 nm (OD_{600}) was measured using a spectrophotometer (Eppendorf BioPhotometer). After centrifugation, the supernatant was separated from the biomass pellet and glucose concentration in the supernatant was determined by YSI 2700 biochemistry analyzer (YSI, Yellow Springs, OH). Concentrations of acetate, butyrate, acetoin, acetone, butanol, and ethanol in the supernatant were determined using an Agilent 1200 Series HPLC (Tomas et al., 2003).

4.2.7 Gas Chromatography-Mass Spectrometry

GC-MS analysis was performed on an Agilent 7890B GC system equipped with a DB-5MS capillary column (30 m, 0.25 mm i.d., 0.25 µm-phase thickness; Agilent J&W Scientific), connected to an Agilent 5977A Mass Spectrometer operating under ionization by electron impact (EI) at 70 eV. Helium flow was maintained at 1 mL/min. The source temperature was maintained at 230°C, the MS quad temperature

at 150°C, the interface temperature at 280°C, and the inlet temperature at 250°C. GC-MS analysis of *tert*-butyldimethylsilyl (TBDMS) derivatized proteinogenic amino acids was performed as described by (Leighty and Antoniewicz, 2012). Mass isotopomer distributions were obtained by integration (Antoniewicz et al., 2007a) and corrected for natural isotope abundances (Fernandez et al., 1996).

4.2.8 GC-MS Analysis of Glucose

Labeling of glucose in the medium was determined by GC–MS analysis of the aldonitrile pentapropionate derivative of glucose (Antoniewicz et al., 2011). For GC–MS analysis, about 5 μL of medium sample was derivatized as described previously (Antoniewicz et al., 2011). The injection volume for GC–MS analysis was 1 μL and samples were injected at 1:40 split ratio. Helium flow was maintained at 1.0 mL/min. The injection port temperature was 250°C. The temperature of the column was started at 80°C for 1 min, increased to 280°C at 15°C/min, and held for 6 min. Labeling of glucose was determined from the mass isotopomer distribution of the fragment at *m/z* 370, which contains carbon atoms C1–C5 of glucose.

4.3 Results

4.3.1 Impact of Butanol and Butyric Acid Stress on Cell Growth

To assess the impact of butanol and butyric acid stress on cell growth, *C. acetobutylicum* was grown anaerobically in mini-bioreactors with a 10 mL working volume. Parallel cultures were grown at 37°C on defined clostridium growth medium containing 40 g/L glucose. At an OD_{600} of 1, the cultures were stressed with four different levels of butanol (0 mM – control; 30 mM – low stress; 60 mM – medium stress; and 90 mM – high stress) and four different levels of butyric acid (0 mM –

control; 30 mM – low stress; 40 mM – medium stress; and 50 mM – high stress), for a total of eight cultures. The concentrations of butanol and butyric acid were chosen to correspond with previous studies focusing on transcriptomic analysis (Venkataramanan et al., 2013; Wang et al., 2013) and proteomic analysis (Venkataramanan et al., 2015) of the metabolite stress response.

Throughout the culture, cell growth was monitored in real-time by measuring net CO_2 production using an on-line mass spectrometer for off-gas analysis. Figure 4.1A shows the CO_2 production rates for the control culture (no stress) and three cultures with three different levels of butanol stress. As expected, the CO_2 production rates increased exponentially during the first 6 hours of exponential cell growth. There were no significant differences between the four cultures. After the cultures were stressed (denoted by the dashed line in the figure), a few changes in growth were observed. There was no significant change in the CO_2 production rate for the low stress culture, and despite the immediate sharp decrease in the CO_2 production rates for the medium and high stress cultures, the two cultures fully recovered by 8 hours. Differences in growth beyond 8 hours were previously also observed in replicate control cultures at the stationary phase (unpublished data), and were not likely the result of varying levels of butanol stress. Overall, off-gas analysis indicated that butanol stress had only a limited and temporary effect on cell growth.

In contrast to butanol stress, off-gas analysis of cultures stressed with butyric acid demonstrated a more severe impact on cell growth. As shown in Figure 4.1B, the CO_2 production rates for the four cultures were similar for the first 7 hours of exponential cell growth. Upon addition of butyric acid stress (indicated by dashed line in the figure), the three stressed cultures displayed a clear decrease in CO_2 production.

Although the growth of the low stress and medium stress cultures recovered within 2 hours after stress addition, the high stress culture did not to recover its pre-stress CO_2 production rate. This indicates that butyric acid stress has a greater effect on growth than was observed for butanol stress.

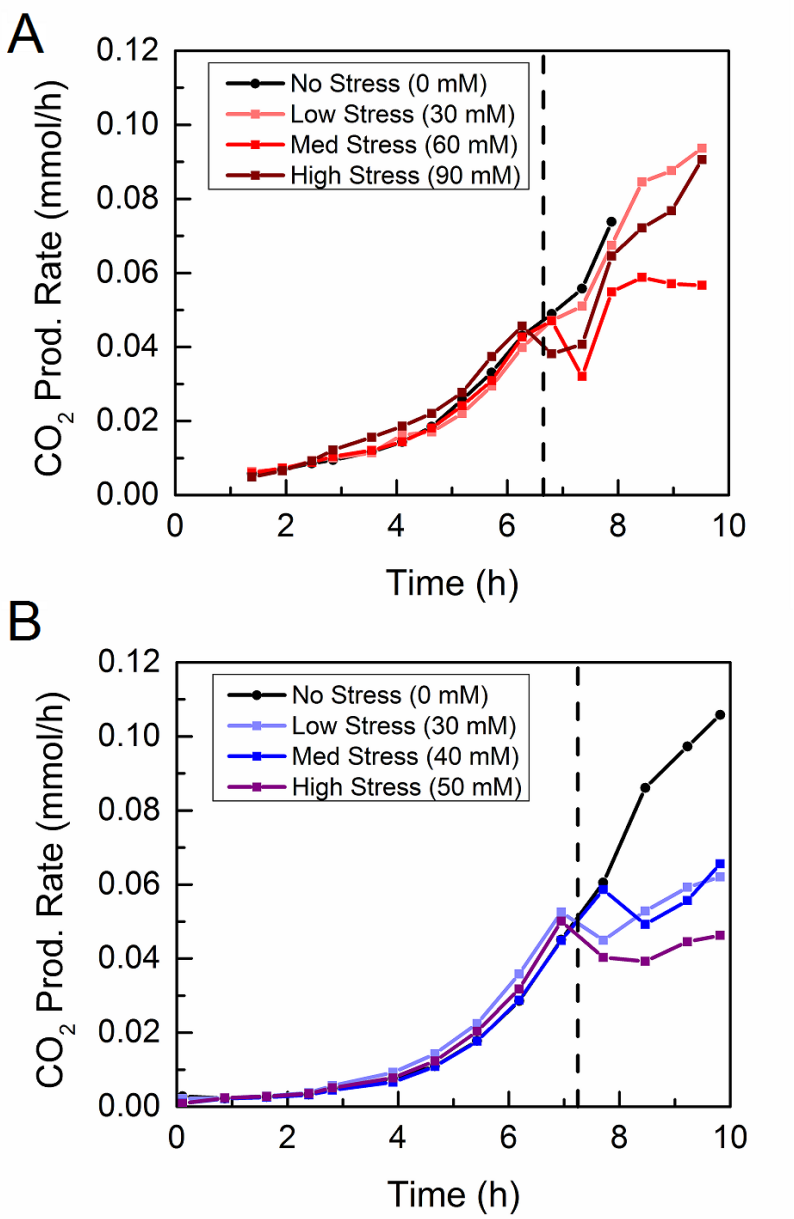

Figure 4.1: Off-gas analysis of *C. acetobutylicum* batch cultures under varying levels of butanol stress. (A) CO_2 production rates for control culture and butanol-stressed cultures. (B) CO_2 production rates for control culture and butyric acid-stressed cultures. Dashed lines in (A) and (B) indicate the approximate time at which the butanol stress was introduced to the cultures.

4.3.2 Short Term Effects of Butanol and Butyric Acid Stress on Intracellular Fluxes

Since off-gas analysis of butanol and butyric acid stressed cultures indicated an immediate impact on cell growth, ^{13}C labeling experiments were used to characterize changes in central metabolic pathways within the first two hours of the stress addition. A parallel labeling strategy was utilized to explore different parts of *C. acetobutylicum* metabolism. Specifically, [1-^{13}C]aspartate was chosen to probe a recently discovered metabolic cycle (see Chapter 3), and [U-^{13}C]glucose was chosen to elucidate general changes to central carbon metabolic pathways. As indicated in Tables 4.1 and 4.2, these tracers and their unlabeled counterparts, and the different levels of stress were introduced to cultures at OD_{600} = 1. Cells were harvested at three time points (0.5 h, 1 h, and 2 h) after the tracer and stress were introduced for subsequent ^{13}C analysis of biomass amino acids.

Figure 4.2 illustrates the time profiles of ^{13}C labeling of key metabolic cycle intermediates (aspartate, threonine, and glycine) in the 2 hours following the addition of tracer and different levels of butanol stress. The percentage of labeled isotopomers for each metabolite (100%-M0) was determined from the measured mass isotopomer distributions after correction for natural isotope abundances. It was expected that any changes in metabolic cycle fluxes as a result of butanol stress would be reflected as differences in ^{13}C labeling profiles between the different levels of stress. As shown in Figure 4.2, the ^{13}C labeling profiles of aspartate, threonine, and glycine were similar between all four butanol stress levels throughout the 2 hours. In both the [1-^{13}C]aspartate and [U-^{13}C]glucose tracer experiments, the labeling dynamics and magnitude of ^{13}C enrichment were similar and independent of the amount of butanol stress introduced (<5% difference in labeling between stress levels). This suggests that

butanol stress had no measureable effect on the flux through this metabolic cycle. ^{13}C labeling profiles of other biomass amino acids (see Appendix B) were also independent of the amount of stress added, which suggests that central carbon metabolism as a whole did not change in response to butanol stress.

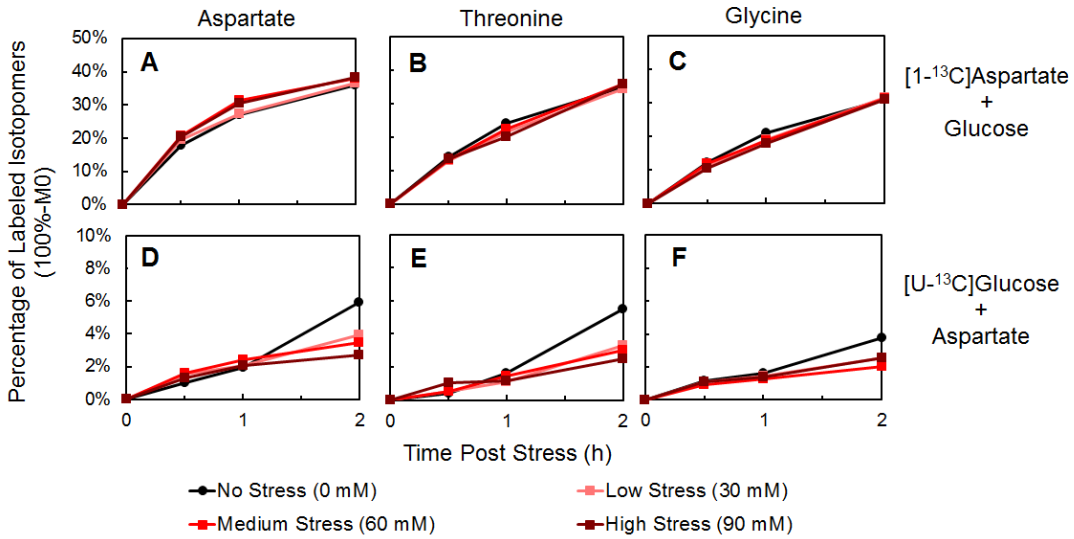

Figure 4.2: Short term effects of butanol stress on labeling of biomass amino acids related to a metabolic cycle in *C. acetobutylicum*. Time profiles of isotopic labeling are shown for (A) aspartate, (B) threonine, and (C) glycine in the two hours after introducing [1-^{13}C]aspartate, unlabeled glucose, and varying levels of butanol stress. Time profiles of isotopic labeling are also shown for (D) aspartate, (E) threonine, and (F) glycine in the two hours after introducing [U-^{13}C]glucose, unlabeled aspartate, and varying levels of butanol stress. Percentages of ^{13}C-labeled mass isotopomers (100%-M0) of intracellular metabolites were determined from the measured mass isotopomer distributions, after correction for natural isotope abundances.

The same ^{13}C labeling experiments were also performed for different levels of butyric acid stress (Figure 4.3 and Appendix B). Some dose dependence was observed in the ^{13}C labeling of amino acids of the stressed cultures. For example, as shown in Figure 4.3B and C, the level of ^{13}C enrichment in threonine and glycine resulting from [1-^{13}C]aspartate decreases with higher levels of butyric acid stress. The greatest difference in labeling, however, was observed when comparing the unstressed culture with the stressed cultures. In general, amino acids from the unstressed cultures displayed much faster labeling dynamics and greater ^{13}C enrichment than amino acids from the butyric acid-stressed cultures. This is apparent in amino acids derived from all parts of central carbon metabolism in both the [1-^{13}C]aspartate and [U-^{13}C]glucose experiments. A similar difference between the unstressed culture and stressed cultures was also observed in the CO_2 production rates (Figure 4.1B). Taken together, it is likely that the observed differences in ^{13}C labeling profiles between the unstressed and butyric acid-stressed cultures are due to a severe effect of butyric acid on cell growth, and not due to changes in relative flux distribution.

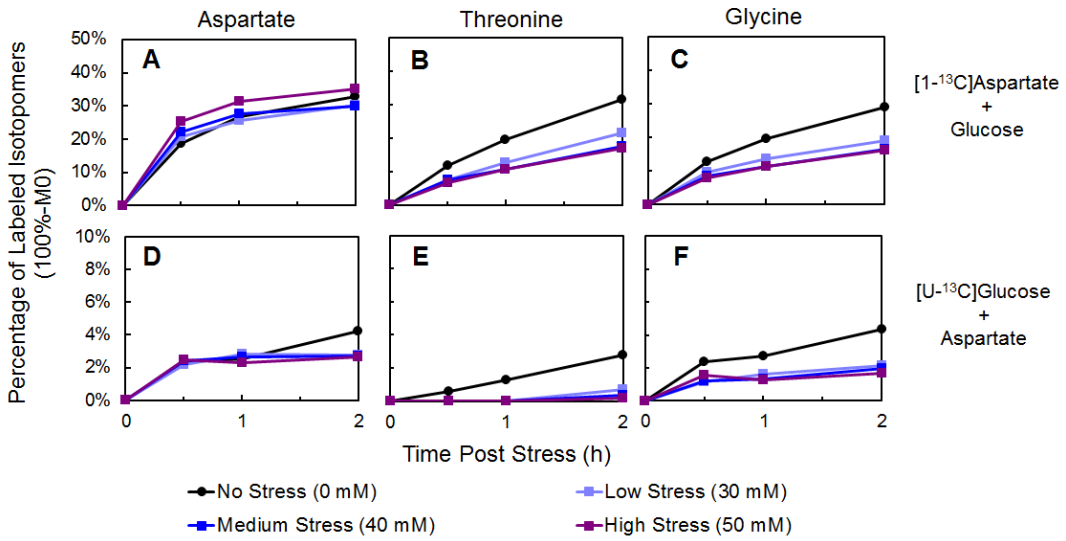

Figure 4.3: Short term effects of butyric acid stress on labeling of biomass amino acids related to a metabolic cycle in *C. acetobutylicum*. Time profiles of isotopic labeling are shown for (A) aspartate, (B) threonine, and (C) glycine in the two hours after introducing [1-^{13}C]aspartate, unlabeled glucose, and varying levels of butyric acid stress. Time profiles of isotopic labeling are also shown for (D) aspartate, (E) threonine, and (F) glycine in the two hours after introducing [U-^{13}C]glucose, unlabeled aspartate, and varying levels of butyric acid stress. Percentages of ^{13}C-labeled mass isotopomers (100%-M0) of intracellular metabolites were determined from the measured mass isotopomer distributions, after correction for natural isotope abundances.

4.3.3 Long Term Effects of Butanol and Butyric Acid Stress on Intracellular Fluxes

Although the ^{13}C labeling experiments suggested that butanol and butyric acid stress did not alter the flux distributions in central carbon metabolism at short time scales, we were curious if the effects of butanol and butyric acid stress would be manifested at longer time scales. Analysis of the proteomic response to both types of stress indicated the upregulation of proteins related to amino acid metabolism, and in

the case of butyric acid stress, the upregulation of proteins related to protein turnover (Venkataramanan et al., 2015). To determine if this proteomic response could be observed in metabolism, [U-^{13}C]glucose was introduced without stress or with high level of stress in cultures at OD_{600} = 1 (see Table 4.3), with 2 replicates for each tracer and stress combination (total of four cultures for each stressor). Cells were harvested at 2, 4, 6, and 8 hours following tracer and stress addition and used for ^{13}C analysis of biomass amino acids. OD_{600} values were taken at the same time points to track cell growth (see Appendix B). Medium samples were also collected to determine glucose labeling in each replicate.

To better compare ^{13}C labeling across cultures, the average carbon labeling (CL) was determined for each amino acid and the glucose in each replicate:

$$CL = \frac{\sum_{i=1}^{n} i(M+i)}{n} \tag{4.1}$$

Here, *n* is the number of carbon atoms in a given amino acid or glucose fragment, and M+*i* are the relative mass isotopomer abundances after correction for natural abundance of ^{13}C. Using the average carbon labeling of glucose and OD_{600} values at the time of tracer and stress addition, an expected labeling curve (assuming no change in fluxes) was determined for each replicate culture:

$$Expected\ labeling = CL_{Gluc}\ \frac{X - X_0}{X} \tag{4.2}$$

Here, X_0 is the OD_{600} of the culture at the time of tracer and stress addition, and X is the OD_{600} at the sampling point. This expected labeling curve projects

labeling of biomass by assuming that any new biomass formed after the tracer and stress addition is produced from the glucose in the medium. It can be reasoned that if the labeling profile of any amino acid differs from this curve, the metabolism of that amino acid has changed, whether due to protein turnover or increased or decreased flux through its biosynthetic pathway.

Figure 4.4 shows the expected labeling curves and labeling profiles for multiple amino acids for an unstressed culture and a culture stressed with a high level of butanol (one replicate each shown in Fig. 4.4). As expected, the labeling of amino acids from the unstressed culture (Figure 4.4A) tracked well with the expected labeling curve, indicating little or no change in amino acid metabolism or protein turnover in the 8 hours after [U-^{13}C]glucose was introduced. The labeling of amino acids from the stressed cultures (Figure 4.4B) also tracked well with the expected labeling curve (<5% difference in labeling between the curves), albeit less smoothly compared to the unstressed cultures. Similar trends were observed in the other replicates for each condition (see Appendix B). Based on these labeling data, we can conclude that the high level of butanol stress did not result in major, long term changes to amino acid metabolism.

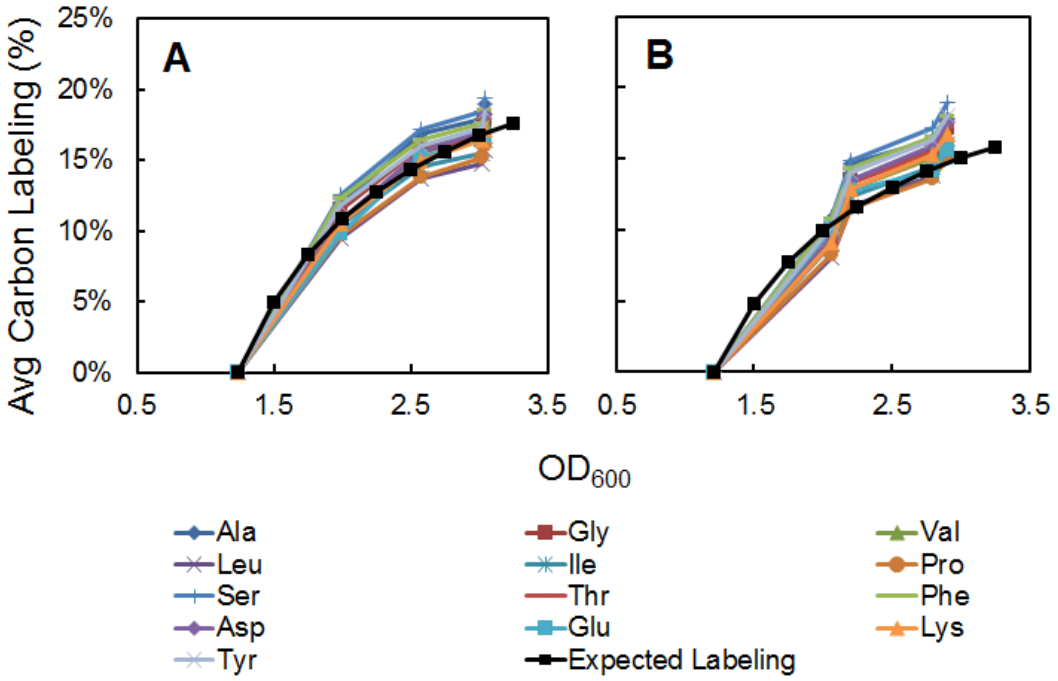

Figure 4.4: Long term effects of butanol stress on labeling of biomass amino acids. Average carbon labeling profiles of biomass amino acids from an (A) unstressed (0 mM butanol) culture and (B) high stress (90 mM butanol) culture. Labeling profiles are plotted against OD_{600} values measured in the eight hours after butanol and [U-^{13}C]glucose addition. Expected labeling curves in (A) and (B) were determined based on the measured percentage of [U-^{13}C]glucose in the medium of each culture.

The cultures stressed with a high level of butyric acid also exhibited similar trends in labeling (Figure 4.5B). Here, the severe impact on growth is quite apparent, with the unstressed culture reaching an OD_{600} of 3.30 and the stressed culture reaching an OD_{600} of 2.09 by 8 hours after butyric acid and [U-^{13}C]glucose were introduced. However, the labeling profiles of each amino acid in the stressed culture tracked well with the expected labeling curve. The replicate cultures for each level of butyric acid

stress (see Appendix B) also show similar trends in labeling, suggesting that in general, the high level of butyric acid stress did not result in major, long term changes to amino acid metabolism.

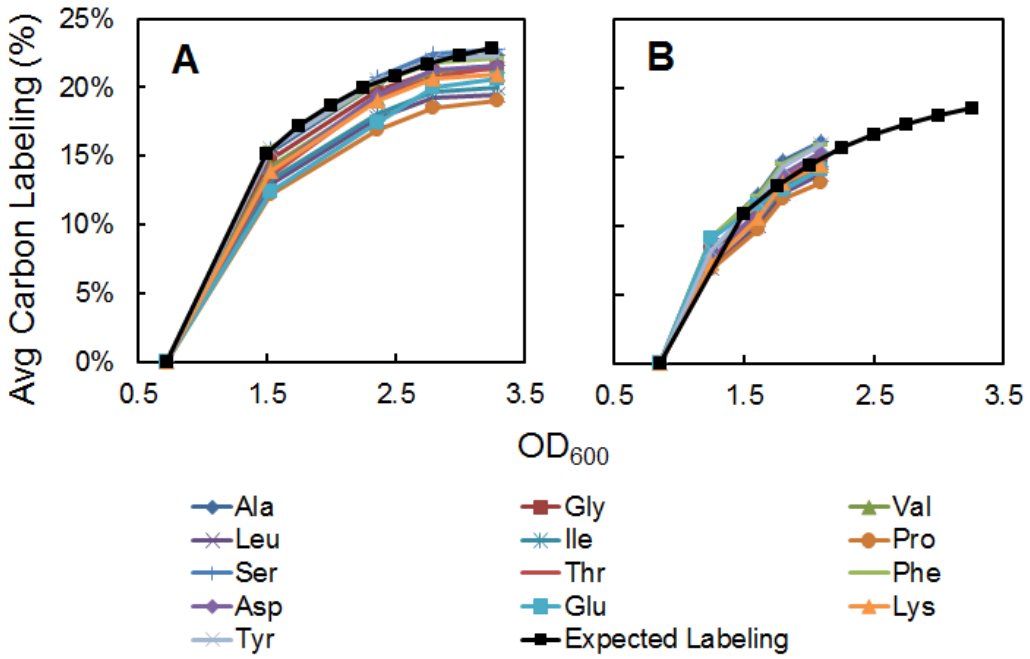

Figure 4.5: Long term effects of butyric acid stress on labeling of biomass amino acids. Average carbon labeling profiles of biomass amino acids from an (A) unstressed (0 mM butyric acid) culture and (B) high stress (50 mM butyric acid) culture. Labeling profiles are plotted against OD_{600} values measured in the eight hours after butyric acid and [U-^{13}C]glucose addition. Expected labeling curves in (A) and (B) were determined based on the measured percentage of [U-^{13}C]glucose in the medium of each culture.

4.3.4 Discussion

The inhibitory nature of butanol and butyric acid in *Clostridium* cultures is well-documented (Ezeji et al., 2010; Nicolaou et al., 2010). Butanol has a chaotropic effect on the cell membrane, which disrupts membrane stability by increasing its fluidity (Bowles and Ellefson, 1985). At high concentrations, this affects a number of cellular processes, such as nutrient transport, ATPase function, and glucose uptake, and disrupts the proton gradient and electrochemical potential across the cell membrane. In their undissociated forms, butyric acid and other carboxylic acids can freely cross the cell membrane, but are non-membrane permeable in their dissociated forms. This causes an accumulation of protons and anions that disrupts the proton gradient across the cell membrane and can damage ribosomal RNA, similarly to oxidative stress.

Given this, it was expected that butanol and butyric acid stress would affect cell growth. Indeed, off-gas analysis showed decreased growth upon stress introduction. Under butanol stress, we observed a temporary decrease in cell growth, with the cells recovering to their pre-stress CO_2 production rates within 2 hours of butanol addition. Under butyric acid stress, we observed a more severe impact on cell growth, with the culture stressed with a high level of butyric acid (50 mM) producing CO_2 at much lower rates compared to the unstressed culture. Interestingly, similarly stressed cultures grown in 4 L reactors, but utilizing pH control and the same clostridial growth medium, showed different effects on growth, i.e. a more severe impact on growth under butanol stress compared to butyric acid stress (Venkataramanan et al., 2015). In that study, cultures stressed with a high level of butanol essentially stopped growing, while the cultures stressed with a high level of butyric acid continued to grow, albeit at a lower rate. Since the stress response and

tolerance are also affected by process parameters (Nicolaou et al., 2010), these differences in the stress response can at least be partially attributed to differences between the 10 mL mini-bioreactors utilized in our work and the 4 L reactors.

Surprisingly, the growth defects observed under butanol and butyric acid stress did not translate to major rewiring of cellular metabolism. As demonstrated by the ^{13}C-labeling profiles of biomass amino acids within 2 hours of stress addition, butanol and butyric acid stress only produced minor differences in labeling (often <5% difference) between the unstressed cultures and stressed cultures, suggesting no significant change in relative fluxes in central carbon metabolism and amino acid metabolism. Within 8 hours of stress introduction, butanol and butyric acid did not produce any changes in the labeling of biomass amino acids beyond what was already expected based on cell growth, suggesting no changes in amino acid metabolism or protein turnover long after stress was introduced. This was the case despite the severe impact on growth observed in the culture stressed with a high amount of butyric acid. Overall, these data indicate that *C. acetobutylicum* metabolic pathways and fluxes are robust to butanol and butyric acid stress.

These findings were unexpected in the context of the transcriptomic and proteomic response to stress in *C. acetobutylicum*. Transcriptomic analysis of the butanol and butyric acid stress response has shown an upregulation of genes related to histidine and branched chain amino acid biosynthesis pathways, as well as differential expression of genes related to arginine and aromatic amino acid metabolism (Wang et al., 2013). Proteomic analysis also showed changes in the expression of proteins related to amino acid metabolism and protein turnover (Venkataramanan et al., 2015). Because the fluxome is believed to be the integrated output of the underlying cellular

processes described by other omics (Tang et al., 2009a), it is surprising that the relative flux distributions in central carbon and amino acid metabolism were similar in both unstressed and stressed cultures. One possible explanation is that the metabolite stress response observed in the transcriptome and proteome is necessary to maintain a constant flux distribution, and therefore maintain cell growth as close to optimal as possible.

Overall, the ^{13}C labeling data generated from this work paints a more complex picture of the stress response and would be best utilized when combined with other omics data. Recent integrative proteomic-transcriptomic analysis of the stress response showed poor correlation between the differentially expressed proteome and differentially expressed RNAseq transcriptome, suggesting significant post-translational regulation that would not be detected using a single omics analysis (Venkataramanan et al., 2015). This suggests that integration of omics data is critical for fully elucidating the stress response and connecting it to tolerance. Future approaches could involve mapping the ^{13}C labeling data to a recently published genome scale model for *C. acetobutylicum* that incorporates regulatory information on the stress response (Dash et al., 2014), providing a more systems level understanding of the stress response and the regulatory interactions between cellular processes.

4.3.5 Conclusion

This is the first study to directly measure the impact of butanol and butyric acid stress on the metabolism of *C. acetobutylicum.* Although off-gas analysis of the stressed cultures indicated significant to severe impairment of cell growth, ^{13}C labeling experiments demonstrated that central carbon metabolism and amino acid

metabolism was robust to both butanol and butyric acid stress, with the relative flux distributions remaining generally unchanged compared to unstressed cultures.

Chapter 5

REVERSE FLUX VIA ENZYME I OF *E. COLI* PHOSPHOTRANSFERASE SYSTEM (PTS) DURING BOTH GLUCONEOGENIC AND GLYCOLYTIC GROWTH

Adapted with permission from Long, C.P.*, Au, J.*, Sandoval, N.R., Gebreselassie, N.A., Antoniewicz, M.R., 2016. Enzyme I facilitates reverse flux from pyruvate to phosphoenolpyruvate in *E. coli*. Submitted. *Equal contribution

5.1 Introduction

The phosphoenolpyruvate-carbohydrate phosphotransferase system (PTS) is used by many bacteria and some archaea for the uptake and phosphorylation of sugar substrates (Deutscher et al., 2014). It is the main mechanism of glucose uptake and utilization in the model organism *Escherichia coli*, where it also has an important role in carbon catabolite repression and regulating central carbon metabolism (Deutscher et al., 2014, 2006; Escalante et al., 2012). The PTS consists of four proteins carrying out successive phosphotransferase reactions, coupling glucose transport and phosphorylation to the lower glycolytic reaction of phosphoenolpyruvate (PEP) to pyruvate. This allows for the coupled regulation of substrate uptake and glycolytic flux, as the PEP/Pyr ratio has been shown to act as part of a flux sensor (Kotte et al., 2010; Kremling et al., 2007) and controller of phosphofructokinase (encoded by *pfkA*) activity via allosteric inhibition by PEP (Fenton and Reinhart, 2009). Due to its central metabolic function and complex regulatory role, the PTS is a frequent target of metabolic engineering interventions (De Anda et al., 2006; Flores et al., 1996; Gosset, 2005; Meza et al., 2012).

Although individual steps of the PTS are known to be reversible (Deutscher et al., 2014, 2006; Postma et al., 1993), current understanding allows only for a net forward flux during the uptake of a PTS sugar (e.g. glucose). Indeed, the conversion from PEP to pyruvate, which is also facilitated by pyruvate kinases (encoded by *pykA* and *pykF* in *E. coli*), is often assumed to be a committed step in lower glycolysis. This assumption has practical implications, for example in the analysis of stable isotope labeling data through ^{13}C metabolic flux analysis and in flux balance analysis studies. The reverse reaction, pyruvate to PEP, is carried out by the gluconeogenic enzyme PEP synthetase (encoded by *ppsA* in *E. coli*). This enzyme is minimally expressed during growth on glycolytic substrates (Trauchessec et al., 2014), as significant activity would cause a wasteful futile cycle. However, *ppsA* is actively expressed under gluconeogenic conditions via transcriptional regulation by *Cra* (Ramseier, 1996).

Here, we show that Enzyme I, the terminal phosphotransferase in the PTS responsible for the conversion of PEP to pyruvate, is also responsible for a significant *in vivo* flux in the reverse direction (i.e. pyruvate to PEP) under both gluconeogenic and glycolytic growth. Knockout strains and ^{13}C alanine tracer experiments were used to directly quantify this reverse flux and determine gene-reaction relationships. We demonstrated that this flux is a major contributor to gluconeogenesis during growth on acetate, and that it is supported interchangeably by both PEP synthetase (*ppsA*) and Enzyme I (*ptsI*). Similar experiments under growth on glycolytic substrates, glucose and xylose, demonstrated that this reverse flux is mainly attributable to Enzyme I, indicating an unexpected role for this enzyme in the context of central carbon

metabolism. Furthermore, we show that this reverse flux is modulated by genetic perturbation of other PTS components.

5.2 Materials and Methods

5.2.1 Materials

Chemicals and minimal M9 medium were purchased from Sigma-Aldrich (St. Louis, MO). [1-^{13}C]Alanine (99 atom% ^{13}C) and [U-^{13}C]alanine (98+ atom% ^{13}C) were purchased from Cambridge Isotope Laboratories (Andover, MA). [1-^{13}C]Aspartate (99.0% ^{13}C), [4-^{13}C]aspartate (99.0% ^{13}C), and [1-^{13}C]serine (99.0% ^{13}C), were purchased from Isotec (St. Louis, MO). M9 minimal medium was used for all experiments. All solutions were sterilized by filtration.

5.2.2 Strains

For wild-type *E. coli* experiments, where cells were grown on acetate or glucose as the main carbon source and [1-^{13}C]aspartate, [4-^{13}C]aspartate, or [1-^{13}C]serine as the tracer, *E. coli* K-12 MG1655 (ATCC Cat. No. 700925, Manassas, VA) was used. For all other cultures, wild-type and single deletion *E. coli* strains were obtained from the Keio collection (GE Dharmacon), which had been generated by one-step inactivation of all non-essential genes in *E. coli* K-12 BW25113 (Δ(*araD*-*araB*)567, Δ*lacZ*4787::*rrnB*-3), lambda−, rph-1, Δ(*rhaD*−*rhaB*)568, *hsdR*514) (Baba et al., 2006). The strains used, with identifying information from the collection, are listed in Table 5.1. Double deletion strains were constructed following the method of Datsenko and Wanner on existing Keio collection strains (Baba et al., 2006; Datsenko and Wanner, 2000). Kanamycin resistance cassettes were cured by transformation of pCP20, which carries the FLP recombinase gene; the pCP20 plasmid was

subsequently cured by growth at 42°C overnight and confirmed via replica plating and PCR amplification. Kanamycin resistance cassettes for second-gene knockouts were amplified from Keio collection single deletion strains using the original Keio collection primers with homologous regions corresponding to the desired deletion. The purified amplicon was electroporated into the cured single deletion host *E. coli* strain expressing 1 mM arabinose-induced λ-Red recombinase genes from the pKD46 plasmid and grown on solid LB with kanamycin at 37°C Successful recombination was confirmed via PCR of both the mutated loci. The recombination plasmid pKD46 was subsequently cured by growth overnight at 42°C and confirmed via replica plating. All strains carrying pCP20 and pKD46 were grown at 30°C.

Table 5.1: *E. coli* strains from the Keio knockout collection used in this study

Knockout Gene	Plate-Row-Col ID	JW_id-Strain
WT / Parent Strain		
ppsA	3-A-3	JW1692-1
ptsG	55-G-3	JW1087-2
crr	57-H-8	JW2410-1
ptsH	57-F-8	JW2408-2
ptsI	57-G-8	JW2409-1

5.2.3 Culture Conditions

E. coli was cultured aerobically in M9 minimal medium at 37°C in mini-bioreactors with 10 mL working volume as described previously (Crown et al., 2015). All cultures were inoculated at OD_{600} of 0.01, and biomass concentration and growth

rates were determined by periodic measurements of OD_{600} using a spectrophotometer (Eppendorf BioPhotometer). Reported growth rates are maximum exponential growth rates.

The medium contained, for the respective experiments, 1.2 g/L acetate, 2 g/L glucose, or 4 g/L xylose. In the acetate experiments, a bolus of 1 mM [1-^{13}C]alanine was added when the cultures reached an OD_{600} of ~0.1, and the cells were harvested for analysis at an OD_{600} of 0.5. In the glucose and xylose experiments, a bolus of 10 mM [U-^{13}C]alanine, 6 mM [1-^{13}C]aspartate, 6 mM [4-^{13}C]aspartate, or 10 mM [1-^{13}C]serine was added when the culture reached an OD_{600} of 0.5, and cells were harvested at an OD_{600} of 1.5. In all experiments, the non-tracer substrate (i.e. acetate, glucose, or xylose) was in excess throughout, and exponential growth was maintained.

5.2.4 Gas Chromatography-Mass Spectrometry

GC-MS analysis was performed on an Agilent 7890B GC system equipped with a DB-5MS capillary column (30 m, 0.25 mm i.d., 0.25 μm-phase thickness; Agilent J&W Scientific), connected to an Agilent 5977A Mass Spectrometer operating under ionization by electron impact (EI) at 70 eV. Helium flow was maintained at 1 mL/min. The source temperature was maintained at 230°C, the MS quad temperature at 150°C, the interface temperature at 280°C, and the inlet temperature at 250 °C. GC-MS analysis of tert-butyldimethylsilyl (TBDMS) derivatized proteinogenic acids was performed as previously described (Leighty and Antoniewicz, 2013). Mass isotopomer distributions were obtained by integration (Antoniewicz et al., 2007a) and corrected for natural isotope abundances (Fernandez et al., 1996).

5.2.5 Calculations

For [1-^{13}C]alanine tracer experiments, the fraction of PEP derived from pyruvate was calculated as follows:

$$\%PEP\ from\ Pyr = \frac{PEP_{M1}}{Pyr_{M1}} = \frac{Phe302_{M1}}{Val288_{M1}} \tag{5.1}$$

For [U-^{13}C]alanine tracer experiments, the fraction of PEP derived from pyruvate was calculated as follows:

$$\%PEP\ from\ Pyr = \frac{PEP_{M3}}{Pyr_{M3}} = \frac{Phe302_{M2}/(1-Ala260_{M0})}{1-\sqrt{(Val260_{M0}-Ala260_{M0})/(1-Ala260_{M0})}} \tag{5.2}$$

Additional details regarding these calculations are provided in Appendix C.

5.3 Results

5.3.1 Enzyme I Supports a Significant Gluconeogenic Flux during Growth on Acetate

There are two possible gluconeogenic routes for acetate metabolism, shown in Figure 5.1A. Acetate enters central carbon metabolism as acetyl-CoA (AcCoA) and can either be metabolized to PEP via PEP carboxykinase (*pck*) (shown in green in Figure 5.1A) or via malic enzyme (*maeAB*) followed by conversion of pyruvate to PEP (shown in purple). This latter reaction is known to be carried out under gluconeogenic conditions by PEP synthetase (*ppsA)*.

To resolve the relative contribution of these two gluconeogenic routes, a novel tracer experiment using [1-^{13}C]alanine was developed (Figures 5.1 and 5.2). The tracer was added during growth on excess acetate (growth rates shown in Figure 5.1B).

Alanine equilibrates with intracellular pyruvate (Figure 5.2D), which results in a pyruvate pool (observed via valine labeling) that is mixed with unlabeled pyruvate (M0) produced from unlabeled sources in central carbon metabolism, and [1-^{13}C]pyruvate (M1) produced from the tracer (Figure 5.2A). As oxaloacetate (observed via aspartate) was almost entirely unlabeled (Figure 5.2B), the relative contribution of each route to PEP production (as measured by phenylalanine labeling, Figure 5.2C) is easily calculated.

In the wild-type, a significant amount (~60%) of PEP was generated from pyruvate (Figure 5.2E). In order to confirm that *ppsA* was responsible for this flux, the tracer experiment was repeated with a Δ*ppsA* knockout strain. Surprisingly, the contribution of pyruvate to PEP (~65%) was very similar to the wild-type. Following a database search for enzymes able to interconvert pyruvate and PEP (Kanehisa et al., 2016), we hypothesized that Enzyme I (encoded by the gene *ptsI*) may be involved. Enzyme I is known to react reversibly (Deutscher et al., 2014, 2006), but is not known to have a role in gluconeogenesis. In the knockout strain Δ*ptsI*, the contribution of pyruvate to PEP (~65%) was still similarly high to the wild-type and Δ*ppsA* strains. To determine if any other enzymes were involved with this flux, a double knockout, Δ*ppsA*Δ*ptsI*, was constructed and the tracer experiment was repeated. In this double knockout, PEP labeling was entirely eliminated, indicating that the flux from pyruvate to PEP was zero (Figure 5.2C, E). These results suggest that both *ppsA* and *ptsI* are able to interchangeably and exclusively support the large gluconeogenic flux from pyruvate to PEP observed in the wild-type during growth on acetate.

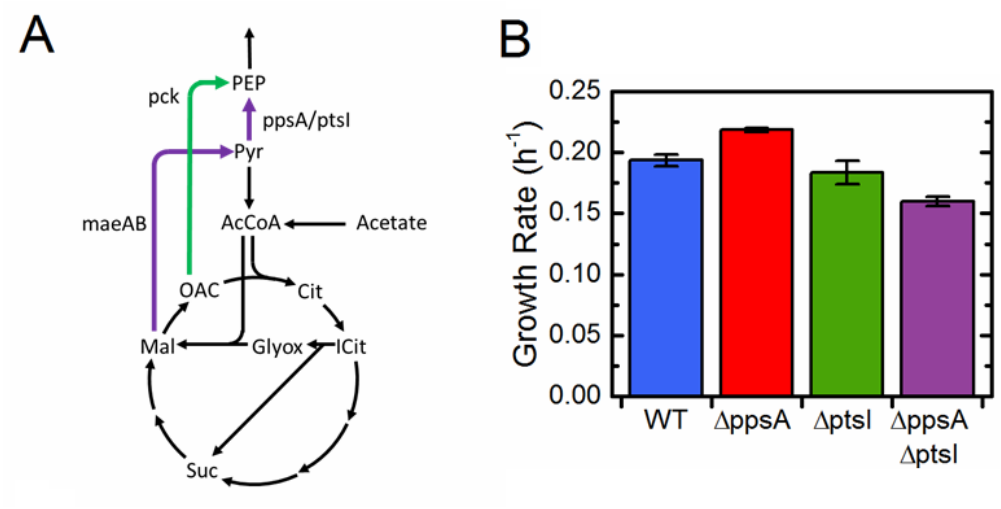

Figure 5.1: Quantification of alternative routes of PEP generation during growth on acetate. (A) Schematic showing two routes of PEP synthesis during growth on acetate. After malate is produced via the glyoxylate shunt, malic enzyme (*maeAB*) can convert malate to pyruvate, from which PEP can be formed by the activity of *ppsA* or *ptsI* (purple reaction). Alternatively, *pck* can convert oxaloacetate (OAC) to PEP directly (green reaction). The relative fluxes of these two routes can be resolved by a tracer experiment utilizing [1-^{13}C]alanine, which equilibrates with pyruvate. (B) Growth rates of four strains during growth on acetate, wild-type (WT) *E. coli*, Δ*ppsA*, Δ*ptsI*, and the double knockout Δ*pps*AΔ*ptsI*. Data presented in B are mean ± SEM of two biological replicates.

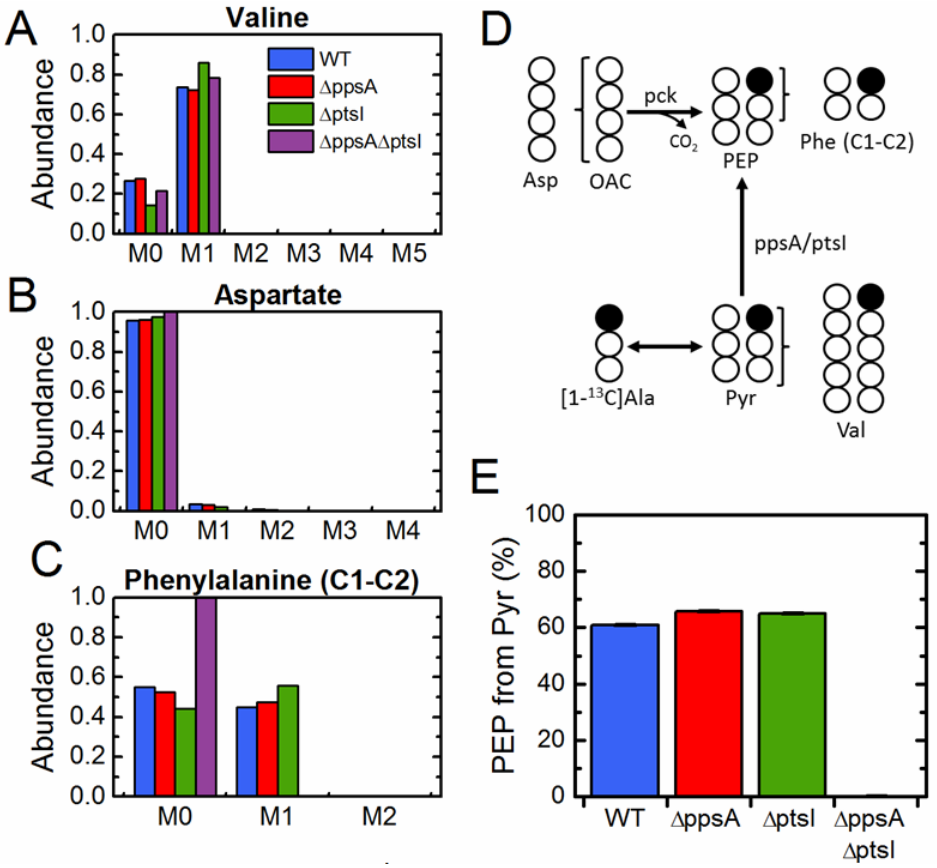

Figure 5.2: Quantification of alternative routes of PEP generation during growth on acetate. (A) Labeling of valine from [1-^{13}C]alanine, reflecting pyruvate labeling. Labeling is M1 (from tracer) and M0 (from unlabeled precursors in central carbon metabolism). (B) Labeling of aspartate from [1-^{13}C]alanine, reflecting oxaloacetate labeling. Aspartate is almost entirely unlabeled (M0). (C) Labeling of the first two (C1-C2) carbons of phenylalanine, reflecting the labeling of the first two carbons in PEP. (D) Schematic depicting the conversion of [1-^{13}C]alanine to PEP and the measured amino acids. Opened and filled circles represent unlabeled (^{12}C) and labeled (^{13}C) carbons, respectively. (E) Percentage of PEP generated from pyruvate. Approximately 60% of PEP is generated from pyruvate in the WT and each single knockout strain; however the flux is completely eliminated in the double knockout, indicating dual responsibility of *ppsA* and *ptsI* for the conversion of pyruvate to PEP. Labeling data presented in A, B, and C have been corrected for unlabeled biomass present prior to tracer introduction. Errors in E were calculated via propagation of measurement error.

5.3.2 A Significant Back-Flux is Measured during Growth on Glucose

Given the surprising activity of Enzyme I under gluconeogenic growth conditions, we next sought to determine whether there was any measureable flux from pyruvate to PEP during growth on glucose. This flux was expected to be minimal or nonexistent, as this would create a futile cycle during glycolytic growth. Glucose is a PTS sugar, meaning that Enzyme I actively participates in the conversion of PEP to pyruvate.

As a preliminary experiment, wild-type *E. coli* was grown on glucose and [1-^{13}C]serine was introduced midway through the culture. [1-^{13}C]Serine can be converted to [1-^{13}C]pyruvate, which can then be converted to [1-^{13}C]PEP (Figure 5.3A). Indeed, as shown in Figure 5.3C, growth under glucose and [1-^{13}C]serine produced labeled phenylalanine (2% M1). Since [1-^{13}C]serine also produced labeled aspartate (6% M1), it was possible that PEP was labeled through the combined activities of pyruvate dehydrogenase, TCA cycle, and PEP carboxykinase (PCK) (Figure 5.3B). To eliminate this possibility, *E. coli* was grown on glucose and with either [1-^{13}C]aspartate or [4-^{13}C]aspartate introduced midway through the cultures. As shown in Figure 5.3C, no phenylalanine labeling was observed with either aspartate tracer, indicating that phenylalanine labeling was the due to PEP generation from pyruvate, and not from oxaloacetate.

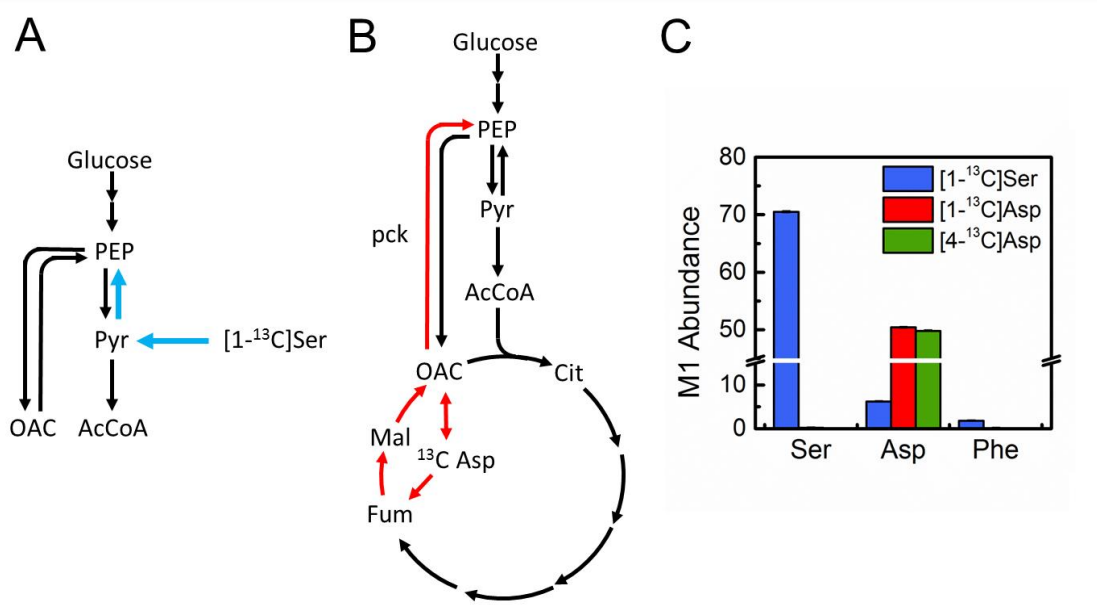

Figure 5.3: PEP to pyruvate flux is observed during glycolytic growth. (A) Schematic showing [1-^{13}C]serine conversion to pyruvate and subsequently to PEP under growth on glucose. (B) Schematic showing potential routes of PEP generation from ^{13}C aspartate under growth on glucose. (C) M1 labeling of serine, aspartate, and phenylalanine in [1-^{13}C]serine, [1-^{13}C]aspartate, and [4-^{13}C]aspartate labeling experiments. Labeling was observed in both aspartate and phenylalanine under growth on [1-^{13}C]serine. No labeling was observed in phenylalanine under growth on [1-^{13}C]aspartate or [4-^{13}C]aspartate, indicating PEP generation from pyruvate, not oxaloacetate. Errors presented in C are from assumed GC/MS errors of 0.2 mol%.

To directly quantify the contribution of PEP from pyruvate, the experimental approach was modified slightly from the acetate case by using [U-^{13}C]alanine instead of [1-^{13}C]alanine (Figure 5.4 and 5.5). Again, pyruvate labeling was observed via valine labeling, and PEP labeling via phenylalanine labeling. As was observed in wild-type *E. coli*, it was assumed that PEP generation from oxaloacetate via the PCK reaction was negligible in the knockout strains. During growth on glucose, the wild-

type was determined to have a statistically significant back-flux through which 10% of PEP was generated from pyruvate. When Δ*ppsA* strain was analyzed, it was found to have the same back-flux as the wild-type (Figure 5.5D). Given the dual contribution of *ppsA* and *ptsI* to gluconeogenic flux under growth on acetate, it was suspected that Enzyme I may also be responsible for this back-flux on glucose. Unfortunately, testing this hypothesis directly was not possible given that *ptsI* was found to be essential for growth on glucose (Figure 5.4B), and therefore the Δ*ptsI* and Δ*ppsA*Δ*ptsI* strains could not be studied under these conditions.

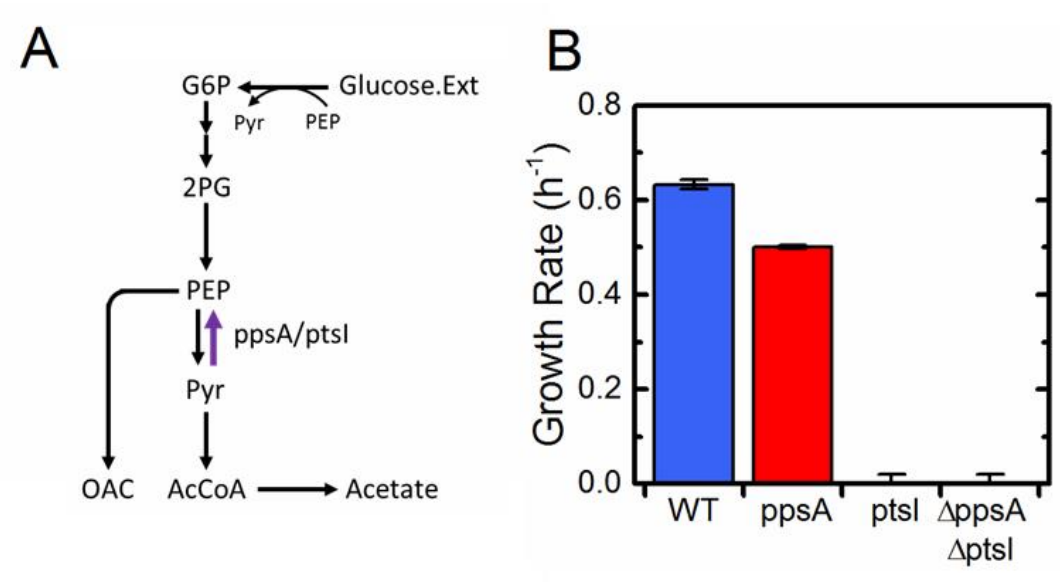

Figure 5.4: During growth on glucose, there is a significant back-flux from pyruvate to PEP not carried out by PEP synthetase (*ppsA*). (A) Schematic of glucose consumption and metabolism related to PEP and pyruvate interconversion. Glucose is transported and phosphorylated by the PTS, simultaneously converting PEP to pyruvate via Enzyme I (*ptsI*). [U-^{13}C]alanine experiments were used to quantify the back-flux from pyruvate to PEP. (B) Growth rates of four strains during growth on glucose; *ptsI* was found to be essential for growth on glucose, precluding direct assessment of its role in the back-flux. Data presented in B are mean ± SEM of two biological replicates.

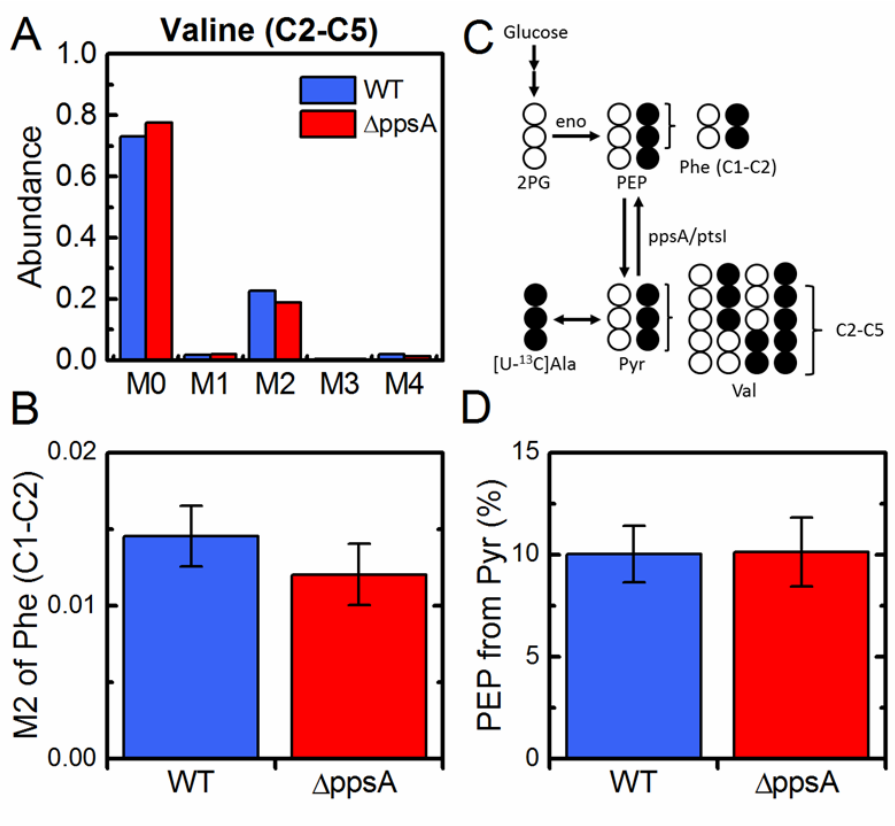

Figure 5.5: During growth on glucose, there is a significant back-flux from pyruvate to PEP not carried out by PEP synthetase (*ppsA*). (A) Labeling of last four carbons (C2-C5) of valine, representing the condensation of the last two carbons (C2-C3) of two pyruvate molecules. Labeling is mainly M2 (i.e. condensation of one fully labeled pyruvate from the tracer and one unlabeled pyruvate from glycolysis) and M0 (condensation of two unlabeled pyruvates). The small amount of M4 reflects condensation of two fully labeled pyruvate molecules. The fractional labeling is consistent with a mixed population of fully labeled and unlabeled pyruvate. (B) M2 labeling of the first two (C1-C2) carbons of phenylalanine, reflecting fully labeled PEP. (C) Schematic depicting the conversion of [U-^{13}C]alanine to PEP and the measured amino acids. Opened and filled circles represent unlabeled (^{12}C) and labeled (^{13}C) carbons, respectively. (D) Percentage of PEP generated from pyruvate. Approximately 10% is generated from pyruvate in both the WT and Δ*ppsA* strains, representing a significant back-flux. Labeling data presented in A have been corrected for unlabeled biomass present prior to tracer introduction. Errors in D were calculated via propagation of measurement error.

5.3.3 Enzyme I is Responsible for a Significant Back-Flux during Growth on Xylose

To assign responsibility for the back-flux of pyruvate to PEP under glycolytic conditions, the [U-^{13}C]alanine tracer experiments were repeated using the non-PTS sugar xylose as substrate (Figure 5.6 and 5.7). Xylose is transported into the cell via an ABC transporter (Linton and Higgins, 1998) (Figure 5.6A), which renders Enzyme I non-essential for growth (Figure 5.6B). During growth on xylose, the back-flux observed in the wild-type was similar to that observed during growth on glucose, with 11% of PEP formed from pyruvate. Once again, this flux was not significantly reduced in the Δ*ppsA* strain. However, this flux was almost completely eliminated in the Δ*ptsI* and Δ*ppsA*Δ*ptsI* strains, directly implicating Enzyme I in the conversion of pyruvate to PEP. Thus, in contrast to the acetate growth condition, *ppsA* and *ptsI* were not interchangeably able to support the back-flux observed in the wild-type, but instead Enzyme I dominated. This is consistent with the known low expression of *ppsA* under glycolytic conditions (Trauchessec et al., 2014).

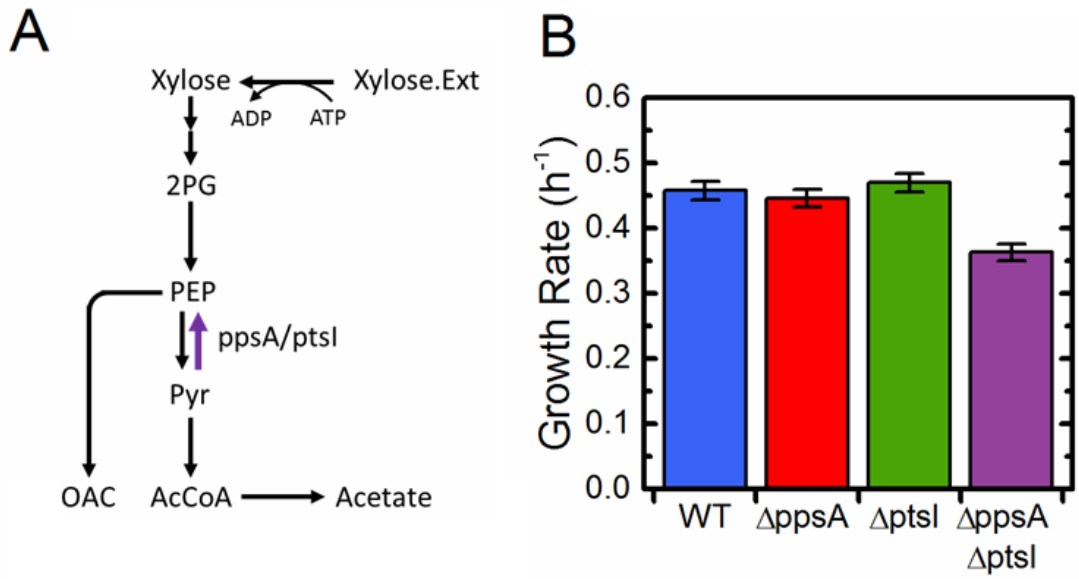

Figure 5.6: Enzyme I (*ptsI*) is responsible for a significant back-flux from pyruvate to PEP during growth on xylose. (A) Schematic of xylose consumption and metabolism related to PEP and pyruvate interconversion. Xylose is transported via an ABC transporter (non-PTS). [U-^{13}C]alanine experiments were used to quantify the back-flux from pyruvate to PEP. (B) Growth rates of four strains during growth on xylose, wild-type (WT) *E. coli*, Δ*ppsA*, Δ*ptsI*, and the double knockout Δ*ppsA*Δ*ptsI*. Data presented in B are mean ± SEM of two biological replicates.

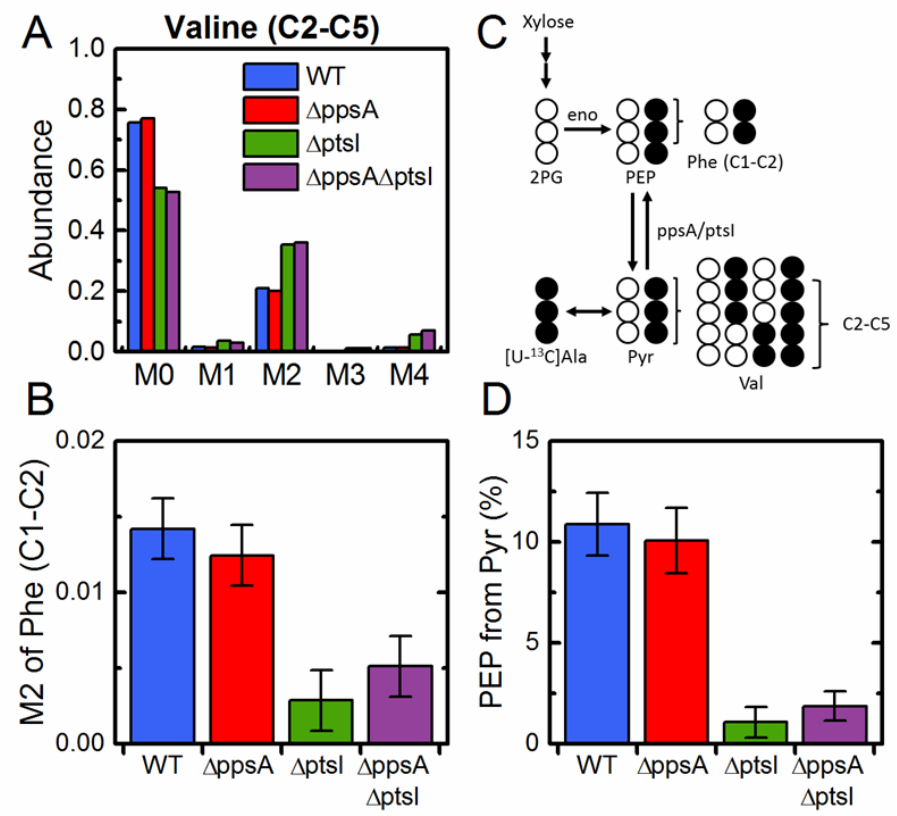

Figure 5.7: Enzyme I (*ptsI*) is responsible for a significant back-flux from pyruvate to PEP during growth on xylose. (A) Labeling of last four carbons (C2-C5) of valine, representing the condensation of the last two carbons (C2-C3) of two pyruvate molecules. Labeling is mainly M2 (i.e. condensation of one fully labeled pyruvate from the tracer and one unlabeled pyruvate from glycolysis) and M0 (condensation of two unlabeled pyruvates). The M4 labeling reflects condensation of two fully labeled pyruvate molecules. The fractional labeling is consistent with a mixed population of fully labeled and unlabeled pyruvate. (B) M2 labeling of the first two (C1-C2) carbons of phenylalanine, reflecting fully labeled PEP. (C) Schematic depicting the conversion of [U-^{13}C]alanine to PEP and the measured amino acids. Opened and filled circles represent unlabeled (^{12}C) and labeled (^{13}C) carbons, respectively. (D) Percentage of PEP generated from pyruvate. Approximately 10% is generated from pyruvate in both the WT and ΔppsA strains, representing a significant back-flux. This flux is nearly completely eliminated in the Δ*ptsI* and Δ*ppsA*Δ*ptsI* strains, indicating a major role for Enzyme I (*ptsI*) in facilitating the back-flux. Labeling data presented in A have been corrected for unlabeled biomass present prior to tracer introduction. Errors in D were calculated via propagation of measurement error.

5.3.4 The Back-Flux is Affected by Genetic Knockouts of PTS Components

Given the strong evidence for Enzyme I involvement in the back-flux from pyruvate to PEP under glycolytic conditions, it was further hypothesized that this activity would be perturbed in knockout mutants of other PTS components. The PTS and its components are shown in Figure 5.8A. The phosphotransferase partner of Enzyme I is HPr (encoded by the gene *ptsH*), which then interacts with the soluble (*crr*) and membrane-bound (*ptsG*) components of the glucose-specific Enzyme II complex ($EIIABC^{Glc}$). The growth rates on glucose and xylose for the mutant strains Δ*ptsG*, Δ*crr*, Δ*ptsH*, and Δ*ptsI* are shown in Figure 5.8B. The only non-growth phenotype observed was for Δ*ptsI* on glucose, as previously discussed. The mannose Enzyme II complex (EII^{Man}) is also able to efficiently transport glucose (Curtis and Epstein, 1975), allowing for the growth of Δ*ptsG* and Δ*crr* strains on glucose. The explanation for the growth of Δ*ptsH* on glucose is less clear, but it has been proposed that the HPr-like protein FPr from the fructose PTS may be able to substitute its activity for HPr (Bettenbrock et al., 2007).

The [U-^{13}C]alanine tracer experiments described above for glucose and xylose were performed for all knockouts of PTS components. There was a striking increase in the back-flux for several knockout strains, as shown in Figure 5.9. For example, in the Δ*ptsG* strain grown on glucose, almost 30% of the PEP was formed from pyruvate. Similarly high back-fluxes were also observed for Δ*crr* on both glucose and xylose. In both cases, the increase during growth on glucose could be a result of disturbed equilibria in the PTS chain, particularly as EII^{Man} replaced EII^{Glc}. The increase during growth on xylose, however, was unexpected and may point to significant phosphotransferase exchange even when the PTS is not used for sugar transport. This could indicate that additional phosphotransferase partners are involved.

To assign responsibility for the increased back-flux in these strains, double knockouts of Δ*ptsG*, Δ*crr*, *ppsA*, and *ptsI* were constructed. The strain Δ*ptsG*Δ*ppsA* had only a modest reduction in the back-flux during growth on glucose relative to the single knockout Δ*ptsG*. The same was true for Δ*crr*Δ*ppsA* on glucose, and there was no decrease compared to Δ*crr* on xylose (Figure 5.9), indicating that ppsA was not facilitating the back-flux. However, the flux was almost entirely eliminated in all ptsI knockout strains including the Δ*crr*Δ*ptsI* strain grown on xylose, thus providing additional support for the hypothesis that Enzyme I (*ptsI*) is mainly responsible for the back-flux (Figure 5.9).

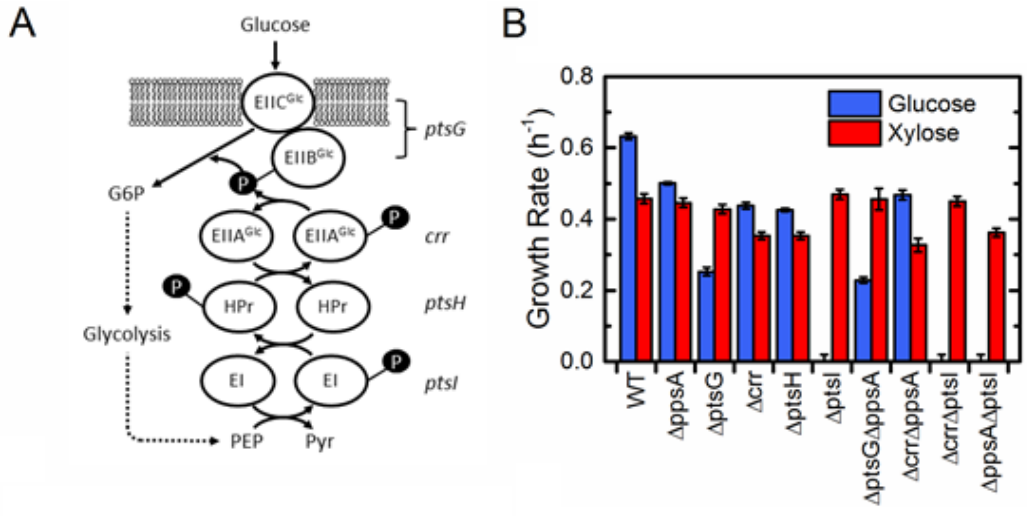

Figure 5.8: Genetic perturbations of PTS components significantly impact the back-flux from pyruvate to PEP. (A) Schematic of the PTS sugar transport system, which couples the transport and phosphorylation of glucose at $EIIBC^{Glc}$ (*ptsG*) to conversion of PEP to pyruvate (*ptsI*), via the phosphotransferases ptsH (*ptsH*) and $EIIA^{Glc}$ (*crr*). (B) Growth rates of wild-type (WT) *E.coli* and 9 knockout strains, including all single knockouts of PTS components and selected double knockouts, grown on glucose and xylose; all *ptsI* knockout strains grew on xylose, but not glucose. Data presented in B are mean ± SEM of two biological replicates.

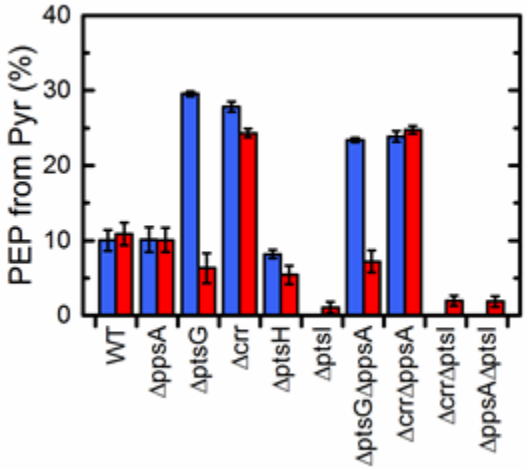

Figure 5.9: Genetic perturbations of PTS components significantly impact the back-flux from pyruvate to PEP. [U-^{13}C]alanine experiments were performed for all strains, and the percentage of PEP derived from pyruvate was determined. Several strains had significantly higher percentages of PEP derived from pyruvate, particularly Δ*ptsG* on glucose and Δ*crr* on glucose and xylose, indicating that PTS component perturbation impacts back-flux. Double knockouts of PTS components and Δ*ppsA* did not significantly reduce the back-flux. In contrast, back-flux was nearly completely eliminated in all ptsI knockout strains, including Δ*crr*Δ*ptsI* grown on xylose, indicating a major role for Enzyme I (*ptsI*) in facilitating the back-flux. Errors were calculated via propagation of measurement error.

5.4 Discussion

The results presented here show a novel and metabolically significant role for Enzyme I in *E. coli* metabolism. This function, the conversion of pyruvate to PEP, is active both under conditions in which the PTS is the primary means of transporting substrate (growth on glucose) and is not (growth on acetate or xylose). Knowledge of

this gene-reaction relationship will improve our understanding and annotation of *E. coli* central carbon metabolism, which is of central importance in metabolic modeling and engineering efforts such as ^{13}C metabolic flux analysis (Long and Antoniewicz, 2014a) and the development of production strains (De Anda et al., 2006; Flores et al., 1996; Gosset, 2005; Meza et al., 2012).

This metabolic activity also raises new biological questions about the PTS, its regulation, and whether there are additional unannotated connectivities in the network. For example, are there other kinases that interact with Enzyme I to provide the phosphoryl groups needed to sustain this large flux from pyruvate to PEP? That this flux is maintained in the knockout mutants of partner PTS components indicates that this must be the case. The large increases in the back-flux for Δ*crr* and Δ*ptsG* are also intriguing, pointing to connected equilibria between Enzyme I and both the PTS and the other kinases. Interestingly, Enzyme I has previously been shown to be able to exchange phosphoryl groups with other kinases such as acetate kinase (*ackA*) (Fox et al., 1986).

Additionally, in Δ*crr* and Δ*ptsG*, the observed back-flux requires the transfer of phosphoryl groups from Enzyme I to pyruvate, which likely affects the phosphorylation state of remaining PTS components or potentially other kinases interacting with the PTS. Regulatory functions spanning from carbon and nitrogen metabolism to chemotaxis are directly influenced by the phosphorylation state of PTS components (Deutscher et al., 2014). Thus, the high back-flux in Δ*crr* and Δ*ptsG* may be a consequence of some factor modulating the phosphorylation state of remaining PTS components, further impacting cellular processes regulated by the PTS. Taken together, the results presented here contribute significantly to our understanding of the

PTS, although further work is needed to more fully elucidate the complex regulatory network governed by the phosphorylation state of its components.

5.5 Author Contributions

NAG performed the experiments and data analysis for growth on acetate and [1-^{13}C]alanine. JA performed the experiments and data analysis for growth on glucose and [1-^{13}C]aspartate, [4-^{13}C]aspartate, or [1-^{13}C]serine. JA and CPL performed the experiments and data analysis for growth on glucose or xylose and [U-^{13}C]alanine. NRS constructed the double knockout strains. CPL, JA, NRS, and MRA wrote the paper.

Chapter 6

^{13}C METABOLIC FLUX ANALYSIS OF MICROBIAL AND MAMMALIAN SYSTEMS IS ENHANCED WITH GC-MS MEASUREMENTS OF GLYCOGEN AND RNA LABELING

Reproduced with permission from Long, C.P.*, Au, J.*, Gonzalez, J.E., Antoniewicz, M.R., 2016. ^{13}C metabolic flux analysis of microbial and mammalian systems is enhanced with GC-MS measurements of glycogen and RNA labeling. Submitted.
*Equal contribution

6.1 Introduction

^{13}C metabolic flux analysis (^{13}C-MFA) is a powerful tool for quantifying cellular metabolism in a wide range of metabolic engineering and biomedical applications (Antoniewicz, 2015b; Young, 2014). A major factor governing the accuracy and precision of flux estimates from ^{13}C-MFA is the selection of informative isotopic labeling measurements. In most ^{13}C-MFA studies to date, flux analysis has been conducted using measurements of isotopic labeling of proteinogenic amino acids and/or isotopic labeling of extracted intracellular metabolites measured with techniques such as mass spectrometry (MS), tandem mass spectrometry (MS/MS), and nuclear magnetic resonance (NMR) (Antoniewicz, 2013c; Antoniewicz et al., 2007a; Masakapalli et al., 2014a; Truong et al., 2014). Recently, improvements in flux precision were also achieved by simultaneously fitting multiple sets of labeling measurements from parallel tracer experiments (Crown et al., 2015).

In these data sets, however, metabolites derived from the upper half of central carbon metabolism (consisting of the upper portion of the glycolysis (EMP) pathway, pentose phosphate pathway (PPP), and Entner-Doudoroff (ED) pathway) are greatly

underrepresented. For example, observability of PPP fluxes in *E. coli* largely depends on accurate measurements of phenylalanine labeling, which is synthesized from erythrose 4-phosphate (E4P) and phosphoenolpyruvate (PEP). Although there are other metabolites derived from upper metabolism, e.g. histidine and serine, these measurements are less informative. In our experience, histidine is typically difficult to reliably detect due to low abundance (Antoniewicz et al., 2007a), and both amino acids are related to one-carbon metabolism for which information may be incomplete. This leaves phenylalanine as the only relevant metabolite for flux analyses of PPP. In mammalian systems, flux analysis is even more challenging given that histidine and phenylalanine are not synthesized by mammalian cells, i.e. these are essential amino acids. Thus, ^{13}C-MFA depends on more distant labeling measurements, for example, of intermediates in the lower glycolytic pathway such as 3PG and PEP (Ahn and Antoniewicz, 2013). LC-MS and LC-MS/MS based approaches have provided direct labeling information on pentose phosphate pathway intermediates and fragments (Hanke et al., 2013; Rühl et al., 2012); however, these methods are often costly and laborious, as analysis of these intracellular metabolites requires rapid quenching and efficient extraction techniques, and in many cases large sample sizes due to low concentrations of these metabolites inside cells.

A recent effort to provide additional labeling data that is more directly related to upper metabolism was focused on fragments of nucleosides derived from DNA and RNA (Miranda-Santos et al., 2015). Specifically, 31 nucleoside fragments were identified and the applicability of these fragments was illustrated in yeast cultures. While this method employed GC-MS instead of LC-MS, the presented protocols required large sample sizes (1.5 to 100 mL of biomass at OD=3.5) and the labeling

data was not solely related to metabolism of PPP, but included other parts of metabolism, e.g. TCA cycle and one-carbon metabolism, which further complicated data analysis. Other research groups have measured ^{13}C-labeling of RNA, glycogen, and glycans, and demonstrated the value of these measurements for flux analysis (Badur et al., 2015; Guzmán et al., 2014; Murphy et al., 2013).

Our work builds on these previous studies. Specifically, we present here a more convenient GC-MS based method for measuring isotopic labeling of multiple fragments of glucose and ribose derived from glycogen and RNA, respectively, for ^{13}C-MFA studies. Our approach is less sample-intensive as well as more informative. We demonstrate the reliability of our approach in two biological systems: *E. coli* as a model microbial system and CHO cells as a model mammalian system. Specifically, we illustrate that isotopic labeling of glucose moiety from glycogen and ribose moiety from RNA permit precise quantification of net and exchange fluxes in PPP. We also use this approach to determine PPP fluxes during co-utilization of glucose and xylose. Overall, we demonstrate that incorporating labeling measurements of glycogen and RNA, which are stable and abundant in microbial and mammalian cells, greatly improves flux observability, thus paving the way for future applications of this approach in metabolic engineering and biomedical research.

6.2 Materials and Methods

6.2.1 Materials

Chemicals and M9 minimal medium were purchased from Sigma-Aldrich (St. Louis, MO). Isotopic tracers were purchased from Cambridge Isotope Laboratories (Tewksbury, MA): [1,6-^{13}C]glucose (99.2 % ^{13}C), [1,2-^{13}C]glucose (99.7 %), [1-

^{13}C]glucose (99.5 %), [2-^{13}C]glucose (99.5 %), [3-^{13}C]glucose (99.5 %), [4,5,6-^{13}C]glucose (99.5 %), and [1,2-^{13}C]xylose (99.2 %). The isotopic enrichment of the purchased tracers and the composition of tracer mixtures used for parallel labeling experiments were validated by GC-MS analysis as described in (Sandberg et al., 2016) and (Cordova and Antoniewicz, 2016). SFM4CHO medium (GE Healthcare Life Sciences SH3054901) and DMEM medium (Corning 17-207-CV, without glucose, glutamine, and sodium pyruvate) were purchased from Fisher Scientific (Pittsburgh, PA).

6.2.2 Strains and Culture Conditions

For *E. coli* tracer experiments, wild-type *E. coli* BW21135 and a *ΔptsG* (Keio collection) strain were used. All *E. coli* strains were purchased from GE Healthcare Dharmacon. *E. coli* was cultured aerobically in M9 minimal medium at 37°C in mini-bioreactors with 10 mL working volume as described previously (Crown et al., 2015). For the wildtype experiments, *E. coli* cultures were inoculated at OD_{600} of 0.01. Tracers were added at the beginning of the culture. Cells were harvested (1 mL samples) for GC-MS analysis at mid-exponential growth when OD_{600} was about 0.6. For the *E. coli* Δ*ptsG* tracer experiment, M9 medium was supplemented with 50 ug/mL of kanamycin (selection marker for the knockout). Cultures were inoculated at OD_{600} of 0.01, and [1,2-^{13}C]glucose and [1,2-^{13}C]xylose were added at the beginning of the culture, each at a concentration of 10 mM. Cells were harvested (1 mL samples) for GC-MS analysis at mid-exponential growth when OD_{600} was about 0.6. For CHO cell tracer experiments, CHO-K1 cells previously adapted to serum-free suspension culture were used (Valente et al., 2015). CHO cells were cultured in 15 mL of SFM4CHO/DMEM (1:1, v/v) medium supplemented with 4 mM glutamine and 1 mM

sodium pyruvate, in vented 125-mL flasks (Corning 431143) in a humidified 5% CO_2 incubator at 37°C with slow shaking (~100 rpm). CHO cell cultures were inoculated at approximately 1.0×10^5 cells/mL. Tracers were added as a bolus when cell density reached 5.0×10^5 cells/mL. Cells were harvested (4 mL sample for hydrolysis of glycogen and RNA, and 6 mL sample for intracellular metabolite extraction) for GC-MS analysis after 23.25 h, when cell density was approximately 1.0×10^6 cells/mL.

6.2.3 Analytical Methods

Cell growth of E. coli cultures was monitored by measuring the optical density at 600nm (OD600) using a spectrophotometer (Eppendorf BioPhotometer). The OD600 values were converted to cell dry weight concentrations using a previously determined OD600-dry cell weight relationship for E. coli (1.0 OD600 = 0.31 gDW/L) (Long et al., 2016). After centrifugation (5 min at 14,000 rpm), the supernatant was separated from the cell pellet, and the cell pellets were washed twice with glucose-free M9 medium. Acetate and xylose concentrations were determined using an Agilent 1200 Series HPLC (Au et al., 2014).

Cell growth of CHO cell cultures was monitored by measuring the cell concentration and cell viability using a Moxi Z Cell Counter and Moxi Z Cassettes Type S (ORFLO Technologies, Ketchum, ID). After centrifugation (2 min at 1,000 rpm), the supernatant was separated from the cell pellet, and the cell pellets were washed twice with D-PBS (Mediatech, Inc., Manassas, VA). For intracellular metabolite extraction of CHO cells, the methanol/chloroform/water extraction method described in (Ahn and Antoniewicz, 2013) was followed. Glucose and lactate concentrations were determined using YSI 2700 biochemistry analyzer (YSI, Yellow Springs, OH).

6.2.4 Hydrolysis of Glycogen and RNA

For hydrolysis of glycogen and RNA, the following two-step hydrochloric acid hydrolysis procedure was used. First, 50 µL of 6N HCl was added to dry cell pellets and the samples were incubated for 30 min at 30 °C. Next, 250 µL of water was added (thus diluting the acid to 1 N) and samples were incubated for 60 min at 110 °C. The samples were then cooled to room temperature, neutralized with 50 µL of 5 N NaOH, and dried under air flow at 65°C. The development of this method was recently described (McConnell and Antoniewicz, 2016).

6.2.5 Derivatization of Glucose and Ribose

Glucose and ribose released from hydrolysis of biomass (i.e. from glycogen and RNA, respectively) were derivatized using the aldonitrile propionate derivatization method described in (Antoniewicz et al., 2011). Briefly, 50 µL of 2 wt% hydroxylamine hydrochloride in pyridine was added to dried samples, which were then incubated for 60 min at 90°C. Next, 100 µL of propionic anhydride was added followed by incubation at 60°C for 30 min. The samples were then immediately transferred to injection vials for GC-MS analysis.

6.2.6 Gas Chromatography-Mass Spectrometry

GC-MS analysis was performed on an Agilent 7890B GC system equipped with a DB-5MS capillary column (30 m, 0.25 mm i.d., 0.25 µm-phase thickness; Agilent J&W Scientific), connected to an Agilent 5977A Mass Spectrometer operating under ionization by electron impact (EI) at 70 eV. Helium flow was maintained at 1 mL/min. The source temperature was maintained at 230°C, the MS quad temperature at 150°C, the interface temperature at 280°C, and the inlet temperature at 250°C. GC-MS analysis of *tert*-butyldimethylsilyl (TBDMS) derivatized proteinogenic amino

acids was performed as described in (Leighty and Antoniewicz, 2013). GC-MS analysis of TBDMS derivatized intracellular metabolites was performed as described in (Ahn and Antoniewicz, 2011). For GC-MS analysis of glucose and ribose, 1 μL of a derivatized sample was injected at 1:2 or 1:10 split ratio. The column was started at 80°C and held for 2 min, increased to 280°C at 10°C/min, and held for 12 min. The *m/z* 173 and *m/z* 370 fragments of the glucose derivative (containing the last two and first five C-atoms of glucose, respectively (Antoniewicz et al., 2011)), and the *m/z* 173 and *m/z* 284 fragments of the ribose derivative (containing the last two and first four C-atoms of ribose, respectively (Long and Antoniewicz, 2014b)), were measured in single ion monitoring. Mass isotopomer distributions were obtained by integration (Antoniewicz et al., 2007a) and corrected for natural isotope abundances (Fernandez et al., 1996).

6.2.7 Metabolic Network Models and ^{13}C-Metabolic Flux Analysis

The metabolic network models used for ^{13}C-MFA in this study are provided in Appendix D. For *E. coli*, the full model described in (Crown et al., 2015) was used, as well as a simplified model containing only the upper portion of central carbon metabolism. For CHO cells, the model described in (Ahn and Antoniewicz, 2013) was used. All ^{13}C-MFA calculations were performed using the Metran software (Yoo et al., 2008), which is based on the elementary metabolite units (EMU) framework (Antoniewicz et al., 2007b). Fluxes were estimated by minimizing the variance-weighted sum of squared residuals (SSR) between the experimentally measured and model predicted mass isotopomer distributions using non-linear least-squares regression (Antoniewicz et al., 2006). For integrated analysis of parallel labeling experiments, the data sets were fitted simultaneously to a single flux model as

described in (Antoniewicz, 2015b; Leighty and Antoniewicz, 2012). Flux estimation was repeated 10 times starting with random initial values for all fluxes to find a global solution. At convergence, accurate 68% and 95% confidence intervals were computed for all estimated fluxes by evaluating the sensitivity of the minimized SSR to flux variations (Antoniewicz et al., 2006).

To model fractional labeling of metabolites, G-value parameters were also included in ^{13}C-MFA (Antoniewicz, 2015a). The G-value represents the fraction of a metabolite pool that is produced during the labeling experiment, while 1-G represents the fraction that is naturally labeled, i.e. from the inoculum. By default, one G-value parameter was included for each measured metabolite in each data set. Reversible reactions were modeled as separate forward and backward fluxes. Net and exchange fluxes were determined as follows: $v_{net} = v_f - v_b$; $v_{exch} = \min(v_f, v_b)$. For visual representation of exchange fluxes, the exchange fluxes were rescaled as follows: exchange flux (%) = $100\% \times v_{exch} / (100 + v_{exch})$.

6.2.8 Goodness-of-Fit Analysis

To determine the goodness-of-fit, ^{13}C-MFA fitting results were subjected to a χ^2-statistical test. In short, assuming that the model is correct and data are without gross measurement errors, the minimized SSR is a stochastic variable with a χ^2-distribution (Antoniewicz et al., 2006). The number of degrees of freedom is equal to the number of fitted measurements *n* minus the number of estimated independent parameters *p*. The acceptable range of SSR values is between $\chi^2_{\alpha/2}(n-p)$ and $\chi^2_{1-\alpha/2}(n-p)$, where α is a certain chosen threshold value, for example 0.05 for 95% confidence interval.

6.3 Results and Discussion

6.3.1 Measuring Glycogen and RNA Labeling with GC-MS

Glycogen and RNA are abundant components of microbial and mammalian biomass. The glucose moiety of glycogen is derived from the glycolytic intermediate glucose-6-phosphate (G6P), and the ribose moiety of RNA is derived from the PPP intermediate ribose-5-phosphate (R5P). Here, we present a convenient procedure for measuring the labeling of glucose and ribose from glycogen and RNA using GC-MS for applications in ^{13}C-MFA. To observe the sugar monomers, the polymers are first hydrolyzed with hydrochloric acid and then derivatized as shown in Figure 6.1. Previously, we validated that this approach is selective for detecting the stable biomass components glycogen and RNA, rather than intracellular metabolites (Long and Antoniewicz, 2014b). For GC-MS analysis, we use the aldonitrile pentapropionate derivatization method that generates two reliable GC-MS fragments for each sugar. The first fragment, *m/z* 173, contains the last two carbons of each sugar, i.e. C5+C6 of glucose and C4+C5 of ribose. The second larger fragment contains the first five carbons of glucose (C1-C5, *m/z* 370), and the first four carbons of ribose (C1-C4, *m/z* 284). The resulting positional labeling information provided by these fragments is critical for precise flux analysis, as is demonstrated in the next sections. The ribose and glucose peaks are clearly identifiable in the chromatograms from hydrolyzed biomass, as shown in Figures 6.1B and 6.1C for *E. coli* and CHO cells, respectively. For CHO cells, we also detected mannose and galactose peaks (Figure 6.1C), which may be useful for other applications such as glycan analysis (Badur et al., 2015).

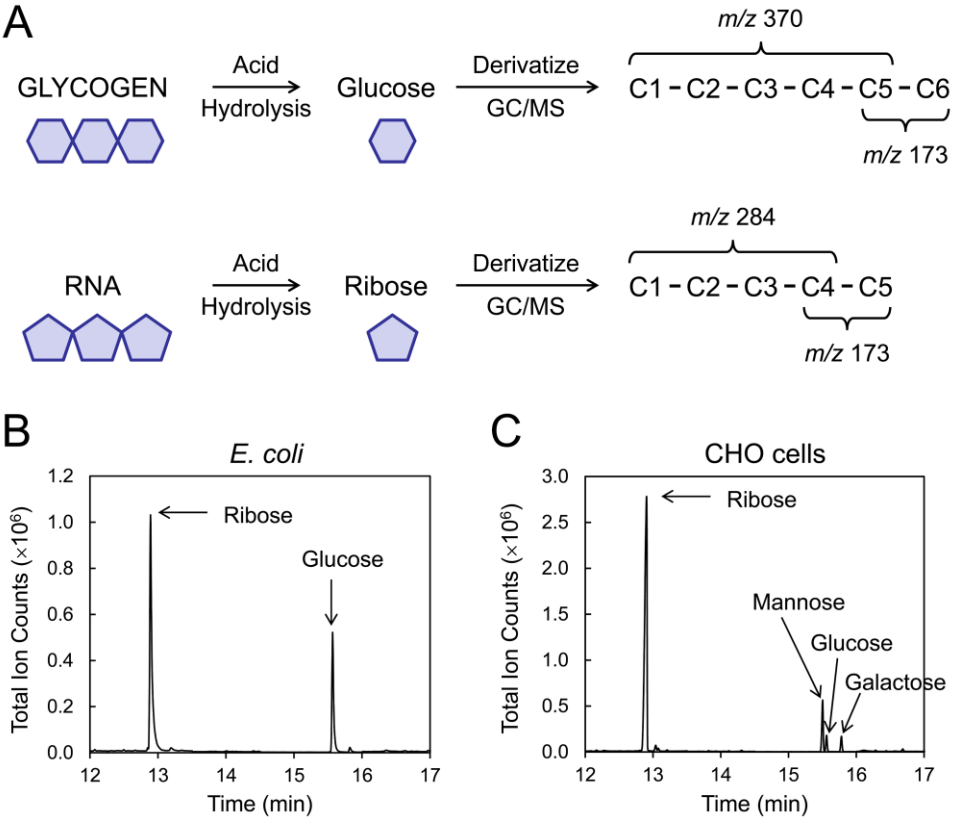

Figure 6.1: GC-MS analysis of glycogen and RNA labeling. A) The biopolymers glycogen and RNA are first broken down into the respective sugar monomers glucose and ribose by acid hydrolysis. The sugars are then subjected to aldonitrile propionate derivatization for subsequent GC-MS analysis. Two fragments of each species are measured to provide positional labeling information. B) Total ion chromatogram from GC-MS analysis of sugars from hydrolyzed *E. coli*, and C) CHO cells. Peaks corresponding to different sugar monomers are clearly resolved.

6.3.2 Glycogen and RNA Labeling Data Improve Resolution of PPP Fluxes in *E. coli*

To demonstrate that glycogen and RNA labeling data can improve flux resolution, we first applied this approach to *E. coli* as a model microbial system. ^{13}C-MFA of *E. coli* currently relies on measurements of protein-bound amino acids. To assess the complementarity of the glycogen and RNA measurements with amino acid

measurements, a test case was performed using the tracer [1,6-^{13}C]glucose and exponentially growing wild-type *E. coli*. In preliminary studies, we identified [1,6-^{13}C]glucose as a promising tracer for ^{13}C-MFA with good performance throughout central carbon metabolism (Crown et al., 2016). After performing the tracer experiment, isotopic labeling of amino acids from hydrolyzed biomass, as well as glucose and ribose moieties of glycogen and RNA, were measured by GC-MS. Fluxes were then estimated, first using only the amino acid labeling data, and then using the amino acid data along with the glycogen and RNA data. The flux results are summarized in Figure 6.2. Acceptable fits were obtained in all cases, assuming a constant measurement error of 0.3 mol% for all GC-MS measurements, demonstrating that all data were in good agreement. Figure 6.2A shows the estimated net fluxes and Figure 6.2B shows the 68% and 95% confidence intervals of several key fluxes in central carbon metabolism. Importantly, the addition of glycogen and RNA labeling data significantly improved the precision of fluxes in upper glycolysis (e.g. PGI flux) and PPP (e.g. oxPPP, TKT, TAL fluxes). The confidence intervals of these fluxes were improved by 4-fold when glycogen and RNA measurements were included (Figure 6.2B).

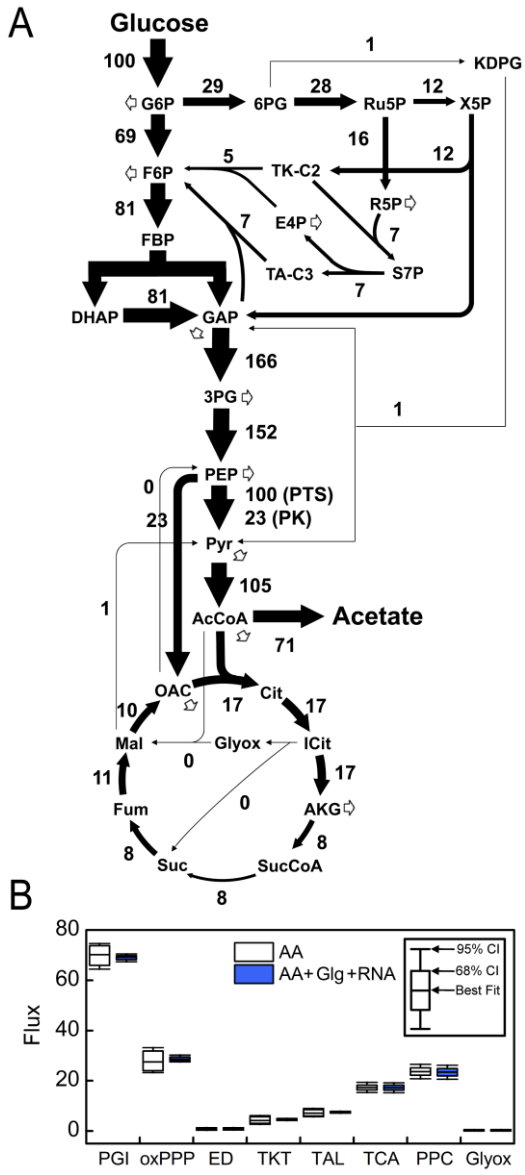

Figure 6.2: ^{13}C metabolic flux analysis of *E. coli* metabolism using amino acid, glycogen and RNA labeling data from a [1,6-^{13}C]glucose tracer experiment. A) Estimated flux map for *E. coli* central carbon metabolism. Fluxes were determined by simultaneously fitting amino acid (AA), glycogen (Glg), and RNA labeling data. White arrows represent outflux to biomass. B) Comparison of flux confidence intervals obtained from ^{13}C-MFA using only amino acid labeling data, and amino acid labeling data combined with glycogen and RNA data. The 68% and 95% flux confidence intervals are shown for eight representative metabolic fluxes in central carbon metabolism.

6.3.3 Estimation of Net and Exchange Fluxes in *E. Coli* Upper Metabolism with Glycogen and RNA Data

Next, we evaluated if glycogen and RNA data alone (i.e. without amino acid data) could be used for reliable flux estimation in the upper half of metabolism, defined here to include the upper portion of the glycolysis (EMP) pathway, pentose phosphate pathway (PPP), and Entner-Doudoroff (ED) pathway. For this analysis we used a simplified network model shown in Figure 6.3A. Of the commonly measured amino acids, only phenylalanine could be used in this case (see Introduction section). To demonstrate the usefulness of glycogen and RNA measurements, a novel parallel tracer experiment scheme was employed here. Specifically, three mixtures of tracers were used (Ahn et al., 2016): [1-^{13}C]glucose + [4,5,6-^{13}C]glucose (1:1), [2-^{13}C]glucose + [4,5,6-^{13}C]glucose (1:1), and [3-^{13}C]glucose + [4,5,6-^{13}C]glucose (1:1). These tracers were selected based on the approaches for optimal tracer experiment design described in (Antoniewicz, 2015b, 2013b; Crown and Antoniewicz, 2012).

After performing the parallel labeling experiments, isotopic labeling of phenylalanine from hydrolyzed proteins, as well as the glucose and ribose moieties of glycogen and RNA, were measured by GC-MS. Flux analysis was then performed three times: first, using only phenylalanine labeling data (using fragments *m/z* 302, 308 and 336); second, using only glycogen and RNA labeling data; and third, using phenylalanine, glycogen and RNA labeling data together. All fits were statistically acceptable, assuming a constant measurement error of 0.3 mol% for all GC-MS measurements. The flux results are shown in Figure 6.3. The differences in flux precision for the different data sets are shown in Figure 6.3B, where for most reactions the glycogen and RNA measurements performed better than phenylalanine measurements alone, and the combined fits provided the most precise flux estimates.

This was the case for all of the reactions except for the ED flux, where glycogen and RNA produced larger confidence intervals than phenylalanine. This is because while phenylalanine has some observability of the products of the ED reactions (i.e. PEP from GAP), glycogen and RNA are upstream and thus have little information about that flux. As shown in Figure 6.3C, the addition of glycogen and RNA measurements allowed good estimation of exchange fluxes. These exchange fluxes are notoriously difficult to estimate with amino acid labeling data alone across a wide spectrum of glucose tracers (Crown et al., 2015). The PGI exchange flux was unobservable using only phenylalanine, but with the addition of glycogen and RNA measurements it was estimated with a narrow confidence interval. Dramatic improvements in precision were also observed for the exchange fluxes of transketolase (TKT) and transaldolase (TAL) half reactions leading to fructose-6-phosphate. Estimates were not improved in other half reactions.

6.3.4 Elucidation of Glucose and Xylose Co-Utilization using Glycogen and RNA Data

To demonstrate a novel and practical application of our methodology, we applied it to elucidate the metabolism of the *E. coli* ΔptsG mutant, which has the ability to co-utilize glucose and xylose (Chiang et al., 2013; Li et al., 2007). A tracer experiment was performed using a 1:1 molar ratio of [1,2-^{13}C]glucose and [1,2-^{13}C]xylose. After performing the labeling experiment, isotopic labeling of phenylalanine, glycogen, and RNA were measured by GC-MS.

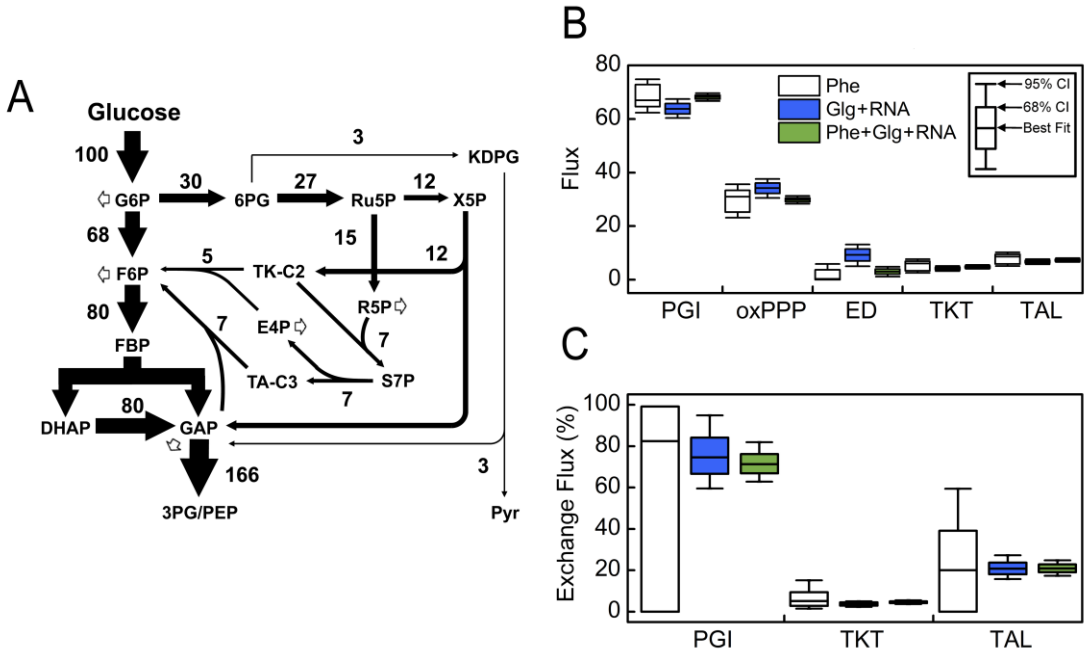

Figure 6.3: ^{13}C metabolic flux analysis of upper metabolism of *E. coli* using phenylalanine, glycogen and RNA labeling data from three parallel labeling experiments. A) Estimated flux map for *E. coli* determined by simultaneously fitting phenylalanine (Phe), glycogen (Glg), and RNA labeling data. White arrows represent outflux to biomass. B) Comparison of flux confidence intervals obtained from ^{13}C-MFA using only phenylalanine labeling data, only glycogen and RNA labeling data, and all three metabolites. The 68% and 95% flux confidence intervals are shown for five representative metabolic fluxes: phosphoglucose isomerase (v_2; PGI); oxidative pentose phosphate pathway (v_9; oxPPP); Entner-Doudoroff pathway (v_{18}; ED); transketolase (v_{14}; TKT); transaldolase (v_{16}; TAL).C) Comparison of confidence intervals for exchange fluxes estimated using different data sets. Note that in both (B) and (C), TKT and TAL refer to the terminal half reactions of transketolase and transaldolase involving fructose 6-phosphate.

^{13}C-MFA was then performed three times as described above using different data sets. All fits were statistically acceptable, assuming a constant measurement error of 0.3 mol% for all GC-MS measurements. The flux results are shown in Figure 6.4

and the differences in flux precision for the different data sets are shown in Figure 6.4B. For ^{13}C-MFA, we did not include the measured glucose and xylose uptake rates as constraints; instead, xylose uptake rate was fixed at 100 and the relative glucose uptake rate was estimated by ^{13}C-MFA so that it could be compared to the measured rate. Overall, including glycogen and RNA labeling data resulted in significantly more precise flux estimates, i.e. narrower confidence intervals, compared to using phenylalanine data alone (Figure 6.4B). Importantly, the addition of glycogen and RNA allowed the glucose uptake rate to be determined precisely, which was not possible with phenylalanine data (Figure 6.4B). Based on ^{13}C-MFA results, the glucose-to-xylose uptake ratio was determined to be 0.23 ± 0.02, which matches perfectly with the measured ratio of 0.22 (i.e. the measured glucose uptake rate was 1.93 mmol/g_{DW}/hr and the measured xylose uptake rate was 8.69 mmol/g_{DW}/hr). Previous studies on glucose and xylose co-utilization have relied on intracellular measurements and amino acid measurements (Aristilde et al., 2015; Cordova and Antoniewicz, 2016). This example clearly illustrates the value of including glycogen and RNA labeling data for precise analysis of glucose and xylose co-utilization.

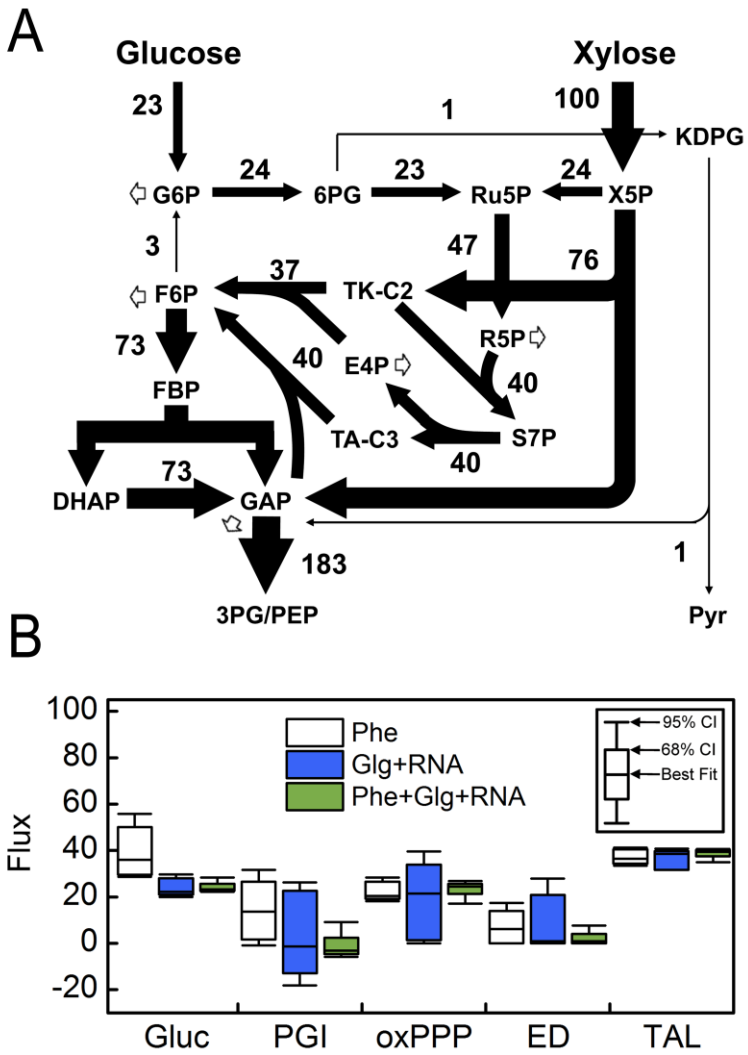

Figure 6.4: ^{13}C metabolic flux analysis of upper metabolism *E. coli* strain ΔptsG co-utilizing glucose and xylose, using phenylalanine, glycogen and RNA labeling data. A) Estimated flux map determined by simultaneously fitting phenylalanine (Phe), glycogen (Glg), and RNA labeling data. White arrows represent outflux to biomass. B) Comparison of flux confidence intervals obtained from ^{13}C-MFA using only phenylalanine labeling data, only glycogen and RNA labeling data, and all three metabolites. The 68% and 95% flux confidence intervals are shown for six key metabolic fluxes: relative glucose uptake (v_1; Gluc); phosphoglucose isomerase (v_2; PGI); oxidative pentose phosphate pathway (v_9; oxPPP); Entner-Doudoroff pathway (v_{18}; ED); transketolase (v_{14}; TKT); transaldolase (v_{16}; TAL).

6.3.5 Estimation of Net and Exchange Fluxes in CHO Cell Upper Metabolism with Glycogen and RNA Data

Lastly, we applied the methodology to analyze the metabolism of CHO cells as a model mammalian system. To demonstrate the efficacy of glycogen and RNA labeling data for ^{13}C-MFA of mammalian cells, the same parallel tracer scheme was used as in section 6.3.3. CHO cells were grown in serum-free suspension culture to the mid-exponential phase (~0.5×10^6 cells/mL), at which point tracers were introduced as a bolus. After ~24 hours, cells were harvested for analysis of 3PG and PEP labeling (intracellular metabolites), and glycogen and RNA labeling by GC-MS.

Flux analysis was then performed three times: first, using only 3PG and PEP labeling data, representing the current standard of using intracellular metabolites for ^{13}C-MFA; second, using only glycogen and RNA labeling data; and third, using 3PG, PEP, glycogen and RNA labeling data together. All fits were statistically acceptable, assuming a measurement error of 0.3 mol% for glycogen and RNA labeling measurements and 0.4 mol% for 3PG and PEP labeling measurements that were more noisy. The flux results are shown in Figure 6.5. As shown in Figure 6.5B, the confidence intervals of fluxes in upper metabolism were largest when fluxes were estimated with 3PG and PEP data alone, were reduced when glycogen and RNA data was used, and were greatly reduced when all measurements were used for ^{13}C-MFA. A similar trend was observed for confidence intervals of exchange fluxes (Figure 6.5C), where the precision of TKT and TAL exchange fluxes was greatly improved when all four metabolites were fitted at the same time. Together, these results demonstrate that glycogen and RNA labeling data are complementary to 3PG and PEP labeling measurements for estimating net and exchange fluxes in upper metabolism of CHO cells.

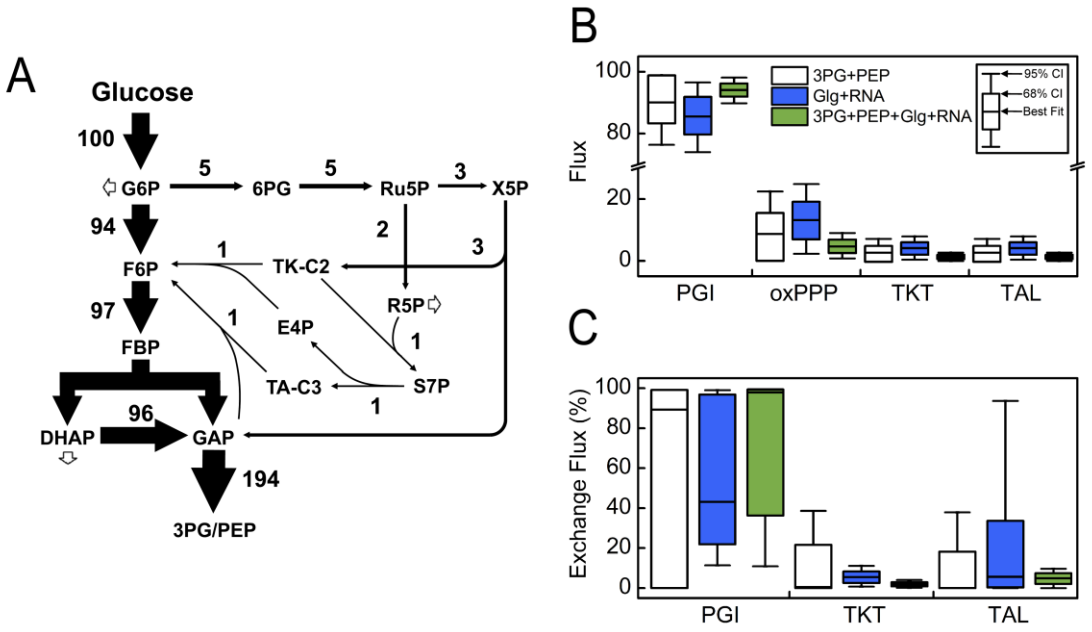

Figure 6.5: ^{13}C metabolic flux analysis of upper metabolism of CHO cells using 3PG, PEP, glycogen and RNA labeling data from three parallel labeling experiments. A) Estimated flux map determined by simultaneously fitting 3PG, PEP, glycogen (Glg), and RNA labeling data. White arrows represent outflux to biomass. B) Comparison of flux confidence intervals obtained from ^{13}C-MFA using only 3PG and PEP labeling data, only glycogen and RNA labeling data, and all four metabolites. The 68% and 95% flux confidence intervals are shown for four representative metabolic fluxes: phosphoglucose isomerase (v_2; PGI); oxidative pentose phosphate pathway (v_8; oxPPP); transketolase (v_{13}; TKT); and transaldolase (v_{15}; TAL). C) Comparison of confidence intervals for exchange fluxes estimated using different data sets. Note that in both (B) and (C), TKT and TAL refer to the terminal half reactions of transketolase and transaldolase involving fructose 6-phosphate.

6.3.6 Determining Turnover Rates of Glycogen and RNA

In addition to determining intracellular fluxes, glycogen and RNA labeling data can also be used to determine turnover rates of glycogen and RNA (Murphy et al.,

2013). For this purpose, the estimated G-values for glycogen and RNA are first used to calculate an apparent labeling rate for each macromolecule. This apparent labeling rate reflects the generation of new biomass (i.e. growth) as well as turnover (i.e. breakdown and regeneration) of the macromolecules. This relationship is described by:

$$\text{Apparent labeling rate} = -\ln(1-G)/t = \text{growth rate} + \text{turnover rate} \quad (6.1)$$

Here, G is the estimated G-value of glycogen (or RNA) from ^{13}C-MFA, and t is the length of the labeling experiment (in this study, t = 23.25 h). To illustrate this approach for determining turnover rates of glycogen and RNA, the growth rate of CHO cells was determined directly by cell counting (Figure 6.6A), and the apparent labeling rate was determined from the estimated G-values (Figure 6.6B). Based on cell counting, a specific cell growth rate of $0.035 \pm 0.001\ h^{-1}$ was determined, and from the estimated G-values for glycogen (G = 0.65) and RNA (G = 0.61), apparent labeling rates of $0.045 \pm 0.001\ h^{-1}$ and $0.040 \pm 0.001\ h^{-1}$ were determined for glycogen and RNA, respectively. Thus, the turnover rate of glycogen was 1.0% per hour (i.e. $0.045 - 0.035\ h^{-1} = 0.010\ h^{-1}$) and the turnover rate of RNA was 0.5% per hour (i.e. $0.040 - 0.035\ h^{-1} = 0.005\ h^{-1}$).

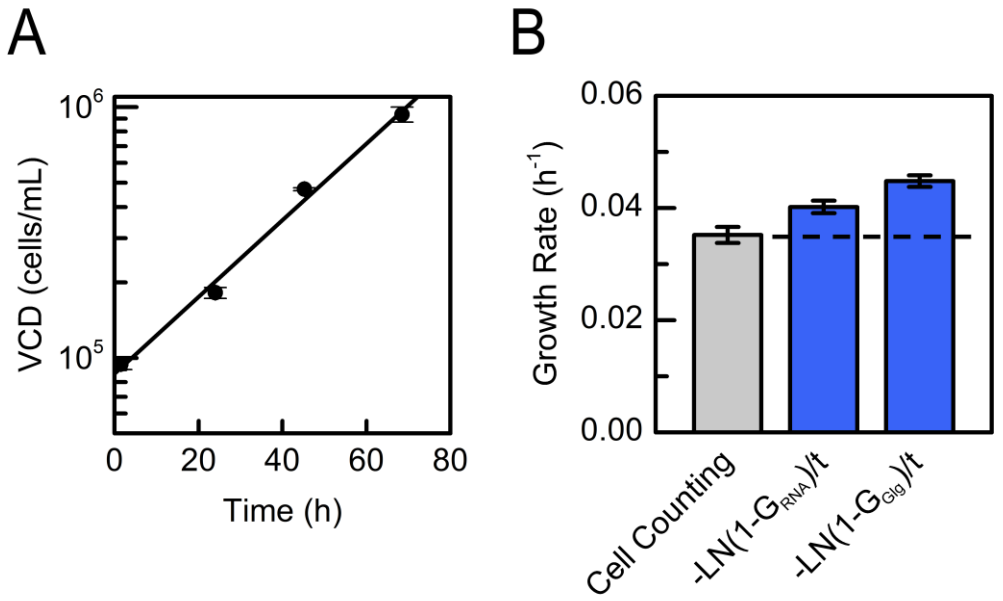

Figure 6.6: Determining turnover rates of glycogen and RNA in CHO cells. A) Time profile of the measured viable cell density of CHO cells in suspension culture. B) Comparison of the growth rate of CHO cells (determined by cell counting) and the apparent labeling rates of glycogen (Glg) and RNA (determined from estimated G-values). The differences between the growth rate of CHO cells and the apparent labeling rates are attributable to turnover of glycogen and RNA. Error bars represent mean ± SD (*n*=3, biological replicates from parallel labeling experiments).

6.4 Conclusion

In this work, we have presented an approach for GC-MS based analysis of isotopic labeling of glycogen and RNA, and demonstrated the usefulness of these measurements for ^{13}C-MFA. Compared to alternative approaches, our method requires relatively little biomass (<0.2 mg of dry biomass for *E. coli*, and <4×10^6 CHO cells), and provides multiple fragments of glucose and ribose moieties with valuable information regarding metabolic fluxes in upper metabolism, including glycolysis and pentose phosphate pathway. Additionally, we demonstrate that these measurements are complementary to other commonly used measurements for ^{13}C-MFA, including

amino acids in microbial systems and intracellular metabolites in mammalian systems. We demonstrate that glycogen and RNA labeling data are valuable for estimating precise glucose and xylose uptake rates when both substrates are co-utilized.

Beyond facilitating more precise flux estimates in combination with other common measurements, glycogen and RNA measurements provide unique observability of net and exchange fluxes in upper metabolism. In *E. coli*, these measurements are sufficient for precise quantification of fluxes in a simplified model of upper central carbon metabolism, performing better and with excellent complementarity to current measurements. In CHO cells, these measurements perform similarly to the commonly measured intracellular metabolites, which require much more laborious sample preparations and larger sample sizes. Similarly, we found strong synergy between these measurements and other commonly used measurements for ^{13}C-MFA. It is important to note that glycogen and RNA measurements allow significant improvements in the precision of exchange fluxes that are often unobservable with other commonly used measurements (Crown et al., 2015). Given the convenience of measuring glycogen and RNA labeling and the high information content of these measurements for resolving metabolic fluxes, we believe that the approach presented in this study will be broadly applied in future ^{13}C-MFA studies.

6.5 Author Contributions

CPL, JEG, and JA performed the experiments and data analysis for wildtype *E. coli*, *E. coli* Δ*ptsG*, and CHO cells, respectively. CPL, JA, JEG, and MRA wrote the paper.

Chapter 7

CONCLUSIONS AND FUTURE WORK

Advances in the design of ^{13}C tracer experiments and ^{13}C-MFA have enabled greater accuracy and precision in flux estimates, leading to a more comprehensive understanding of cellular metabolism. This dissertation highlighted the use of parallel labeling experiments, ^{13}C amino acid tracers, and RNA and glycogen measurements in validating metabolic network models and estimating metabolic fluxes. We applied these techniques to characterize the metabolism of *C. acetobutylicum*, *E. coli*, and CHO cells.

7.1 Summary of Conclusions

In Chapter 2, we applied parallel labeling experiments, ^{13}C-MFA, and statistical analysis to quantitatively resolve the metabolism of *C. acetobutylicum* for the first time. Using goodness-of-fit analysis and evaluation of 95% confidence intervals, we established a minimal metabolic network model that fit all experimental data from the four [U-^{13}C]glucose and [1-^{13}C]glucose parallel cultures. Estimated fluxes determined with this minimal model indicated that the TCA cycle is incomplete with no measurable flux between α-ketoglutarate and succinyl-CoA, succinate and fumarate, and malate and oxaloacetate. We also found that isoleucine is produced exclusively through the citramalate synthase pathway. Overall, the validated network model can be used for future ^{13}C-MFA studies of *C. acetobutylicum*. From a broader perspective, the combined analysis of the parallel data sets provides a large number of

redundant measurements, which are valuable for validating metabolic network models and producing precise flux estimates.

In Chapter 3, we used multiple ^{13}C amino acid tracers ([1-^{13}C]aspartate, [4-^{13}C]aspartate, and [1-^{13}C]serine) to detect the presence of cycling between amino acid metabolism and central carbon metabolism. We demonstrated that the conversion of serine to pyruvate is active in wildtype *E. coli*. In *C. acetobutylicum,* we provided the first conclusive evidence that a metabolic cycle is active where carbon atoms flow from aspartate to threonine, to serine, to pyruvate, to oxaloacetate, and back to aspartate. Two reactions in this cycle, the conversion of oxaloacetate to aspartate and the conversion of glycine to serine, were also shown to be reversible. In general, this work tested a common assumption in ^{13}C-MFA, namely that no carbon flows from secondary pathways, such as amino acid metabolism, back to central carbon metabolism. We emphasized the importance of considering such reactions in ^{13}C-MFA, particularly in the analysis of strains with altered phenotypes. This work also serves as an example of how multiple ^{13}C amino acid tracers can be used to probe reactions and cycles that are difficult to detect using traditional ^{13}C glucose tracers.

In Chapter 4, we applied ^{13}C tracers and mass isotopomer analysis to directly measure the effects of butanol and butyric acid stress on the metabolic pathways and fluxes of *C. acetobutylicum*. Off-gas analysis of the stressed cultures indicated significant to severe impairment of cell growth. However, ^{13}C labeling experiments demonstrated that central carbon metabolism and amino acid metabolism were robust to both butanol and butyric acid stress, with the relative flux distributions remaining generally unchanged compared to unstressed cultures, both on short time scales (within 2 hours of stress introduction) and long time scales (within 8 hours of stress

introduction). This work adds to our current understanding of the metabolite stress response in *C. acetobutylicum*. If combined with other omics data, the ^{13}C labeling data may contribute to a more systems level understanding of the metabolite stress response and potentially better strategies for rationally engineering *C. acetobutylicum* for industrial scale production of butanol and butyric acid.

In Chapter 5, we quantified a back-flux from pyruvate to phosphoenoelpyruvate in *E. coli* using ^{13}C alanine tracers and knockout strains. We showed that this flux is a major contributor to gluconeogenic flux during growth on acetate and is interchangeably supported by both PEP synthetase (*ppsA*) and Enzyme I (*ptsI*), the terminal phosphotransferase of the PTS. Unexpectedly, we found that this back-flux is significant under glycolytic growth (specifically growth on glucose and xylose) and that Enzyme I is primarily responsible. Single and double knockouts of genes related to other PTS components, specifically Δ*ptsG* and Δ*crr*, also displayed a significant amount of back-flux, suggesting the involvement of other phosphotransferases or sources of phosphoryl groups. Overall, these findings contribute to our understanding and annotation of *E. coli* central carbon metabolism, which is of central importance in metabolic modeling and engineering efforts such as ^{13}C-MFA and the development of production strains.

In Chapter 6, we demonstrated that isotopic labeling of glycogen and RNA provides additional valuable information for ^{13}C-MFA. The presented GC-MS based method supplies labeling data for multiple fragments of the glucose and ribose moieties of glycogen and RNA, respectively. Using *E. coli* as a model microbial system and CHO cells as a model mammalian system, we demonstrated that these labeling data allow for significant improvements in flux precision in upper glycolysis

and the pentose phosphate pathway, and are complementary to other commonly used measurements, such as biomass amino acids or intracellular metabolites. Furthermore, the inclusion of glycogen and RNA labeling proved to be valuable in estimating precise glucose and xylose uptake rates in the sugar co-utilizing strain *E. coli* Δ*ptsG*. Compared to alternative methods, this approach uses a relatively small amount of biomass and avoids the pitfalls of LC-MS and LC-MS/MS based techniques. The availability of glycogen and RNA labeling data also expands the repertoire of reliable isotopic measurements that can be used for ^{13}C-MFA.

7.2 Recommendations for Future Work

Future Directions for Elucidating Clostridial Metabolism

Although ^{13}C labeling experiments showed no major rewiring of *C. acetobutylicum* metabolism in response to butanol and butyric acid stress, it may be of potential value to compare the fluxes of a high-butanol-producing or high-butyric acid-producing strain with the fluxes of the parental strain. A similar strategy has been undertaken using other omics approaches. For example, comparative genomic analysis of *C. acetobutylicum* JB200, a mutant strain capable of producing up to 21 g/L butanol in batch fermentations, and *C. acetobutylicum* ATCC 55025, the parental strain, revealed a mutation in the gene encoding histidine kinase (Xu et al., 2014). Disruption of this gene in ATCC 55025 imparted the resulting knockout strain with higher butanol productivity and titer than the parental strain, implicating the role of this gene in solvent production and tolerance. The same approach could be applied to fluxomics using the validated *C. acetobutylicum* network model as a starting point. Differences in fluxes may provide valuable insights into the high-titer phenotype, as well as

information for next generation genome scale models that can be used to elucidate underlying regulatory processes.

Another potential area of study is to apply ^{13}C-MFA to study acetogenic clostridia. These organisms are rapidly gaining attention due to the potential for increased product yields from carbohydrate feedstocks through anaerobic, non-phothosynthetic mixotrophic fermentation (Fast et al., 2015). ^{13}C labeling experiments would likely utilize ^{13}C gases (e.g. ^{13}CO or $^{13}CO_2$) to probe the Wood-Ljungdahl pathway, the carbon fixation pathway in acetogenic clostridia. Thus the autotrophic component of metabolism would also present an opportunity to make improvements to the isotopic non-stationary ^{13}C metabolic flux analysis (^{13}C-NMFA) methodology, which is experimentally complex and laborious (Wiechert and Nöh, 2013). This by itself would represent a significant development in ^{13}C flux analysis.

Future Directions for Investigating the PTS in E. coli

As referenced in Chapter 5, the high back-flux from pyruvate to PEP observed in *E. coli* Δ*ptsG* and Δ*crr* suggests that other proteins or metabolites may interact with PTS components to supply phosphoryl groups to sustain this flux. It was previously demonstrated that Enzyme I is able to exchange phosphoryl groups with other kinases, such as acetate kinase (*ackA*) (Fox et al., 1986). It has also been suggested that acetyl-phosphate can directly phosphorylate regulatory proteins (Boll and Hendrixson, 2011). Thus, a potential next step would be to use similar ^{13}C alanine experiments to determine if the back flux is eliminated in the double knockout strains (Δ*ptsG*Δ*ackA* or Δ*crr*Δ*ackA*) or perhaps, Δ*ptsG* or Δ*crr* that is deficient in acetyl-phosphate. Similar

experiments with other relevant knockout strains may also help further elucidate the interactions of the PTS with other parts of metabolism.

Future Directions for ^{13}C-MFA Methodologies

A recent method for identifying optimal tracers for parallel labeling experiments introduced a new scoring system to evaluate ^{13}C glucose tracer schemes for increased flux precision (Crown et al., 2016). A logical extension of this would be to apply this scoring system to evaluate tracer schemes that include ^{13}C substrates besides glucose (e.g. xylose, acetate, various amino acids). This may be particularly useful due to the interest in sugar co-utilizing organisms or strains, as well as the relevance of amino acid metabolism in mammalian systems. Also, an extension to alternative ^{13}C substrates would aid in designing experiments to quantify flux through pathways that are difficult to detect using ^{13}C glucose tracers (e.g. the metabolic cycle identified in Chapter 3).

Additionally, the new advances highlighted in this dissertation, namely the utility of parallel labeling experiments, ^{13}C amino acid tracers, and RNA and glycogen labeling measurements, increase the number of possible designs for ^{13}C labeling experiments. This is expected to continue to increase as custom tracers become easier and less costly to synthesize. Furthermore, improvements to metabolomics techniques are likely to increase the availability and ease of acquiring new measurements for ^{13}C analysis. Since flux precision is a function of experimental layout, tracer selection, and measurement selection, methodologies should be developed to design ^{13}C labeling experiments with all three factors in consideration. These methodologies would enable

a more rational decision-making process when designing ^{13}C labeling experiments for precise flux estimation.

REFERENCES

Adler, P., Frey, L.J., Berger, A., Bolten, C.J., Hansen, C.E., Wittmann, C., 2014. The key to acetate: metabolic fluxes of acetic acid bacteria under cocoa pulp fermentation-simulating conditions. Appl. Environ. Microbiol. 80, 4702–16.

Ahn, W.S., Antoniewicz, M.R., 2011. Metabolic flux analysis of CHO cells at growth and non-growth phases using isotopic tracers and mass spectrometry. Metab. Eng. 13, 598–609.

Ahn, W.S., Antoniewicz, M.R., 2013. Parallel labeling experiments with [1,2-^{13}C]glucose and [U-^{13}C]glutamine provide new insights into CHO cell metabolism. Metab. Eng. 15, 34–47.

Ahn, W.S., Crown, S.B., Antoniewicz, M.R., 2016. Evidence for transketolase-like TKTL1 flux in CHO cells based on parallel labeling experiments and ^{13}C-metabolic flux analysis. Metab. Eng. 37, 72–78.

Alsaker, K. V, Paredes, C., Papoutsakis, E.T., 2010. Metabolite stress and tolerance in the production of biofuels and chemicals: gene-expression-based systems analysis of butanol, butyrate, and acetate stresses in the anaerobe Clostridium acetobutylicum. Biotechnol. Bioeng. 105, 1131–47.

Alsaker, K. V, Spitzer, T.R., Eleftherios, T., Papoutsakis, E.T., 2004. Transcriptional Analysis of spo0A Overexpression in Clostridium acetobutylicum and Its Effect on the Cell ' s Response to Butanol Stress Transcriptional Analysis of spo0A Overexpression in Clostridium acetobutylicum and Its Effect on the Cell ' s Response. J. Bacteriol. 186, 1959–1971.

Amador-Noguez, D., Brasg, I. a, Feng, X.-J., Roquet, N., Rabinowitz, J.D., 2011. Metabolome remodeling during the acidogenic-solventogenic transition in Clostridium acetobutylicum. Appl. Environ. Microbiol. 77, 7984–97.

Amador-Noguez, D., Feng, X.-J., Fan, J., Roquet, N., Rabitz, H., Rabinowitz, J.D., 2010. Systems-level metabolic flux profiling elucidates a complete, bifurcated tricarboxylic acid cycle in Clostridium acetobutylicum. J. Bacteriol. 192, 4452–61.

Antoniewicz, M.R., 2013a. Using multiple tracers for ^{13}C metabolic flux analysis.

Methods Mol. Biol., Methods in Molecular Biology 985, 353–365.

Antoniewicz, M.R., 2013b. ^{13}C metabolic flux analysis: optimal design of isotopic labeling experiments. Curr. Opin. Biotechnol. 24, 1116–1121.

Antoniewicz, M.R., 2013c. Tandem mass spectrometry for measuring stable-isotope labeling. Curr. Opin. Biotechnol. 24, 48–53.

Antoniewicz, M.R., 2013d. Dynamic metabolic flux analysis-tools for probing transient states of metabolic networks. Curr. Opin. Biotechnol. 1–6.

Antoniewicz, M.R., 2015a. Methods and advances in metabolic flux analysis: a mini-review. J. Ind. Microbiol. Biotechnol. 42, 317–325.

Antoniewicz, M.R., 2015b. Parallel labeling experiments for pathway elucidation and ^{13}C metabolic flux analysis. Curr. Opin. Biotechnol. 36, 91–97.

Antoniewicz, M.R., Kelleher, J.K., Stephanopoulos, G., 2006. Determination of confidence intervals of metabolic fluxes estimated from stable isotope measurements. Metab. Eng. 8, 324–37.

Antoniewicz, M.R., Kelleher, J.K., Stephanopoulos, G., 2007a. Accurate assessment of amino acid mass isotopomer distributions for metabolic flux analysis. Anal. Chem. 79, 7554–9.

Antoniewicz, M.R., Kelleher, J.K., Stephanopoulos, G., 2007b. Elementary metabolite units (EMU): a novel framework for modeling isotopic distributions. Metab. Eng. 9, 68–86.

Antoniewicz, M.R., Kelleher, J.K., Stephanopoulos, G., 2011. Measuring deuterium enrichment of glucose hydrogen atoms by gas chromatography/mass spectrometry. Anal. Chem. 83, 3211–6.

Antoniewicz, M.R., Kraynie, D.F., Laffend, L. a, González-Lergier, J., Kelleher, J.K., Stephanopoulos, G., 2007c. Metabolic flux analysis in a nonstationary system: fed-batch fermentation of a high yielding strain of E. coli producing 1,3-propanediol. Metab. Eng. 9, 277–92.

Arifin, Y., Archer, C., Lim, S., Quek, L.-E., Sugiarto, H., Marcellin, E., Vickers, C.E., Krömer, J.O., Nielsen, L.K., 2014. Escherichia coli W shows fast, highly oxidative sucrose metabolism and low acetate formation. Appl. Microbiol. Biotechnol. 98, 9033–44.

Aristilde, L., Lewis, I.A., Park, J.O., Rabinowitz, J.D., 2015. Hierarchy in Pentose

Sugar Metabolism in Clostridium acetobutylicum. Appl. Environ. Microbiol. 81, 1452–1462.

Au, J., Choi, J., Jones, S.W., Venkataramanan, K.P., Antoniewicz, M.R., 2014. Parallel labeling experiments validate Clostridium acetobutylicum metabolic network model for ^{13}C metabolic flux analysis. Metab. Eng. 26, 23–33.

Baba, T., Ara, T., Hasegawa, M., Takai, Y., Okumura, Y., Baba, M., Datsenko, K.A., Tomita, M., Wanner, B.L., Mori, H., 2006. Construction of Escherichia coli K-12 in-frame, single-gene knockout mutants: the Keio collection. Mol. Syst. Biol. 2, 1–11.

Badur, M.G., Zhang, H., Metallo, C.M., 2015. Enzymatic passaging of human embryonic stem cells alters central carbon metabolism and glycan abundance. Biotechnol. J. 10, 1600–1611.

Bailey, J.E., 1991. Toward a Science of Metabolic Engineering Published by : American Association for the Advancement of Science Stable. Science (80-.). 252, 1668–1675.

Bettenbrock, K., Sauter, T., Jahreis, K., Kremling, A., Lengeler, J.W., Gilles, E.D., 2007. Correlation between growth rates, EIIACrr phosphorylation, and intracellular cyclic AMP levels in Escherichia coli K-12. J. Bacteriol. 189, 6891–6900.

Boll, J.M., Hendrixson, D.R., 2011. A specificity determinant for phosphorylation in a response regulator prevents in vivo cross-talk and modification by acetyl phosphate. Proc Natl Acad Sci U S A 108, 20160–20165.

Borden, J.R., Jones, S.W., Indurthi, D., Chen, Y., Terry Papoutsakis, E., 2010. A genomic-library based discovery of a novel, possibly synthetic, acid-tolerance mechanism in Clostridium acetobutylicum involving non-coding RNAs and ribosomal RNA processing. Metab. Eng. 12, 268–281.

Borden, J.R., Papoutsakis, E.T., 2007. Dynamics of genomic-library enrichment and identification of solvent tolerance genes for Clostridium acetobutylicum. Appl. Environ. Microbiol. 73, 3061–3068.

Bowles, L., Ellefson, W., 1985. Effects of Butanol on Clostridium-Acetobutylicum. Appl. Environ. Microbiol. 50, 1165–1170.

Buescher, J.M., Antoniewicz, M.R., Boros, L.G., Burgess, S.C., Brunengraber, H., Clish, C.B., DeBerardinis, R.J., Feron, O., Frezza, C., Ghesquiere, B., Gottlieb, E., Hiller, K., Jones, R.G., Kamphorst, J.J., Kibbey, R.G., Kimmelman, A.C.,

Locasale, J.W., Lunt, S.Y., Maddocks, O.D., Malloy, C., Metallo, C.M., Meuillet, E.J., Munger, J., Nöh, K., Rabinowitz, J.D., Ralser, M., Sauer, U., Stephanopoulos, G., St-Pierre, J., Tennant, D. a, Wittmann, C., Vander Heiden, M.G., Vazquez, A., Vousden, K., Young, J.D., Zamboni, N., Fendt, S.-M., 2015. A roadmap for interpreting ^{13}C metabolite labeling patterns from cells. Curr. Opin. Biotechnol. 34, 189–201.

Cameron, D.C., Tong, I.-T., 1993. Cellular and metabolic engineering. Appl. Biochem. Biotechnol. 38, 105–140.

Caspi, R., Altman, T., Dreher, K., Fulcher, C.A., Subhraveti, P., Keseler, I.M., Kothari, A., Krummenacker, M., Latendresse, M., Mueller, L.A., Ong, Q., Paley, S., Pujar, A., Shearer, A.G., Travers, M., Weerasinghe, D., Zhang, P., Karp, P.D., 2012. The MetaCyc database of metabolic pathways and enzymes and the BioCyc collection of pathway / genome databases. Nucleic Acids Res. 40, 742–753.

Chen, X., Alonso, A.P., Allen, D.K., Reed, J.L., Shachar-Hill, Y., 2011. Synergy between (13)C-metabolic flux analysis and flux balance analysis for understanding metabolic adaptation to anaerobiosis in E. coli. Metab. Eng. 13, 38–48.

Chiang, C., Lee, H.M., Guo, H.J., Wang, Z.W., Lin, L., 2013. Systematic Approach To Engineer Escherichia coli Pathways for Co-Utilization of a Glucose-Xylose Mixture. J. Agric. Food Chem. 61, 7583–7590.

Choi, J., Antoniewicz, M.R., 2011. Tandem mass spectrometry: a novel approach for metabolic flux analysis. Metab. Eng. 13, 225–33.

Choi, J., Grossbach, M.T., Antoniewicz, M.R., 2012. Measuring complete isotopomer distribution of aspartate using gas chromatography/tandem mass spectrometry. Anal. Chem. 84, 4628–32.

Cordova, L.T., Antoniewicz, M.R., 2016. ^{13}C metabolic flux analysis of the extremely thermophilic, fast growing, xylose-utilizing Geobacillus strain LC300. Metab. Eng. 33, 148–157.

Crown, S.B., Antoniewicz, M.R., 2012. Selection of tracers for ^{13}C-metabolic flux analysis using elementary metabolite units (EMU) basis vector methodology. Metab. Eng. 14, 150–61.

Crown, S.B., Antoniewicz, M.R., 2013a. Parallel labeling experiments and metabolic flux analysis: Past, present and future methodologies. Metab. Eng. 16, 21–32.

Crown, S.B., Antoniewicz, M.R., 2013b. Publishing ^{13}C metabolic flux analysis studies: A review and future perspectives. Metab. Eng. 20C, 42–48.

Crown, S.B., Indurthi, D.C., Ahn, W.S., Choi, J., Papoutsakis, E.T., Antoniewicz, M.R., 2011. Resolving the TCA cycle and pentose-phosphate pathway of Clostridium acetobutylicum ATCC 824: Isotopomer analysis, in vitro activities and expression analysis. Biotechnol. J. 6, 300–5.

Crown, S.B., Long, C.P., Antoniewicz, M.R., 2015. Integrated ^{13}C-metabolic flux analysis of 14 parallel labeling experiments in Escherichia coli. Metab. Eng. 28, 151–158.

Crown, S.B., Long, C.P., Antoniewicz, M.R., 2016. Optimal tracers for parallel labeling experiments and ^{13}C metabolic flux analysis: A new precision and synergy scoring system. Submitt. to Metab. Eng.

Curtis, S.J., Epstein, W., 1975. Phosphorylation of D-glucose in Escherichia coli mutants defective in glucosephosphotransferase, mannosephosphotransferase, and glucokinase. J. Bacteriol. 122, 1189–1199.

Dash, S., Mueller, T.J., Venkataramanan, K.P., Papoutsakis, E.T., Maranas, C.D., 2014. Capturing the response of Clostridium acetobutylicum to chemical stressors using a regulated genome-scale metabolic model. Biotechnol. Biofuels 7, 144.

Datsenko, K. a, Wanner, B.L., 2000. One-step inactivation of chromosomal genes in Escherichia coli K-12 using PCR products. Proc. Natl. Acad. Sci. U. S. A. 97, 6640–5.

De Anda, R., Lara, A.R., Hernández, V., Hernández-Montalvo, V., Gosset, G., Bolívar, F., Ramírez, O.T., 2006. Replacement of the glucose phosphotransferase transport system by galactose permease reduces acetate accumulation and improves process performance of Escherichia coli for recombinant protein production without impairment of growth rate. Metab. Eng. 8, 281–290.

Deutscher, J., Aké, F.M.D., Derkaoui, M., Zébré, A.C., Cao, T.N., Bouraoui, H., Kentache, T., Mokhtari, A., Milohanic, E., Joyet, P., 2014. The bacterial phosphoenolpyruvate:carbohydrate phosphotransferase system: regulation by protein phosphorylation and phosphorylation-dependent protein-protein interactions. Microbiol. Mol. Biol. Rev. 78, 231–56.

Deutscher, J., Francke, C., Postma, P.W., 2006. How phosphotransferase system-related protein phosphorylation regulates carbohydrate metabolism in bacteria. Microbiol. Mol. Biol. Rev. 70, 939–1031.

Dürre, P., 1998. New insights and novel developments in clostridial acetone/butanol/isopropanol fermentation. Appl. Microbiol. Biotechnol. 639–648.

Escalante, A., Cervantes, A.S., Gosset, G., Bolívar, F., 2012. Current knowledge of the Escherichia coli phosphoenolpyruvate-carbohydrate phosphotransferase system: Peculiarities of regulation and impact on growth and product formation. Appl. Microbiol. Biotechnol. 94, 1483–1494.

Ezeji, T., Milne, C., Price, N.D., Blaschek, H.P., 2010. Achievements and perspectives to overcome the poor solvent resistance in acetone and butanol-producing microorganisms. Appl. Microbiol. Biotechnol. 85, 1697–712.

Fast, A.G., Schmidt, E.D., Jones, S.W., Tracy, B.P., 2015. Acetogenic mixotrophy: novel options for yield improvement in biofuels and biochemicals production. Curr. Opin. Biotechnol. 33, 60–72.

Fenton, A.W., Reinhart, G.D., 2009. Disentangling the Web of Allosteric Communication in a Homotetramer: Heterotropic Inhibition in Phosphofructokinase from *Escherichia coli*. Biochemistry 48, 12323–12328.

Fernandez, C.A., Des Rosiers, C., Previs, S.F., David, F., Brunengraber, H., 1996. Correction of ^{13}C mass isotopomer distributions for natural stable isotope abundance. J. Mass Spectrom. 31, 255–62.

Flores, N., Xiao, J., Berry, A., Bolivar, F., Valle, F., 1996. Pathway engineering for the production of aromatic compounds in Escherichia coli. Nat. Biotechnol. 14, 620–623.

Fox, D.K., Meadow, N.D., Roseman, S., 1986. Phosphate transfer between acetate kinase and Enzyme I of the bacterial phosphotransferase system. J. Biol. Chem. 261, 13498–13503.

Fu, Y., Yoon, J.M., Jarboe, L., Shanks, J. V, 2015. Metabolic flux analysis of Escherichia coli MG1655 under octanoic acid (C8) stress. Appl. Microbiol. Biotechnol.

Furdui, C., Ragsdale, S.W., 2000. The role of pyruvate ferredoxin oxidoreductase in pyruvate synthesis during autotrophic growth by the Wood-Ljungdahl pathway. J. Biol. Chem. 275, 28494–9.

Gopalakrishnan, S., Maranas, C.D., 2015. 13C metabolic flux analysis at a genome-scale. Metab. Eng. 32, 12–22.

Gosset, G., 2005. Improvement of Escherichia coli production strains by modification of the phosphoenolpyruvate:sugar phosphotransferase system. Microb. Cell Fact. 4, 14.

Guisbert, E., Yura, T., Rhodius, V.A., Gross, C.A., 2008. Convergence of Molecular, Modeling, and Systems Approaches for an Understanding of the Escherichia coli Heat Shock Response. Microbiol. Mol. Biol. Rev. 72, 545–554.

Guzmán, S., Marin, S., Miranda, A., Selivanov, V. a, Centelles, J.J., Harmancey, R., Smih, F., Turkieh, A., Durocher, Y., Zorzano, A., Rouet, P., Cascante, M., 2014. ^{13}C metabolic flux analysis shows that resistin impairs the metabolic response to insulin in L6E9 myotubes. BMC Syst. Biol. 8, 109.

Hanke, T., Nöh, K., Noack, S., Polen, T., Bringer, S., Sahm, H., Wiechert, W., Bott, M., 2013. Combined fluxomics and transcriptomics analysis of glucose catabolism via a partially cyclic pentose phosphate pathway in Gluconobacter oxydans 621H. Appl. Environ. Microbiol. 79, 2336–48.

Hiller, K., Metallo, C.M., 2013. Profiling metabolic networks to study cancer metabolism. Curr. Opin. Biotechnol. 24, 60–8.

Hönicke, D., Janssen, H., Grimmler, C., Ehrenreich, A., Lütke-Eversloh, T., 2012. Global transcriptional changes of Clostridium acetobutylicum cultures with increased butanol: Acetone ratios. N. Biotechnol. 29, 485–493.

Hou, S., Jones, S.W., Choe, L.H., Papoutsakis, E.T., Lee, K.H., 2013. Workflow for quantitative proteomic analysis of Clostridium acetobutylicum ATCC 824 using iTRAQ tags. Methods 61, 269–76.

Huffer, S., Clark, M.E., Ning, J.C., Blanch, H.W., Clark, D.S., 2011. Role of alcohols in growth, lipid composition, and membrane fluidity of yeasts, bacteria, and archaea. Appl. Environ. Microbiol. 77, 6400–6408.

Janssen, H., Grimmler, C., Ehrenreich, A., Bahl, H., Fischer, R.-J., 2012. A transcriptional study of acidogenic chemostat cells of Clostridium acetobutylicum--solvent stress caused by a transient n-butanol pulse. J. Biotechnol. 161, 354–65.

Jeffrey, F.M.H., Roach, J.S., Storey, C.J., Sherry, A.D., Malloy, C.R., 2002. ^{13}C Isotopomer Analysis of Glutamate by Tandem Mass Spectrometry. Anal. Biochem. 300, 192–205.

Jones, D.T., Woods, D.R., 1986. Acetone-butanol fermentation revisited. Microbiol. Rev. 50, 484–524.

Junker, B.H., 2014. Flux analysis in plant metabolic networks: increasing throughput and coverage. Curr. Opin. Biotechnol. 26C, 183–188.

Kanehisa, M., Goto, S., 2000. KEGG : Kyoto Encyclopedia of Genes and Genomes. Nucleic Acids Res. 28, 27–30.

Kanehisa, M., Goto, S., Sato, Y., Furumichi, M., Tanabe, M., 2012. KEGG for integration and interpretation of large-scale molecular data sets. Nucleic Acids Res. 40, 109–114.

Kanehisa, M., Sato, Y., Kawashima, M., Furumichi, M., Tanabe, M., 2016. KEGG as a reference resource for gene and protein annotation. Nucleic Acids Res. 44, D457–D462.

Keibler, M.A., Fendt, S., Stephanopoulos, G., 2012. Expanding the Concepts and Tools of Metabolic Engineering to Elucidate Cancer Metabolism. Biotechnol. Prog. 28, 1409–18.

Kind, S., Becker, J., Wittmann, C., 2013. Increased lysine production by flux coupling of the tricarboxylic acid cycle and the lysine biosynthetic pathway--metabolic engineering of the availability of succinyl-CoA in Corynebacterium glutamicum. Metab. Eng. 15, 184–95.

Kotte, O., Zaugg, J.B., Heinemann, M., 2010. Bacterial adaptation through distributed sensing of metabolic fluxes. Mol. Syst. Biol. 6, 1–9.

Kremling, A., Bettenbrock, K., Gilles, E.D., 2007. Analysis of global control of Escherichia coli carbohydrate uptake. BMC Syst. Biol. 1, 42.

Lee, J., Yun, H., Feist, A.M., Palsson, B.Ø., Lee, S.Y., 2008. Genome-scale reconstruction and in silico analysis of the Clostridium acetobutylicum ATCC 824 metabolic network. Appl. Microbiol. Biotechnol. 80, 849–62.

Lee, S.K., Chou, H., Ham, T.S., Lee, T.S., Keasling, J.D., 2008. Metabolic engineering of microorganisms for biofuels production : from bugs to synthetic biology to fuels. Curr. Opin. Biotechnol. 19, 556–563.

Leighty, R.W., Antoniewicz, M.R., 2011. Dynamic metabolic flux analysis (DMFA): a framework for determining fluxes at metabolic non-steady state. Metab. Eng. 13, 745–55.

Leighty, R.W., Antoniewicz, M.R., 2012. Parallel labeling experiments with [U-^{13}C]glucose validate E. coli metabolic network model for ^{13}C metabolic flux analysis. Metab. Eng. 14, 533–41.

Leighty, R.W., Antoniewicz, M.R., 2013. COMPLETE-MFA: Complementary parallel labeling experiments technique for metabolic flux analysis. Metab. Eng. 20C, 49–55.

Li, R., Chen, Q., Wang, P.G., Qi, Q., 2007. A novel-designed Escherichia coli for the production of various polyhydroxyalkanoates from inexpensive substrate mixture. Appl. Microbiol. Biotechnol. 75, 1103–1109.

Linton, K.J., Higgins, C.F., 1998. The Escherichia coli ATP-binding cassette (ABC) proteins. Mol. Microbiol. 28, 5–13.

Long, C.P., Antoniewicz, M.R., 2014a. Metabolic flux analysis of Escherichia coli knockouts: lessons from the Keio collection and future outlook. Curr. Opin. Biotechnol. 28, 127–133.

Long, C.P., Antoniewicz, M.R., 2014b. Quantifying biomass composition by gas chromatography/mass spectrometry. Anal. Chem. 86, 9423–9427.

Long, C.P., Gonzalez, J.E., Sandoval, N.R., Antoniewicz, M.R., 2016. Characterization of physiological responses to 22 gene knockouts in Escherichia coli central carbon metabolism. Metab. Eng. In Press.

Mao, S., Luo, Y., Bao, G., Zhang, Y., Li, Y., Ma, Y., 2011. Comparative analysis on the membrane proteome of Clostridium acetobutylicum wild type strain and its butanol-tolerant mutant. Mol. Biosyst. 7, 1660–1677.

Mao, S., Luo, Y., Zhang, T., Li, J., Bao, G., Zhu, Y., Chen, Z., Zhang, Y., Li, Y., Ma, Y., 2010. Proteome reference map and comparative proteomic analysis between a wild type clostridium acetobutylicumDSM 1731 and its mutant with enhanced butanol tolerance and butanol yield. J. Proteome Res. 9, 3046–3061.

Masakapalli, S.K., Kruger, N.J., Ratcliffe, R.G., 2013. The metabolic flux phenotype of heterotrophic Arabidopsis cells reveals a complex response to changes in nitrogen supply. Plant J. 74, 569–82.

Masakapalli, S.K., Ratcliffe, R.G., Williams, T.C.R., 2014a. Quantification of ^{13}C enrichments and isotopomer abundances for metabolic flux analysis using 1D NMR spectroscopy. Methods Mol. Biol. 1090, 73–86.

Masakapalli, S.K., Ritala, A., Dong, L., van der Krol, A.R., Oksman-Caldentey, K.-M., Ratcliffe, R.G., Sweetlove, L.J., 2014b. Metabolic flux phenotype of tobacco hairy roots engineered for increased geraniol production. Phytochemistry 99, 73–85.

Matsuoka, Y., Shimizu, K., 2010. Current status of 13C-metabolic flux analysis and future perspectives. Process Biochem. 45, 1873–1881.

McConnell, B.O., Antoniewicz, M.R., 2016. Measuring the Composition and Stable-Isotope Labeling of Algal Biomass Carbohydrates via Gas Chromatography/Mass Spectrometry. Anal. Chem. acs.analchem.6b00779.

Metallo, C.M., Walther, J.L., Stephanopoulos, G., 2009. Evaluation of 13C isotopic tracers for metabolic flux analysis in mammalian cells. J. Biotechnol. 144, 167–174.

Meza, E., Becker, J., Bolivar, F., Gosset, G., Wittmann, C., 2012. Consequences of phosphoenolpyruvate:sugar phosphotranferase system and pyruvate kinase isozymes inactivation in central carbon metabolism flux distribution in Escherichia coli. Microb. Cell Fact. 11, 127.

Miranda-Santos, I., Gramacho, S., Pineiro, M., Martinez-Gomez, K., Fritz, M., Hollemeyer, K., Salvador, A., Heinzle, E., 2015. Mass isotopomer analysis of nucleosides isolated from RNA and DNA using GC/MS. Anal. Chem. 87, 617–623.

Moon, H.G., Jang, Y., Cho, C., Lee, J., Binkley, R., Lee, S.Y., 2016. One hundred years of clostridial butanol fermentation.

Murphy, T. a, Dang, C. V, Young, J.D., 2013. Isotopically nonstationary ^{13}C flux analysis of Myc-induced metabolic reprogramming in B-cells. Metab. Eng. 15, 206–17.

Nargund, S., Misra, A., Zhang, X., Coleman, G.D., Sriram, G., 2014. Flux and reflux: metabolite reflux in plant suspension cells and its implications for isotope-assisted metabolic flux analysis. Mol. Biosyst. 10, 1496–508.

Nargund, S., Sriram, G., 2013. Designer labels for plant metabolism: statistical design of isotope labeling experiments for improved quantification of flux in complex plant metabolic networks. Mol. Biosyst. 9, 99–112.

Nicolaou, S. a, Gaida, S.M., Papoutsakis, E.T., 2010. A comparative view of metabolite and substrate stress and tolerance in microbial bioprocessing: From biofuels and chemicals, to biocatalysis and bioremediation. Metab. Eng. 12, 307–31.

Niklas, J., Schneider, K., Heinzle, E., 2010. Metabolic flux analysis in eukaryotes. Curr. Opin. Biotechnol. 21, 63–9.

Nolling, J., Breton, G., Omelchenko, M. V., Makarova, K.S., Zeng, Q., Gibson, R., Lee, H.M., Dubois, J., Qiu, D., Hitti, J., Teams, G.S.C.P.F. and B., Wolf, Y.I., Tatusov, R.L., Sabathe, F., Doucette-stamm, L., Soucaille, P., Daly, M.J., Bennett, G.N., Koonin, E. V, Smith, D.R., 2001. Genome Sequence and Comparative Analysis of the Solvent-Producing Bacterium Clostridium acetobutylicum. J. Bacteriol. 183, 4823–4838.

Okahashi, N., Kajihata, S., Furusawa, C., Shimizu, H., 2014. Reliable Metabolic Flux Estimation in Escherichia coli Central Carbon Metabolism Using Intracellular Free Amino Acids. Metabolites 4, 408–20.

Papoutsakis, E.T., 1984. Equations and calculations for fermentations of butyric acid bacteria. Biotechnol. Bioeng. 26, 174–87.

Papoutsakis, E.T., 2008. Engineering solventogenic clostridia. Curr. Opin. Biotechnol. 19, 420–9.

Paredes, C.J., Alsaker, K. V, Papoutsakis, E.T., 2005. A comparative genomic view of clostridial sporulation and physiology. Nat. Rev. Microbiol. 3, 969–78.

Peabody, G., Kao, K.C., 2016. Recent progress in bio-butanol tolerance in microbial systems with an emphasis on Clostridium. FEMS Microbiol. Lett. 363, 1–6.

Postma, P.W., Lengeler, J.W., Jacobson, G.R., 1993. Phosphoenolpyruvate:carbohydrate phosphotransferase systems of bacteria. Microbiol. Rev. 57, 543–594.

Quek, L.-E., Dietmair, S., Krömer, J.O., Nielsen, L.K., 2010. Metabolic flux analysis in mammalian cell culture. Metab. Eng. 12, 161–171.

Ramseier, T.M., 1996. Cra and the control of carbon flux via metabolic pathways. Res. Microbiol. 147, 489–493.

Ranganathan, S., Tee, T.W., Chowdhury, A., Zomorrodi, A.R., Yoon, J.M., Fu, Y., Shanks, J. V, Maranas, C.D., 2012. An integrated computational and experimental study for overproducing fatty acids in Escherichia coli. Metab. Eng. 14, 687–704.

Rühl, M., Rupp, B., Nöh, K., Wiechert, W., Sauer, U., Zamboni, N., 2012. Collisional fragmentation of central carbon metabolites in LC-MS/MS increases precision of ^{13}C metabolic flux analysis. Biotechnol. Bioeng. 109, 763–771.

Sandberg, T.E., Long, C.P., Gonzalez, J.E., Feist, A.M., Antoniewicz, M.R., Palsson, B.O., 2016. Evolution of E. coli on [U-^{13}C]Glucose Reveals a Negligible Isotopic

Influence on Metabolism and Physiology. PLoS One 11, e0151130.

Schellenberger, J., Zielinski, D.C., Choi, W., Madireddi, S., Portnoy, V., Scott, D.A., Reed, J.L., Osterman, A.L., Palsson, B., 2012. Predicting outcomes of steady-state ^{13}C isotope tracing experiments using Monte Carlo sampling. BMC Syst. Biol. 6, 1–14.

Schirch, V., Hopkins, S., Villar, E., Angelaccio, S., 1985. Serine hydroxymethyltransferase from *Escherichia coli*: purification and properties. J. Bacteriol. 163, 1–7.

Schwarz, K.M., Kuit, W., Grimmler, C., Ehrenreich, A., Kengen, S.W., 2012. A transcriptional study of acidogenic chemostat cells of Clostridium acetobutylicum - Cellular behavior in adaptation to n-butanol. J Biotechnol 161, 366–77.

Senger, R.S., Papoutsakis, E.T., 2008. Genome-scale model for Clostridium acetobutylicum: Part I. Metabolic network resolution and analysis. Biotechnol. Bioeng. 101, 1036–52.

Sheikholeslami, Z., Jolicoeur, M., Henry, O., 2014. Elucidating the effects of postinduction glutamine feeding on the growth and productivity of CHO cells. Biotechnol. Prog. 30, 535–46.

Stephanopoulos, G., 2007. Challenges in Engineering Microbes for Biofuels Production. Science (80-.). 315, 801–805.

Stephanopoulos, G., 2008. Metabolic engineering: enabling technology for biofuels production. Metab. Eng. 10, 293–4.

Stephanopoulos, G., Aristidou, A.A., Nielsen, J., 1998. Metabolic Engineering: Principles and Methodologies.

Swarup, A., Lu, J., Dewoody, K.C., Antoniewicz, M.R., 2014. Metabolic network reconstruction, growth characterization and ^{13}C-metabolic flux analysis of the extremophile Thermus thermophilus HB8. Metab. Eng. 24, 173–180.

Tang, J.K., You, L., Blankenship, R.E., Tang, Y.J., 2012. Recent advances in mapping environmental microbial metabolisms through ^{13}C isotopic fingerprints. J. R. Soc. interface 9, 2767–2780.

Tang, Y.J., Martin, H.G., Myers, S., Rodriguez, S., Baidoo, E.E.K., Keasling, J.D., 2009a. Advances in analysis of microbial metabolic fluxes via 13C isotopic labeling. Mass Spectrom. Rev. 28, 362–375.

Tang, Y.J., Sapra, R., Joyner, D., Hazen, T.C., Myers, S., Reichmuth, D., Blanch, H., Keasling, J.D., 2009b. Analysis of metabolic pathways and fluxes in a newly discovered thermophilic and ethanol-tolerant geobacillus strain. Biotechnol. Bioeng. 102, 1377–1386.

Templeton, N., Lewis, A., Dorai, H., Qian, E. a, Campbell, M.P., Smith, K.D., Lang, S.E., Betenbaugh, M.J., Young, J.D., 2014. The impact of anti-apoptotic gene Bcl-2Δ expression on CHO central metabolism. Metab. Eng. 25, 92–102.

Tomas, C. a., Welker, N.E., Papoutsakis, E.T., 2003. Overexpression of groESL in Clostridium acetobutylicum results in increased solvent production and tolerance, prolonged metabolism, and changes in the cell's transcriptional program. Appl. Environ. Microbiol. 69, 4951–4965.

Tomas, C.A., Beamish, J., Papoutsakis, E.T., 2004. Transcriptional Analysis of Butanol Stress and Tolerance in Clostridium acetobutylicum. J. Bacteriol. 186, 2006–18.

Toya, Y., Shimizu, H., 2013. Flux analysis and metabolomics for systematic metabolic engineering of microorganisms. Biotechnol. Adv. 31, 818–826.

Tracy, B.P., Jones, S.W., Fast, A.G., Indurthi, D.C., Papoutsakis, E.T., 2012. Clostridia: the importance of their exceptional substrate and metabolite diversity for biofuel and biorefinery applications. Curr. Opin. Biotechnol. 23, 364–81.

Trauchessec, M., Jaquinod, M., Bonvalot, A., Brun, V., Bruley, C., Ropers, D., de Jong, H., Garin, J., Bestel-Corre, G., Ferro, M., 2014. Mass Spectrometry-based Workflow for Accurate Quantification of Escherichia coli Enzymes: How Proteomics Can Play a Key Role in Metabolic Engineering. Mol. Cell. Proteomics 13, 954–968.

Truong, Q.X., Yoon, J.M., Shanks, J. V, 2014. Isotopomer measurement techniques in metabolic flux analysis I: nuclear magnetic resonance. Methods Mol. Biol. 1083, 65–83.

Valente, K.N., Lenhoff, A.M., Lee, K.H., 2015. Expression of difficult-to-remove host cell protein impurities during extended Chinese hamster ovary cell culture and their impact on continuous bioprocessing. Biotechnol. Bioeng. 112, 1232–1242.

Venkataramanan, K.P., Jones, S.W., McCormick, K.P., Kunjeti, S.G., Ralston, M.T., Meyers, B.C., Papoutsakis, E.T., 2013. The Clostridium small RNome that responds to stress: the paradigm and importance of toxic metabolite stress in C. acetobutylicum. BMC Genomics 14, 849.

Venkataramanan, K.P., Min, L., Hou, S., Jones, S.W., Ralston, M.T., Lee, K.H., Papoutsakis, E.T., 2015. Complex and extensive post-transcriptional regulation revealed by integrative proteomic and transcriptomic analysis of metabolite stress response in Clostridium acetobutylicum. Biotechnol. Biofuels 8, 81.

Walther, J.L., Metallo, C.M., Zhang, J., Stephanopoulos, G., 2012. Optimization of ^{13}C isotopic tracers for metabolic flux analysis in mammalian cells. Metab. Eng. 14, 162–71.

Wang, Q., Venkataramanan, K.P., Huang, H., Papoutsakis, E.T., Wu, C.H., 2013. Transcription factors and genetic circuits orchestrating the complex, multilayered response of Clostridium acetobutylicum to butanol and butyrate stress. BMC Syst. Biol. 7, 120.

Wiechert, W., 2001. 13C metabolic flux analysis. Metab. Eng. 3, 195–206.

Wiechert, W., Nöh, K., 2013. Isotopically non-stationary metabolic flux analysis: complex yet highly informative. Curr. Opin. Biotechnol.

Wu, B., Zhang, B., Feng, X., Rubens, J.R., Huang, R., Hicks, L.M., Pakrasi, H.B., Tang, Y.J., 2010. Alternative isoleucine synthesis pathway in cyanobacterial species. Microbiology 156, 596–602.

Wurm, F.M., 2004. Production of recombinant protein therapeutics in cultivated mammalian cells. Nat. Biotechnol. 22, 1393–1398.

Xu, M., Zhao, J., Yu, L., Tang, I.C., Xue, C., Yang, S.T., 2014. Engineering Clostridium acetobutylicum with a histidine kinase knockout for enhanced n-butanol tolerance and production. Appl. Microbiol. Biotechnol. 99, 1011–1022.

Yoo, H., Antoniewicz, M.R., Stephanopoulos, G., Kelleher, J.K., 2008. Quantifying reductive carboxylation flux of glutamine to lipid in a brown adipocyte cell line. J. Biol. Chem. 283, 20621–7.

Young, J., Walther, J., Antoniewicz, M.R., Yoo, H., Stephanopoulos, G., 2008. An elementary metabolite unit (EMU) based method of isotopically nonstationary flux analysis. Biotechnol. Bioeng. 99, 686–699.

Young, J.D., 2014. ^{13}C metabolic flux analysis of recombinant expression hosts. Curr. Opin. Biotechnol. 30, 238–245.

Zamboni, N., 2011. 13C metabolic flux analysis in complex systems. Curr. Opin. Biotechnol. 22, 103–8.

Appendix A

SUPPLEMENTARY DATA FOR CHAPTER 2

Table A.1: Metabolic network models of *Clostridium acetobutylicum* used for ^{13}C metabolic flux analysis.

B = base model (initial model, constructed based on KEGG and BioCyc databases and two published genome-scale models)

E = extended model (model with additional reactions that were found to improve the fits of ^{13}C-labeling data)

M = minimal model (smallest model that could still produce an acceptable fit of all ^{13}C-labeling data in this study)

Glycolysis

[B E M] v_1 Gluc.ext (abcdef) + ATP → G6P (abcdef) + ADP

[B E M] v_2 G6P (abcdef) ↔ F6P (abcdef)

[B E M] v_3 F6P (abcdef) + ATP → FBP (abcdef) + ADP

[B E M] v_4 FBP (abcdef) ↔ DHAP (cba) + GAP (def)

[B E M] v_5 DHAP (abc) ↔ GAP (abc)

[B E M] v_6 GAP (abc) + ADP + NAD ↔ 3PG (abc) + ATP + NADH

[B E M] v_7 3PG (abc) ↔ PEP (abc)

Table A.1 continued

[B E M] v_8 PEP (abc) + ADP → Pyr (abc) + ATP

Pentose Phosphate Pathway

[B E] v_9 G6P (abcdef) + NADP → 6PG (abcdef) + NADPH

[B E] v_{10} 6PG (abcdef) + NADP → Ru5P (bcdef) + CO2 (a) + NADPH

[B E M] v_{11} Ru5P (abcde) ↔ X5P (abcde)

[B E M] v_{12} Ru5P (abcde) ↔ R5P (abcde)

[B E M] v_{13} X5P (abcde) ↔ TK-C2 (ab) + GAP (cde)

[B E M] v_{14} F6P (abcdef) ↔ TK-C2 (ab) + E4P (cdef)

[B E M] v_{15} S7P (abcdefg) ↔ TK-C2 (ab) + R5P (cdefg)

[B E M] v_{16} F6P (abcdef) ↔ TA-C3 (abc) + GAP (def)

[B E M] v_{17} S7P (abcdefg) ↔ TA-C3 (abc) + E4P (defg)

Entner-Doudoroff Pathway

[B E] v_{18} 6PG (abcdef) → KDPG (abcdef)

[B E] v_{19} KDPG (abcdef) → Pyr (abc) + GAP (def)

Pyruvate Metabolism

[B E M] v_{20} Pyr (abc) → AcCoA (bc) + Form (a)

[E M]* v_{21} Pyr (abc) ↔ PFOR-C2 (bc) + CO2 (a)

Table A.1 continued

[B E M] v_{22} PFOR-C2 (ab) + 2 oxFd → AcCoA (ab) + 2 redFd

TCA Cycle

[B E M] v_{23} OAC (abcd) + AcCoA (ef) → Cit (efbcda)

[B E M] v_{24} Cit (abcdef) ↔ ICit (abcdef)

[B E M] v_{25} ICit (abcdef) + NADP ↔ AKG (abcde) + CO2 (f) + NADPH

[B E] v_{26} AKG (abcde) + 2 oxFd → SucCoA (bcde) + CO2 (a) + 2 redFd

[B E M] v_{27} SucCoA (abcd) + ADP ↔ Suc (½ abcd + ½ dcba) + ATP

[B E] v_{28} Suc (½ abcd + ½ dcba) + NAD → Fum (½ abcd + ½ dcba) + NADH

[B E M] v_{29} Fum (½ abcd + ½ dcba) ↔ Mal (abcd)

[B E] v_{30} Mal (abcd) + NAD ↔ OAC (abcd) + NADH

Amphibolic Reactions

[B E M] v_{31} Mal (abcd) + NADP → Pyr (abc) + CO2 (d) + NADPH

[B E M] v_{32} Pyr (abc) + CO2 (d) + ATP → OAC (abcd) + ADP

Acid and Solvent Formation

[B E M] v_{33} AcCoA (ab) + ADP → Ac (ab) + ATP

[B E M] v_{34} Pyr (abc) + Pyr (def) → Acn (cbef) + CO2 (a) + CO2 (d)

[B E M] v_{35} Pyr (abc) → Acetal (bc) + CO2 (a)

Table A.1 continued

[B E M] v_{36} Acetal (ab) + NADH ↔ EtOH (ab) + NAD

[B E M] v_{37} AcCoA (ab) + NADH → Acetal (ab) + NAD

[B E M] v_{38} AcCoA (ab) + AcCoA (cd) ↔ AcAcCoA (abcd)

[B E M] v_{39} AcAc (abcd) → Acne (bcd) + CO2 (a)

[B E M] v_{40} AcAcCoA (abcd) + NADPH + NADH → BtCoA (abcd) + NADP + NAD

[B E M] v_{41} BtCoA (abcd) + ADP → Bt (abcd) + ATP

[B E M] v_{42} BtCoA (abcd) + 2 NADH → BtOH (abcd) + 2 NAD

[B E M] v_{43} Bt (abcd) + AcAcCoA (efgh) → BtCoA (abcd) + AcAc (efgh)

[B E M] v_{44} Ac (ab) + AcAcCoA (cdef) → AcCoA (ab) + AcAc (cdef)

Amino Acid Biosynthesis

[B E M] v_{45} AKG (abcde) + NADPH + NH3 ↔ Glu (abcde) + NADP

[B E M] v_{46} Glu (abcde) + ATP + NH3 ↔ Gln (abcde) + ADP

[B E M] v_{47} Glu (abcde) + ATP + 2 NADPH → Pro (abcde) + ADP + 2 NADP

[B E M] v_{48} Glu (abcde) + CO2 (f) + Gln (ghijk) + Asp (lmno) + 4 ATP + NADPH →
Arg (abcdef) + AKG (ghijk) + Fum (lmno) + 3 ADP + AMP + NADP

[B E M] v_{49} OAC (abcd) + Glu (efghi) → Asp (abcd) + AKG (efghi)

[B E M] v_{50} Asp (abcd) + Gln (efghi) + ATP ↔ Asn (abcd) + Glu (efghi) + AMP

[B E M] v_{51} Pyr (abc) + Glu (defgh) ↔ Ala (abc) + AKG (defgh)

[B E M] v_{52} 3PG (abc) + Glu (defgh) + NAD → Ser (abc) + AKG (defgh) + NADH

Table A.1 continued

[B E M]	v_{53}	Pyr (abc) ↔ Ser (abc)
[B E M]	v_{54}	Ser (abc) ↔ Gly (ab) + MEETHF (c)
[B E]	v_{55}	Gly (ab) + NAD ↔ CO2 (a) + MEETHF (b) + NADH + NH3
[B E M]*	v_{56}	Thr (abcd) → Gly (ab) + Acetal (cd)
[B E M]	v_{57}	Ser (abc) + AcCoA (de) + 2 ATP + 3 NADPH + redTRX + SO4 → Cys (abc) + Ac (de) + ADP + AMP + 3 NADP + oxTRX
[B E M]	v_{58}	Asp (abcd) + Pyr (efg) + Glu (hijkl) + SucCoA (mnop) + ATP + 2 NADPH → LL-DAP (½ abcdgfe + ½ efgdcba) + AKG (hijkl) + Suc (½ mnop + ½ ponm) + ADP + 2 NADP
[B E M]	v_{59}	LL-DAP (½ abcdefg + ½ gfedcba) → Lys (abcdef) + CO2 (g)
[B E M]	v_{60}	Asp (abcd) + 2 ATP + 2 NADPH → Thr (abcd) + 2 ADP + 2 NADP
[B E M]	v_{61}	Asp (abcd) + METHF (e) + Cys (fgh) + SucCoA (ijkl) + ATP + 2 NADPH → Met (abcde) + Pyr (fgh) + Suc (½ ijkl + ½ lkji) + ADP + 2 NADP + NH3
[B E M]	v_{62}	Pyr (abc) + Pyr (def) + Glu (ghijk) + NADPH → Val (abcef) + CO2 (d) + AKG (ghijk) + NADP
[B E M]	v_{63}	AcCoA (ab) + Pyr (cde) + Pyr (fgh) + Glu (ijklm) + NADPH + NAD → Leu (abdghe) + CO2 (c) + CO2 (f) + AKG (ijklm) + NADP + NADH
[E]	v_{64}	Thr (abcd) + Pyr (efg) + Glu (hijkl) + NADPH → Ile (abfcdg) + CO2 (e) + AKG (hijkl) + NADP + NH3

Table A.1 continued

[B E] v_{65} Asp (abcd) + Pyr (efg) + Glu (hijkl) + SucCoA (mnop) + ATP + 3 NADPH → Ile (abfcdg) + CO2 (e) + AKG (hijkl) + Suc(mnop) + ADP + 3 NADP + NH3

[E M] v_{66} Pyr (abc) + Pyr (def) + AcCoA (gh) + Glu (ijklm) + NAD + NADPH → Ile (ghbefc) + CO2 (a) + CO2 (d) + AKG(ijklm) + NADH + NADP

[B E M] v_{67} PEP (abc) + PEP (def) + E4P (ghij) + Glu (klmno) + ATP + NADPH → Phe (abcefghij) + CO2 (d) + AKG (klmno) + ADP + NADP

[B E M] v_{68} PEP (abc) + PEP (def) + E4P (ghij) + Glu (klmno) + ATP + NAD + NADPH →

Tyr (abcefghij) + CO2 (d) + AKG (klmno) + ADP + NADH + NADP

[B E M] v_{69} Ser (abc) + R5P (defgh) + PEP (ijk) + E4P (lmno) + PEP (pqr) + Gln (stuvw) + 2 ATP + NADPH → Trp (abcedklmnoj) + CO2 (i) + GAP (fgh) + Pyr (pqr) + Glu (stuvw) + ADP + AMP + NADP

[B E M] v_{70} R5P (abcde) + FTHF (f) + Gln (ghijk) + Asp (lmno) + 4 ATP + 2 NAD → His (edcbaf) + AKG (ghijk) + Fum (lmno) + 3 ADP + AMP + 2 NADH

One-Carbon Metabolism

[B E M] v_{71} MEETHF (a) + NADH → METHF (a) + NAD

[B E M] v_{72} MEETHF (a) + NADP ↔ FTHF (a) + NADPH

[B E M] v_{73} Form (a) + ATP → FTHF (a) + ADP

Table A.1 continued

Redox Metabolism

[B E M] v_{74} 2 redFd + NAD ↔ 2 oxFd + NADH

[B E M] v_{75} 2 redFd + NADP ↔ 2 oxFd + NADPH

[B E M] v_{76} 2 redFd → 2 oxFd + H2

Energy metabolism

[B E M]* v_{77} ATP → ADP

[B E M] v_{78} ATP + AMP → 2 ADP

Transport

[B E M] v_{79} CO2 (a) → CO2.ext (a)

[B E M] v_{80} H2 → H2.ext

[B E M] v_{81} Ac (ab) → Ac.ext (ab)

[B E M] v_{82} Bt (abcd) → Bt.ext (abcd)

[B E M] v_{83} Acne (abc) → Acne.ext (abc)

[B E M] v_{84} BtOH (abcd) → BtOH.ext (abcd)

[B E M] v_{85} EtOH (ab) → EtOH.ext (ab)

[B E M] v_{86} Acn (abcd) → Acn.ext (abcd)

[B E M] v_{87} NH3.ext → NH3

[B E M] v_{88} SO4.ext → SO4

Table A.1 continued

Biomass Formation

[B E M]* v_{89} 0.410 Ala + 0.070 Arg + 0.082 Asn + 0.082 Asp + 0.643 Cys + 0.067 Glu + 0.067 Gln + 0.570 Gly + 0.077 His + 0.230 Ile + 0.227 Leu + 0.188 Lys + 0.414 Met + 0.098 Phe + 0.241 Pro + 0.226 Ser + 0.217 Thr + 0.023 Trp + 0.423 Tyr + 0.619 Val + 0.267 G6P + 0.225 F6P + 0.338 R5P + 0.597 GAP + 0.256 3PG + 0.107 PEP + 0.335 Pyr + 1.813 AcCoA + 0.112 AKG + 0.284 OAC + 0.194 MEETHF + 26.281 ATP + 0.763 NAD + 4.207 NADPH → 37.28 Biomass + 26.281 ADP + 0.763 NADH + 4.207 NADP

Dilution fluxes

[E M]* v_{90} CO2.unlabeled (a) + CO2 (b) → CO2 (a) + CO2.sink (b)

[E M]* v_{91} Ac.unlabeled (ab) + AcCoA (cd) → AcCoA (ab) + Ac.sink (cd)

Notes:

- Reaction 21 was initially treated as irreversible in the base model (i.e. reactions 21 and 22 were lumped together).
- Reaction 56 was treated as reversible in the base model and extended model. The reaction was treated as irreversible in the minimal model.
- Reaction 77 describes utilization of ATP for cellular processes not captured in the rest of the model.
- Reaction 89. The biomass composition reported in the genome-scale model by Lee et al. (2008) was used for the biomass reaction.

- Reaction 90. The net effect of this reaction is the exchange of intracellular CO_2 for an unlabeled CO_2 without affecting intracellular carbon balances. This reaction captures endogenous production of unlabeled CO_2, for example, due to metabolism of unlabeled biomass metabolites.
- Reaction 91. This reaction captures the uptake and metabolism of unlabeled acetate that was present in our growth medium. The net effect of this reaction is the exchange of intracellular AcCoA for an unlabeled AcCoA without affecting intracellular carbon balances.

Table A.2: Results of ^{13}C-MFA for C. acetobutylicum grown in parallel batch cultures with [1-^{13}C] and [U-^{13}C]glucose tracers.

Shown are the estimated net and exchange fluxes (normalized to glucose uptake rate of 100).
Accurate 95% confidence intervals of fluxes (LB95 = lower bound, UB95 = upper bound) were determined by evaluating the sensitivity of the minimized SSR to flux variations (Antoniewicz et al., 2006)

	Model used for ^{13}C-MFA:	Extended Model			Minimal Model		
	Data sets used for ^{13}C-MFA :	[U]Gluc, Repl. 1 [U]Gluc, Repl. 2 [1]Gluc, Repl. 1 [1]Gluc, Repl. 2			[U]Gluc, Repl. 1 [U]Gluc, Repl. 2 [1]Gluc, Repl. 1 [1]Gluc, Repl. 2		
	SSR :	312			320		
	Fit statistically accepted :	Yes			Yes		
INTRACELLULAR FLUXES							
Flux No.	Reaction	Best Fit	LB95	UB95	Best Fit	LB95	UB95
1	Gluc.Ext + ATP -> G6P + ADP	100.0	99.9	100.1	100.0	99.9	100.1
2	G6P <=> F6P (net)	99.5	99.3	99.6	99.5	99.4	99.6
3	F6P + ATP -> FBP + ADP	98.2	97.9	98.4	98.2	97.9	98.5
4	FBP <=> DHAP + GAP (net)	98.2	97.9	98.4	98.2	97.9	98.5
5	DHAP <=> GAP (net)	98.2	97.9	98.4	98.2	97.9	98.5
6	GAP + NAD + ADP <=> 3PG + ATP + NADH (net)	194.3	193.5	195.1	194.4	193.6	195.2
7	3PG <=> PEP (net)	187.8	184.2	191.5	189.0	185.8	192.2
8	PEP + ADP -> Pyr + ATP	185.6	181.9	189.3	186.8	183.5	190.1
9	G6P + NADP -> 6PG + NADPH	0.0	0.0	0.2	not present in model		
10	6PG + NADP -> Ru5P + CO2 + NADPH	0.0	0.0	0.2	not present in model		
11	Ru5P <=> X5P (net)	-0.9	-1.0	-0.8	-0.9	-1.0	-0.8
12	Ru5P <=> R5P (net)	0.9	0.8	1.0	0.9	0.8	1.0
13	X5P <=> GAP + E-C2 (net)	-0.9	-1.0	-0.8	-0.9	-1.0	-0.8
14	F6P <=> E4P + E-C2 (net)	1.0	0.8	1.1	0.9	0.8	1.1
15	S7P <=> R5P + E-C2 (net)	-0.1	-0.1	-0.1	-0.1	-0.1	-0.1
16	F6P <=> GAP + E-C3 (net)	-0.1	-0.1	-0.1	-0.1	-0.1	-0.1
17	S7P <=> E4P + E-C3 (net)	0.1	0.1	0.1	0.1	0.1	0.1
18	6PG -> KDPG	0.0	0.0	0.2	not present in model		

Table A.2 continued

19	KDPG -> GAP + Pyr	0.0	0.0	0.2	not present in model		
20	Pyr -> AcCoA + Form	2.3	0.9	3.0	2.0	1.5	2.6
21	Pyr <=> CO2 + PFOR-C2 (net)	177.5	174.3	180.5	177.7	174.2	180.8
22	PFOR-C2 + 2 oxfd -> AcCoA + 2 refd	177.5	174.3	180.5	177.7	174.2	180.8
23	AcCoA + OAC -> Cit	1.0	0.9	1.4	1.0	0.9	1.2
24	Cit <=> ICit (net)	1.0	0.9	1.4	1.0	0.9	1.2
25	ICit + NADP <=> AKG + CO2 + NADPH (net)	1.0	0.9	1.4	1.0	0.9	1.2
26	AKG + 2 oxfd -> SucCoA + CO2 + 2 refd	0.0	0.0	0.4	not present in model		
27	SucCoA + ADP <=> Suc + ATP (net)	-1.1	-1.3	-0.8	-1.1	-1.3	-1.0
28	Suc + NAD -> Fum + NADH	0.0	0.0	0.4	not present in model		
29	Fum <=> Mal (net)	0.3	0.2	0.7	0.3	0.2	0.3
30	Mal + NAD <=> OAC + NADH (net)	-21.6	-217.1	0.0	not present in model		
31	Mal + NADP -> Pyr + CO2 + NADPH	21.9	0.2	217.3	0.3	0.2	0.3
32	Pyr + CO2 + ATP -> OAC + ADP	26.9	4.4	223.0	5.5	4.7	6.3
33	AcCoA + ADP -> Ac + ATP	30.4	24.8	35.0	30.9	24.8	35.1
34	2 Pyr -> Acn + 2 CO2	0.1	0.0	1.0	0.1	0.0	1.0
35	Pyr -> Acetal + CO2	0.0	0.0	0.6	0.0	0.0	0.5
36	Acetal + NADH <=> EtOH + NAD (net)	1.6	0.6	2.2	1.8	1.2	2.4
37	AcCoA + NADH -> Acetal + NAD	0.0	0.0	0.4	0.0	0.0	0.5
38	2 AcCoA <=> AcAcCoA (net)	72.0	69.5	74.5	72.0	69.3	74.5
39	AcAc -> Acne + CO2	2.3	0.4	4.2	2.3	0.4	4.2
40	AcAcCoA + NADPH + NADH -> BtCoA + NADP + NAD	69.7	66.7	72.7	69.7	66.5	72.7
41	BtCoA + ADP -> Bt + ATP	65.0	61.5	69.5	64.6	61.4	69.6
42	BtCoA + 2 NADH -> BtOH + 2 NAD	5.1	4.1	6.0	5.1	4.1	6.0
43	Bt + AcAcCoA -> BtCoA + AcAc	0.4	0.0	4.2	0.0	0.0	4.2
44	AcAcCoA + Ac -> AcAc + AcCoA	1.9	0.0	4.2	2.3	0.0	4.2

Table A.2 continued

45	AKG + NH3 + NADPH <=> Glu + NADP (net)	15.0	11.1	18.6	14.0	10.2	17.8
46	Glu + ATP + NH3 <=> Gln + ADP (net)	0.6	0.5	0.7	0.6	0.5	0.7
47	Glu + ATP + 2 NADPH -> Pro + ADP + 2 NADP	0.5	0.4	0.5	0.4	0.4	0.5
48	Glu + CO2 + Gln + Asp + 4 ATP + NADPH -> Arg + AKG + Fum + 3 ADP + AMP +	0.1	0.1	0.1	0.1	0.1	0.1
49	OAC + Glu <=> Asp + AKG (net)	3.7	2.9	4.4	3.9	3.2	4.6
50	Asp + Gln + ATP <=> Asn + Glu + AMP (net)	0.2	0.1	0.2	0.2	0.1	0.2
51	Pyr + Glu <=> Ala + AKG (net)	0.8	0.7	0.9	0.8	0.7	0.9
52	3PG + Glu + NAD -> Ser + NADH + AKG	6.0	2.5	9.5	4.9	2.1	8.0
53	Pyr + NH3 <=> Ser (net)	-4.3	-8.1	-0.3	-3.2	-7.0	0.0
54	Ser <=> Gly + MEETHF (net)	-0.8	-1.2	0.0	-0.8	-1.4	-0.2
55	Gly + NAD <=> CO2 + MEETHF + NH3 + NADH (net)	-0.2	-0.8	0.3	not present in model		
56	Thr <=> Gly + Acetal (net)	1.6	0.9	2.2	1.8	1.2	2.4
57	SO4 + AcCoA + Ser + reTRX + 3 NADPH + 2 ATP -> Cys + Ac + oxTRX + 3 NADP +	2.0	1.7	2.3	2.0	1.7	2.2
58	Asp + Pyr + Glu + SucCoA + ATP + 2 NADPH -> LL-DAP + AKG + Suc + ADP +	0.4	0.3	0.4	0.3	0.3	0.4
59	LL-DAP -> Lys + CO2	0.4	0.3	0.4	0.3	0.3	0.4
60	Asp + 2 ATP + 2 NADPH -> Thr + 2 ADP + 2 NADP	2.0	1.3	2.6	2.2	1.6	2.8
61	Asp + SucCoA + Cys + METHF + ATP + 2 NADPH -> Met + Suc + Pyr + NH3 +	0.8	0.7	0.9	0.8	0.7	0.9
62	2 Pyr + Glu + NADPH -> Val + CO2 + AKG + NADP	1.2	1.0	1.3	1.2	1.0	1.3
63	2 Pyr + AcCoA + Glu + NADPH + NAD -> Leu + 2 CO2 + AKG + NADP + NADH	0.4	0.4	0.5	0.4	0.4	0.5

Table A.2 continued

64	Thr + Pyr + Glu + NADPH -> Ile + CO2 + AKG + NADP + NH3	0.0	0.0	0.0	not present in model		
65	Asp + SucCoA + Pyr + Glu + ATP + 3 NADPH -> Ile + CO2 + AKG + Suc + NH3 +	0.0	0.0	0.0	not present in model		
66	AcCoA + 2 Pyr + NAD + NADPH + Glu -> Ile + 2 CO2 + NADH + NADP + AKG	0.4	0.4	0.5	0.4	0.4	0.5
67	2 PEP + E4P + Glu + ATP + NADPH -> Phe + AKG + CO2 + ADP + NADP	0.2	0.2	0.2	0.2	0.2	0.2
68	2 PEP + E4P + Glu + NADPH + NAD + ATP -> Tyr + CO2 + AKG + NADP + NADH +	0.8	0.7	0.9	0.8	0.7	0.9
69	2 PEP + E4P + R5P + Gln + Ser + 2 ATP + NADPH -> Trp + GAP + Pyr + Glu +	0.0	0.0	0.0	0.0	0.0	0.0
70	R5P + Gln + Asp + 4 ATP + 2 NAD + FTHF -> His + AKG + Fum + AMP + 3 ADP +	0.1	0.1	0.2	0.1	0.1	0.2
71	MEETHF + NADH -> METHF + NAD	0.8	0.7	0.9	0.8	0.7	0.9
72	MEETHF + NADP <=> FTHF + NADPH (net)	-2.1	-2.9	-0.7	-1.9	-2.5	-1.3
73	Form + ATP -> FTHF + ADP	2.3	0.9	3.0	2.0	1.5	2.6
74	2 refd + NAD <=> 2 oxfd + NADH (net)	-99.7	-126.3	97.8	-120.2	-124.6	-115.9
75	2 refd + NADP <=> 2 oxfd + NADPH (net)	88.2	-111.8	116.0	108.7	102.1	115.3
76	2 refd -> 2 oxfd + H2	189.1	182.0	196.6	189.2	181.3	197.1
77	ATP -> ADP	182.6	0.0	217.4	205.7	191.5	220.0
78	ATP + AMP -> 2 ADP	2.5	2.1	2.8	2.4	2.1	2.8
79	CO2 -> CO2.Ext	179.8	176.4	183.1	180.0	176.4	183.6
80	H2 -> H2.Ext	189.1	182.0	196.6	189.2	181.3	197.1
81	Ac -> Ac.Ext	30.6	26.8	34.4	30.6	26.8	34.4
82	Bt -> Bt.Ext	64.6	61.5	67.7	64.6	61.4	67.8
83	Acne -> Acne.Ext	2.3	0.4	4.2	2.3	0.4	4.2
84	BtOH -> BtOH.Ext	5.1	4.1	6.0	5.1	4.1	6.0
85	EtOH -> EtOH.Ext	1.6	0.6	2.2	1.8	1.2	2.4

Table A.2 continued

86	Acn -> Acn.Ext	0.1	0.0	1.0	0.1	0.0	1.0
87	NH3.Ext -> NH3	10.7	9.4	12.2	10.6	9.2	12.0
88	SO4.Ext -> SO4	2.0	1.7	2.3	2.0	1.7	2.2
89	0.410 Ala + 0.070 Arg + 0.082 Asn + 0.082 Asp + … -> Biomass + …	1.9	1.6	2.1	1.9	1.6	2.1
90	CO2.unlabeled + CO2 -> CO2 + CO2.sink	18.8	16.9	20.1	19.3	17.5	21.1
91	Ac.unlabeled + AcCoA -> AcCoA + Ac.sink	82.1	78.0	86.8	80.6	76.6	84.8
EXCHANGE FLUXES							
2	G6P <=> F6P (exch)	130.0	0.0	Inf	604.8	0.0	Inf
4	FBP <=> DHAP + GAP (exch)	12.1	0.0	Inf	3.1	0.0	Inf
5	DHAP <=> GAP (exch)	73.3	0.0	Inf	48.4	0.0	Inf
6	GAP + NAD + ADP <=> 3PG + ATP + NADH (exch)	9.7	0.0	Inf	161.8	0.0	Inf
7	3PG <=> PEP (exch)	34.6	0.0	Inf	127.0	0.0	Inf
11	Ru5P <=> X5P (exch)	144.0	0.0	Inf	6.4	0.0	Inf
12	Ru5P <=> R5P (exch)	0.0	0.0	Inf	58.1	0.0	Inf
13	X5P <=> GAP + E-C2 (exch)	127.6	0.0	Inf	26.7	0.0	Inf
14	F6P <=> E4P + E-C2 (exch)	12.3	11.2	13.8	12.3	10.7	13.8
15	S7P <=> R5P + E-C2 (exch)	0.0	0.0	Inf	47.2	0.0	Inf
16	F6P <=> GAP + E-C3 (exch)	0.0	0.0	2.2	0.0	0.0	2.2
17	S7P <=> E4P + E-C3 (exch)	11.8	0.0	Inf	0.0	0.0	Inf
21	Pyr <=> CO2 + PFOR-C2 (exch)	244.4	238.5	253.5	246.2	236.4	256.7
24	Cit <=> ICit (exch)	64.7	0.0	Inf	22.9	0.0	Inf
25	ICit + NADP <=> AKG + CO2 + NADPH (exch)	21.8	0.0	Inf	104.6	0.0	Inf
27	SucCoA + ADP <=> Suc + ATP (exch)	25.5	0.0	Inf	141.3	0.0	Inf
29	Fum <=> Mal (exch)	0.0	0.0	Inf	149.5	0.0	Inf
30	Mal + NAD <=> OAC + NADH (exch)	0.0	0.0	Inf	not present in model		
36	Acetal + NADH <=> EtOH + NAD (exch)	13.8	0.0	Inf	57.9	0.0	Inf
38	2 AcCoA <=> AcAcCoA (exch)	46.2	0.0	Inf	85.0	0.0	Inf

Table A.2 continued

45	AKG + NH3 + NADPH <=> Glu + NADP (exch)	66.0	0.0	Inf	46.6	0.0	Inf
46	Glu + ATP + NH3 <=> Gln + ADP (exch)	49.8	0.0	Inf	12.7	0.0	Inf
49	OAC + Glu <=> Asp + AKG (exch)	12.2	0.0	Inf	27.5	0.0	Inf
50	Asp + Gln + ATP <=> Asn + Glu + AMP (exch)	12.2	0.0	Inf	0.0	0.0	Inf
51	Pyr + Glu <=> Ala + AKG (exch)	0.0	0.0	Inf	73.9	0.0	Inf
53	Pyr + NH3 <=> Ser (exch)	0.0	0.0	0.1	0.0	0.0	0.1
54	Ser <=> Gly + MEETHF (exch)	0.5	0.2	1.4	0.3	0.2	0.4
55	Gly + NAD <=> CO2 + MEETHF + NH3 + NADH (exch)	0.0	0.0	1.3	not present in model		
56	Thr <=> Gly + Acetal (exch)	0.1	0.0	0.1	not present in model		
72	MEETHF + NADP <=> FTHF + NADPH (exch)	38.2	0.0	Inf	1019.0	0.0	Inf
74	2 refd + NAD <=> 2 oxfd + NADH (exch)	0.0	0.0	Inf	31.7	0.0	Inf
75	2 refd + NADP <=> 2 oxfd + NADPH (exch)	60.8	0.0	Inf	16.6	0.0	Inf
FRACTIONALABELING OF GLUCOSE (D-VALUE)							
1	Fractional labeling of Gluc.ext	56%	56%	56%	56%	56%	56%
FRACTIONALABELING OF AMINO ACIDS (G-VALUES)							
1	Fractional labeling of Ala (data set #1)	82%	81%	82%	82%	81%	83%
2	Fractional labeling of Gly (data set #1)	80%	79%	81%	80%	79%	81%
3	Fractional labeling of Val (data set #1)	80%	80%	81%	80%	80%	81%
4	Fractional labeling of Leu (data set #1)	78%	77%	79%	78%	77%	79%
5	Fractional labeling of Ile (data set #1)	80%	79%	81%	80%	79%	81%
6	Fractional labeling of Pro (data set #1)	78%	77%	79%	78%	77%	79%

Table A.2 continued

7	Fractional labeling of Ser (data set #1)	81%	81%	82%	82%	81%	82%
8	Fractional labeling of Thr (data set #1)	80%	79%	80%	80%	79%	81%
9	Fractional labeling of Phe (data set #1)	82%	81%	82%	82%	81%	83%
10	Fractional labeling of Asp (data set #1)	81%	80%	81%	81%	80%	82%
11	Fractional labeling of Glu (data set #1)	81%	80%	82%	81%	80%	82%
12	Fractional labeling of Tyr (data set #1)	84%	83%	85%	84%	83%	86%
13	Fractional labeling of Ala (data set #2)	82%	81%	83%	82%	81%	83%
14	Fractional labeling of Gly (data set #2)	80%	79%	81%	80%	79%	81%
15	Fractional labeling of Val (data set #2)	81%	80%	81%	81%	80%	82%
16	Fractional labeling of Leu (data set #2)	78%	77%	79%	78%	77%	79%
17	Fractional labeling of Ile (data set #2)	80%	79%	81%	80%	79%	81%
18	Fractional labeling of Pro (data set #2)	79%	78%	80%	79%	78%	80%
19	Fractional labeling of Ser (data set #2)	81%	81%	82%	82%	81%	82%
20	Fractional labeling of Thr (data set #2)	80%	79%	81%	80%	80%	81%
21	Fractional labeling of Phe (data set #2)	82%	81%	82%	82%	81%	82%
22	Fractional labeling of Asp (data set #2)	81%	80%	81%	81%	80%	81%
23	Fractional labeling of Glu (data set #2)	82%	81%	82%	82%	81%	83%
24	Fractional labeling of Tyr (data set #2)	85%	83%	86%	85%	83%	86%
25	Fractional labeling of Ala (data set #3)	73%	72%	75%	73%	72%	75%
26	Fractional labeling of Gly (data set #3)	4%	0%	100%	0%	0%	100%
27	Fractional labeling of Val (data set #3)	73%	72%	75%	74%	72%	75%

Table A.2 continued

28	Fractional labeling of Leu (data set #3)	71%	70%	73%	71%	70%	73%
29	Fractional labeling of Ile (data set #3)	72%	70%	74%	72%	70%	73%
30	Fractional labeling of Pro (data set #3)	72%	70%	74%	72%	70%	74%
31	Fractional labeling of Ser (data set #3)	72%	68%	75%	73%	71%	75%
32	Fractional labeling of Thr (data set #3)	70%	69%	72%	70%	69%	72%
33	Fractional labeling of Phe (data set #3)	76%	74%	78%	76%	74%	78%
34	Fractional labeling of Asp (data set #3)	72%	70%	74%	72%	71%	74%
35	Fractional labeling of Glu (data set #3)	74%	73%	75%	74%	73%	76%
36	Fractional labeling of Tyr (data set #3)	83%	0%	100%	0%	0%	100%
37	Fractional labeling of Ala (data set #4)	71%	70%	73%	71%	70%	73%
38	Fractional labeling of Gly (data set #4)	12%	0%	100%	1%	0%	100%
39	Fractional labeling of Val (data set #4)	72%	70%	73%	72%	70%	73%
40	Fractional labeling of Leu (data set #4)	69%	67%	70%	69%	67%	70%
41	Fractional labeling of Ile (data set #4)	69%	68%	71%	69%	68%	71%
42	Fractional labeling of Pro (data set #4)	70%	68%	71%	70%	68%	72%
43	Fractional labeling of Ser (data set #4)	70%	67%	73%	71%	69%	73%
44	Fractional labeling of Thr (data set #4)	70%	68%	71%	70%	68%	71%
45	Fractional labeling of Phe (data set #4)	75%	73%	76%	75%	73%	76%
46	Fractional labeling of Asp (data set #4)	71%	69%	72%	71%	69%	72%
47	Fractional labeling of Glu (data set #4)	71%	69%	72%	71%	69%	72%
48	Fractional labeling of Tyr (data set #4)	84%	0%	100%	17%	0%	100%

Table A.3: Growth data for C. acetobutylicum grown in parallel batch cultures with [1-^{13}C] and [U-^{13}C]glucose tracers.

[U-^{13}C]glucose tracer experiment - biological replicate 1

Time [hr]	OD600 [-]	YSI Glucose [mM]	HPLC Glucose [mM]	HPLC Acetate [mM]	HPLC Butyrate [mM]
1.5	0.049	104.0	113.7	45.3	N/D
6.0	0.162	106.0	111.5	45.7	0.2
7.0	0.276	205.0	210.6	37.5	1.8
9.5	1.260	213.0	209.6	40.2	8.5

[U-^{13}C]glucose tracer experiment - biological replicate 2

Time [hr]	OD600 [-]	YSI Glucose [mM]	HPLC Glucose [mM]	HPLC Acetate [mM]	HPLC Butyrate [mM]
1.5	0.051	104.0	117.6	46.3	N/D
6.0	0.151	106.0	115.4	46.0	0.6
7.0	0.236	201.5	221.0	41.4	0.8
9.5	1.329	206.0	205.6	42.2	8.6

[1-^{13}C]glucose tracer experiment - biological replicate 1

Time [hr]	OD600 [-]	YSI Glucose [mM]	HPLC Glucose [mM]	HPLC Acetate [mM]	HPLC Butyrate [mM]
1.5	0.052	105.0	118.0	44.7	N/D
6.0	0.197	105.0	112.2	45.9	0.9
7.0	0.576	200.0	204.8	39.3	7.4
9.5	1.531	191.0	189.3	43.3	10.2

Table A.3 continued

[1-^{13}C]glucose tracer experiment - biological replicate 1					
Time [hr]	OD600 [-]	YSI Glucose [mM]	HPLC Glucose [mM]	HPLC Acetate [mM]	HPLC Butyrate [mM]
1.5	0.050	105.0	117.0	46.3	N/D
6.0	0.307	104.0	107.5	44.5	1.9
7.0	0.444	210.0	212.6	41.9	3.2
9.5	1.886	194.0	195.6	44.3	12.0

* Bolus of [U-^{13}C]glucose or [1-^{13}C]glucose added at 6.5 h
* Cells harvested at 9.5 h for GC-MS analysis

Appendix B

SUPPLEMENTARY DATA FOR CHAPTER 4

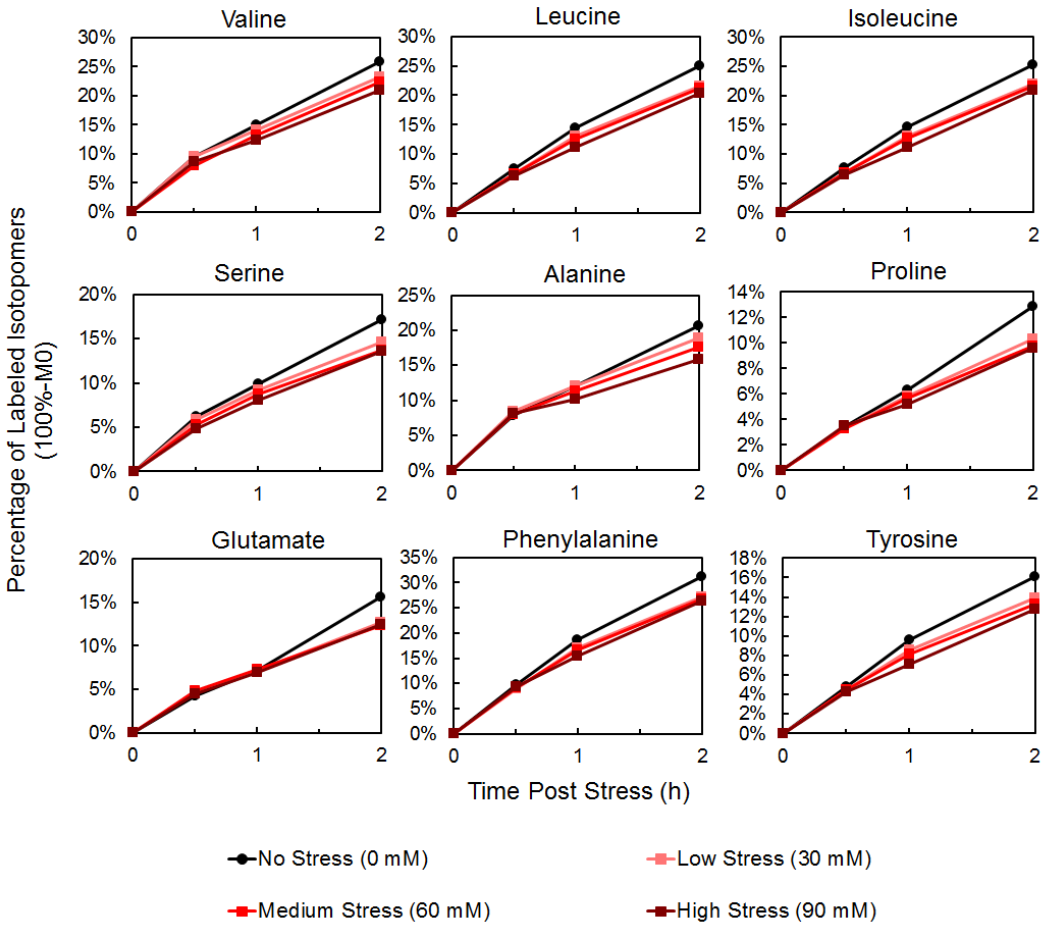

Figure B.1: Short term effects of butanol stress on labeling of biomass amino acids in *C. acetobutylicum*. Time profiles of isotopic labeling are shown for the two hours after introducing [U-^{13}C]glucose, unlabeled aspartate, and varying levels of butanol stress. Percentages of ^{13}C-labeled mass isotopomers (100%-M0) of intracellular metabolites were determined from the measured mass isotopomer distributions, after correction for natural isotope abundances.

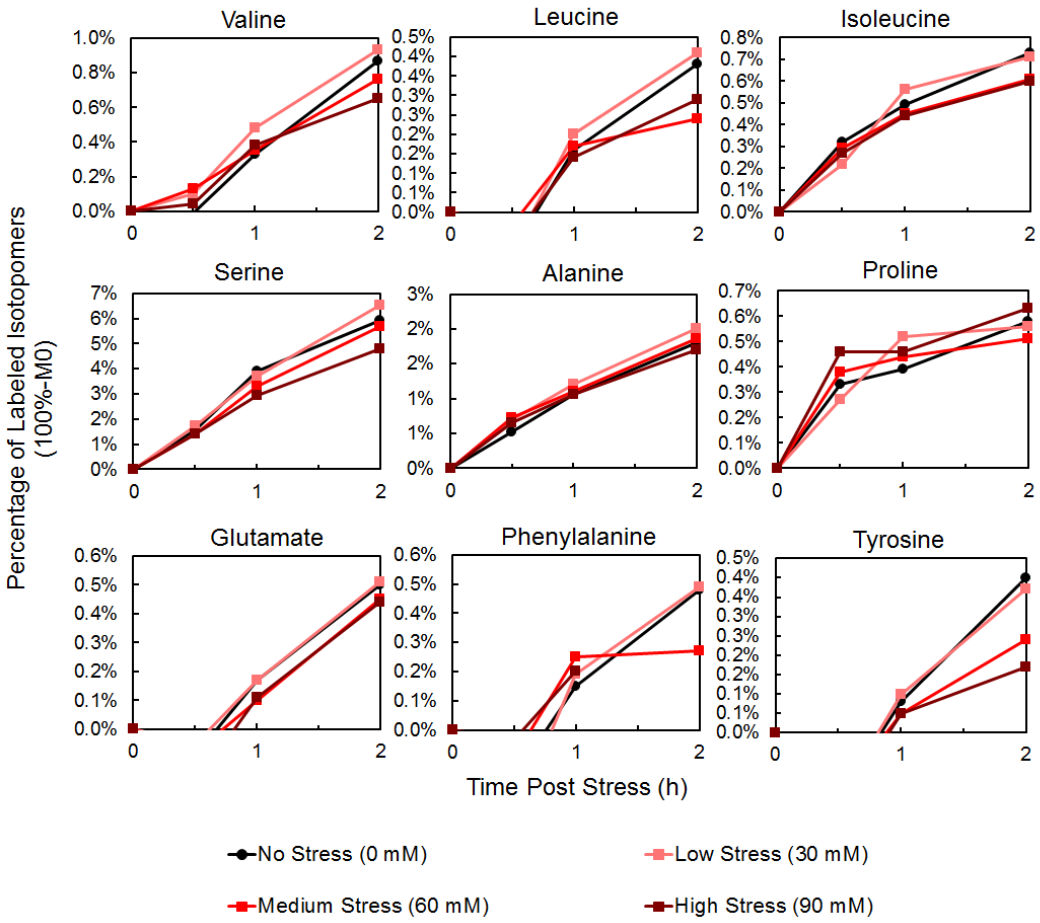

Figure B.2: Short term effects of butanol stress on labeling of biomass amino acids in *C. acetobutylicum*. Time profiles of isotopic labeling are shown for the two hours after introducing [1-^{13}C]aspartate, unlabeled glucose, and varying levels of butanol stress. Percentages of ^{13}C-labeled mass isotopomers (100%-M0) of intracellular metabolites were determined from the measured mass isotopomer distributions, after correction for natural isotope abundances.

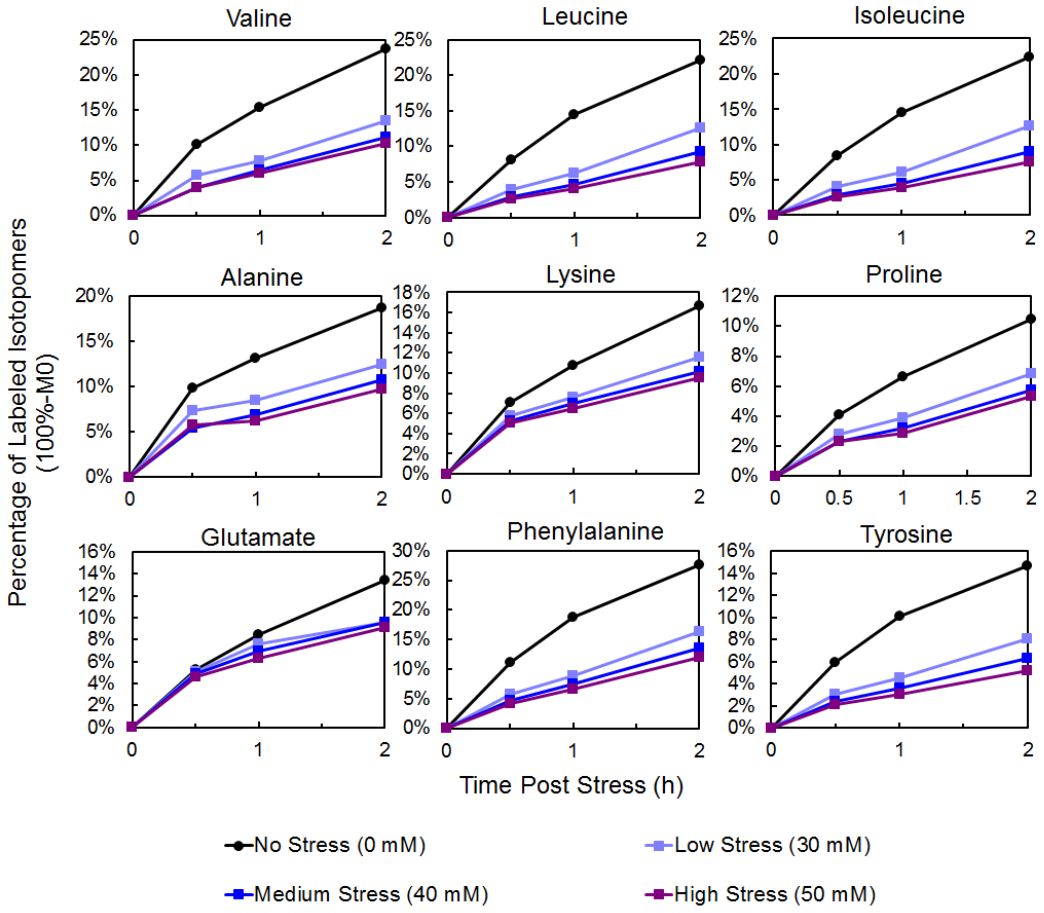

Figure B.3: Short term effects of butyric acid stress on labeling of biomass amino acids in *C. acetobutylicum*. Time profiles of isotopic labeling are shown for the two hours after introducing [U-^{13}C]glucose, unlabeled aspartate, and varying levels of butyric acid stress. Percentages of ^{13}C-labeled mass isotopomers (100%-M0) of intracellular metabolites were determined from the measured mass isotopomer distributions, after correction for natural isotope abundances.

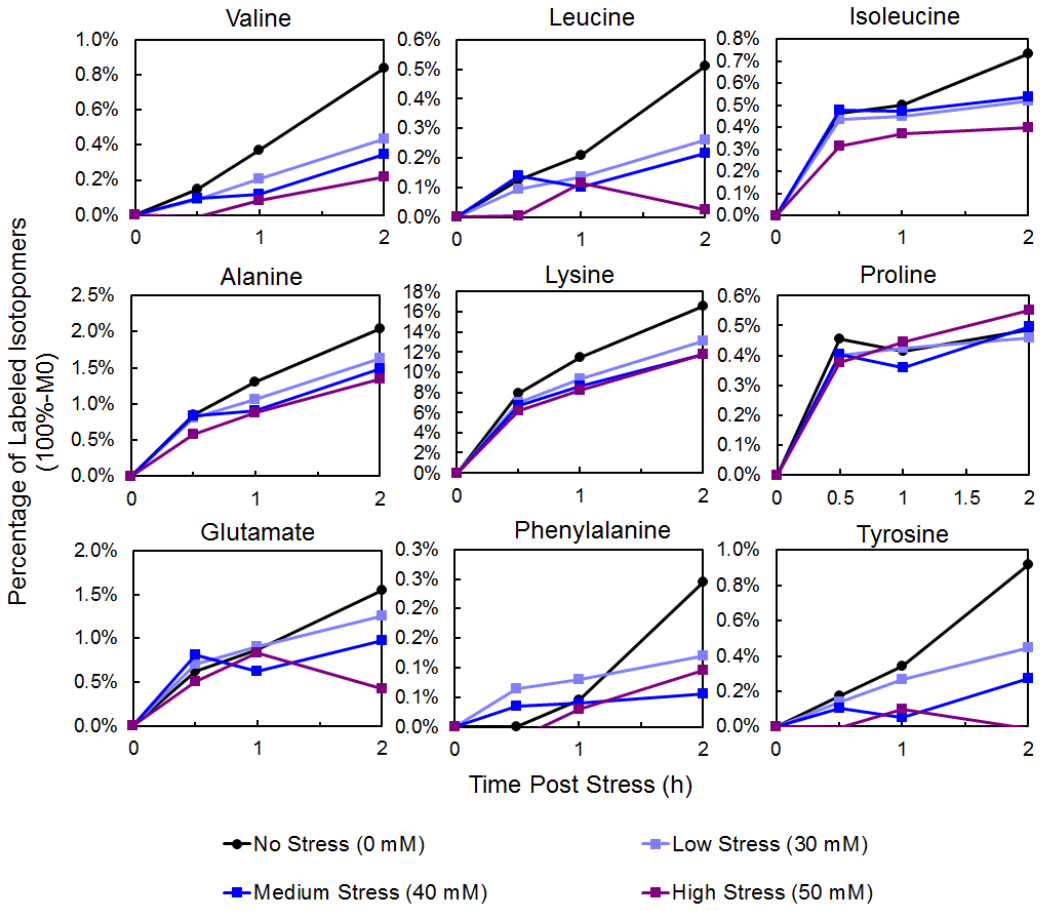

Figure B.4: Short term effects of butyric acid stress on labeling of biomass amino acids in *C. acetobutylicum*. Time profiles of isotopic labeling are shown for the two hours after introducing [1-^{13}C]aspartate, unlabeled glucose, and varying levels of butyric acid stress. Percentages of ^{13}C-labeled mass isotopomers (100%-M0) of intracellular metabolites were determined from the measured mass isotopomer distributions, after correction for natural isotope abundances.

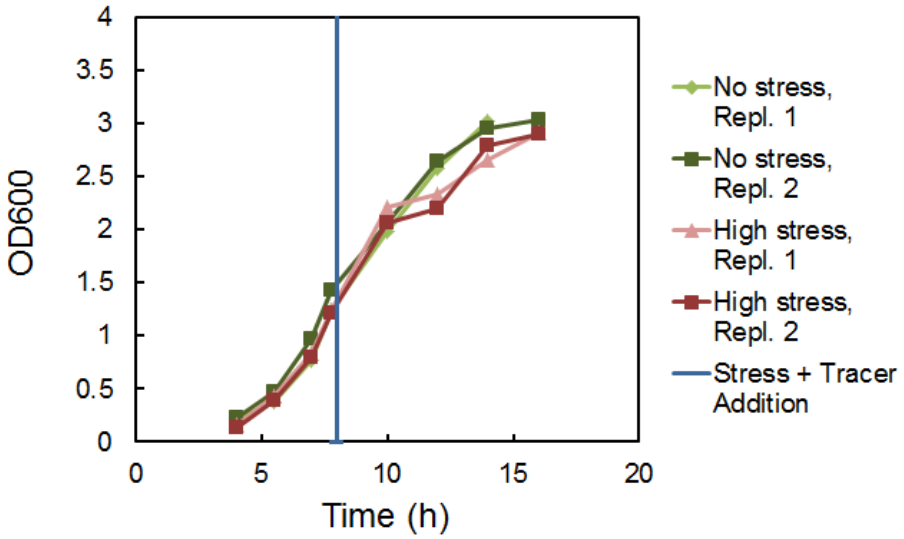

Figure B.5: Growth profiles of cultures with no stress and a high level of butanol stress in long term stress experiments. Two replicates are shown for each condition. Blue line indicates time at which [U-^{13}C]glucose and butanol were added to the cultures.

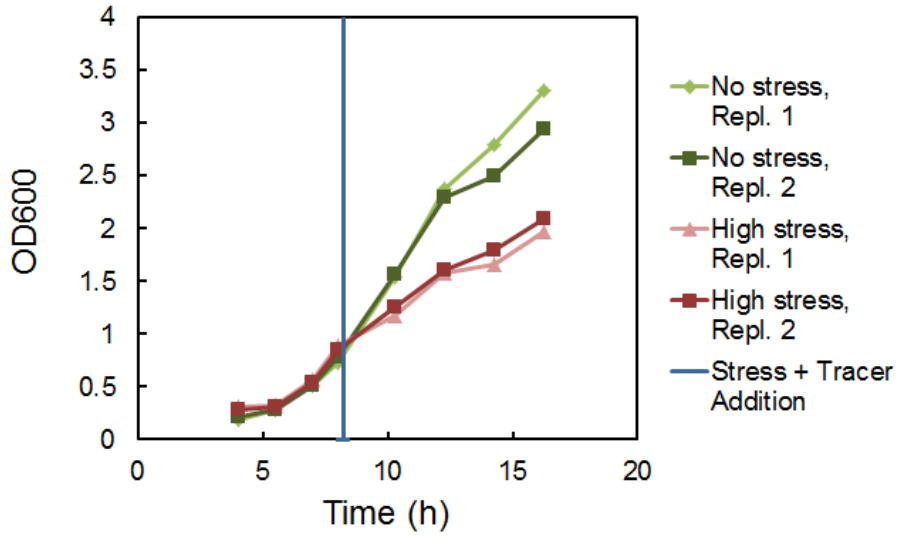

Figure B.6: Growth profiles of cultures with no stress and a high level of butyric acid stress in long term stress experiments. Two replicates are shown for each condition. Blue line indicates time at which [U-^{13}C]glucose and butyric acid were added to the cultures.

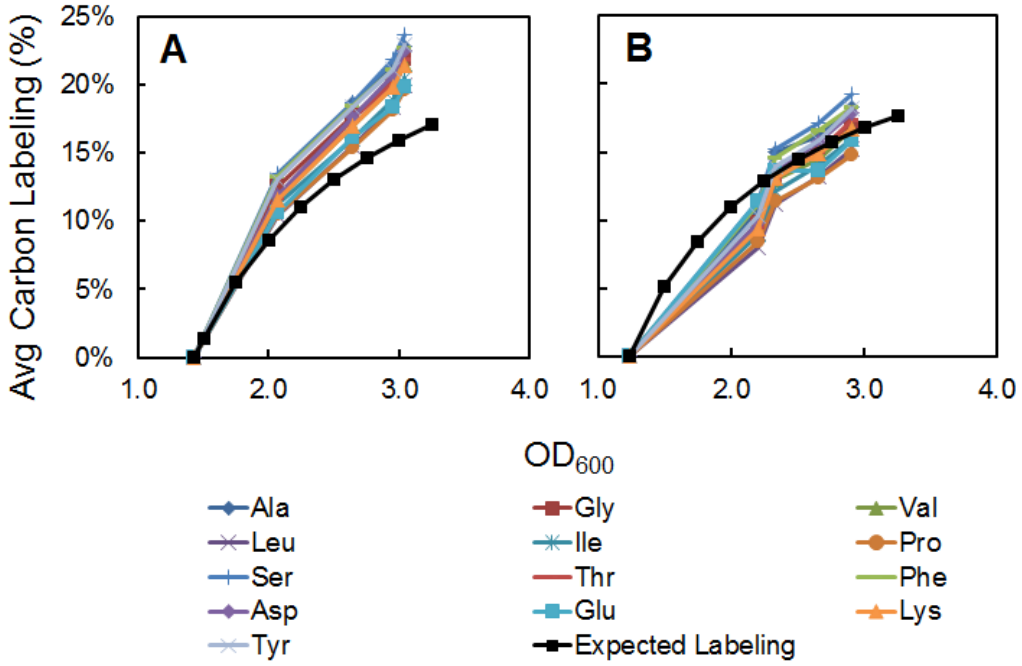

Figure B.7: Long term effects of butanol stress on labeling of biomass amino acids. Average carbon labeling profiles of biomass amino acids from an (A) unstressed (0 mM butanol) culture and (B) high stress (90 mM butanol) culture. The first replicate of each culture is shown in Fig. 4.4. Labeling profiles are plotted against OD_{600} values measured in the eight hours after butanol and [U-^{13}C]glucose addition. Expected labeling curves in (A) and (B) were determined based on the measured percentage of [U-^{13}C]glucose in the medium of each culture.

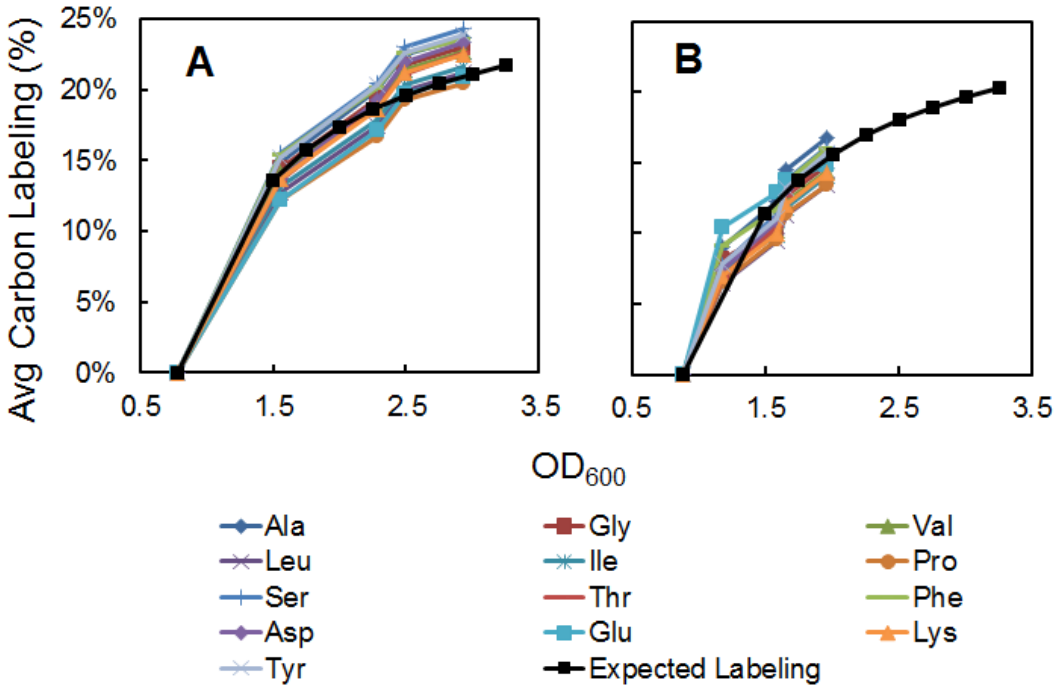

Figure B.8: Long term effects of butyric acid stress on labeling of biomass amino acids. Average carbon labeling profiles of biomass amino acids from an (A) unstressed (0 mM butyric acid) culture and (B) high stress (50 mM butyric acid) culture. The first replicate of each culture is shown in Fig.4.5. Labeling profiles are plotted against OD_{600} values measured in the eight hours after butyric acid and [U-^{13}C]glucose addition. Expected labeling curves in (A) and (B) were determined based on the measured percentage of [U-^{13}C]glucose in the medium of each culture.

Appendix C

CALCULATING THE PERCENTAGE OF PEP FROM PYRUVATE

C.1 Correction of Amino Acid Data for Unlabeled Biomass (After Natural Abundance Correction)

Since we are measuring labeling of amino acids from hydrolyzed biomass proteins, the mass isotopomer data must be corrected for unlabeled biomass that was present prior to the introduction of ^{13}C-alanine. The fraction of *old unlabeled* biomass and fraction of *new* biomass (i.e. generated after the introduction of ^{13}C-alanine) is calculated as follows:

Fraction of *old unlabeled* biomass = Ala_{M0}

Fraction of *new* biomass = $1 - Ala_{M0}$

The mass isotopomer data of other amino acids, e.g. valine, can then be corrected for the presence of *old unlabeled* biomass as follows:

$$Val_{M0}^{corr} = \frac{Val_{M0} - Ala_{M0}}{1 - Ala_{M0}} \qquad \text{(for M0)}$$

$$Val_{Mi}^{corr} = \frac{Val_{Mi}}{1 - Ala_{M0}} \qquad \text{(for Mi, i> 0)}$$

C.2 Tracer Experiments with [1-^{13}C]Alanine

For [1-^{13}C]alanine tracer experiments, the fraction of PEP derived from pyruvate is calculated from the M1 labeling of pyruvate and M1 labeling of PEP. Labeling of pyruvate is inferred from that of valine. GC-MS analysis of valine produces *m/z* 288 fragment which contains C1-5 of valine. C1 of valine is derived from C1 of pyruvate, and the remaining carbons are derived from C2-3 of pyruvate. Since carbons C2-3 of pyruvate are unlabeled, the M1 labeling of *m/z* 288 fragment reflects the M1 labeling of pyruvate:

$$Pyr_{M1} = Val288_{M1}^{corr}$$

The M1 labeling of PEP is inferred from the M1 labeling of *m/z* 302 fragment of phenylalanine, which contains C1-2 of phenylalanine that are derived from C1-2 of PEP:

$$PEP_{M1} = Phe302_{M1}^{corr}$$

Thus, the fraction of PEP derived from pyruvate is calculated as follows:

$$\%PEP\ from\ Pyr = \frac{PEP_{M1}}{Pyr_{M1}} = \frac{Phe302_{M1}^{corr}}{Val288_{M1}^{corr}} = \frac{Phe302_{M1}/(1-Ala260_{M0})}{Val288_{M1}/(1-Ala260_{M0})} = \frac{Phe302_{M1}}{Val288_{M1}}$$

In the above equation, we have assumed that the contribution of oxaloacetate to PEP_{M1} is minimal, which we have confirmed by measuring aspartate M1 labeling, which was negligible (see Fig 5.2 in Chapter 5).

C.3 Tracer Experiments with [U-^{13}C]Alanine

For [U-^{13}C]alanine tracer experiments, the fraction of PEP derived from pyruvate is calculated from the inferred M3 labeling of pyruvate and M3 labeling of PEP. Cells grown on glucose or xylose should only produce either unlabeled (M0) or fully labeled (M3) pyruvate. Given the minimal partial labeling (as confirmed by analyzing *m/z* 260 and 288 fragments of valine), the abundance of unlabeled (M0) pyruvate can be estimated by taking the square root of the M0 abundance of the *m/z* 260 fragment of valine, which is derived from C2-3 + C2-3 of pyruvate. Subtracting this value from 1 yields an estimate for the amount of fully labeled (M3) pyruvate.

$$Pyr_{M0} = \sqrt{Val260_{M1}^{corr}}$$

$$Pyr_{M3} = 1 - \sqrt{Val260_{M1}^{corr}}$$

The phenylalanine *m/z* 302 fragment is used to infer the labeling of PEP.

$$PEP_{M3} = Phe302_{M2}^{corr}$$

Thus, the fraction of PEP derived from pyruvate is calculated as follows:

$$\%PEP\ from\ Pyr = \frac{PEP_{M3}}{Pyr_{M3}} = \frac{Phe302_{M2}^{corr}}{1 - \sqrt{Val260_{M0}^{corr}}}$$
$$= \frac{Phe302_{M2}/(1 - Ala260_{M0})}{1 - \sqrt{(Val260_{M0} - Ala260_{M0})/(1 - Ala260_{M0})}}$$

In the above equation, we have assumed that the contribution of oxaloacetate to PEP_{M3} is minimal. It has been demonstrated for wild-type *E. coli* that the PCK reaction (oxaloacetate to PEP) carries no significant flux during growth on glucose (Crown et al., 2015; Leighty and Antoniewicz, 2013). We have assumed that the same is true for all *E. coli* strains studied here, when grown on glucose or xylose.

Appendix D

METABOLIC NETWORK MODELS USED IN CHAPTER 6

Table D.1: Metabolic network model for ^{13}C-MFA of *E. coli* (full model)

Glycolysis

v_1 Gluc.ext (abcdef) + PEP (ghi) → G6P (abcdef) + Pyr (ghi)

v_2 G6P (abcdef) ↔ F6P (abcdef)

v_3 F6P (abcdef) + ATP → FBP (abcdef)

v_4 FBP (abcdef) ↔ DHAP (cba) + GAP (def)

v_5 DHAP (abc) ↔ GAP (abc)

v_6 GAP (abc) ↔ 3PG (abc) + ATP + NADH

v_7 3PG (abc) ↔ PEP (abc)

v_8 PEP (abc) → Pyr (abc) + ATP

Pentose Phosphate Pathway

v_9 G6P (abcdef) → 6PG (abcdef) + NADPH

v_{10} 6PG (abcdef) → Ru5P (bcdef) + CO2 (a) + NADPH

v_{11} Ru5P (abcde) ↔ X5P (abcde)

Table D.1 continued

v_{12} Ru5P (abcde) ↔ R5P (abcde)

v_{13} X5P (abcde) ↔ TK-C2 (ab) + GAP (cde)

v_{14} F6P (abcdef) ↔ TK-C2 (ab) + E4P (cdef)

v_{15} S7P (abcdefg) ↔ TK-C2 (ab) + R5P (cdefg)

v_{16} F6P (abcdef) ↔ TA-C3 (abc) + GAP (def)

v_{17} S7P (abcdefg) ↔ TA-C3 (abc) + E4P (defg)

Entner-Doudoroff Pathway

v_{18} 6PG (abcdef) → KDPG (abcdef)

v_{19} KDPG (abcdef) → Pyr (abc) + GAP (def)

TCA Cycle

v_{20} Pyr (abc) → AcCoA (bc) + CO2 (a) + NADH

v_{21} OAC (abcd) + AcCoA (ef) → Cit (dcbfea)

v_{22} Cit (abcdef) ↔ ICit (abcdef)

v_{23} ICit (abcdef) ↔ AKG (abcde) + CO2 (f) + NADPH

v_{24} AKG (abcde) → SucCoA (bcde) + CO2 (a) + NADH

v_{25} SucCoA (abcd) ↔ Suc (½ abcd + ½ dcba) + ATP

v_{26} Suc (½ abcd + ½ dcba) ↔ Fum (½ abcd + ½ dcba) + FADH2

Table D.1 continued

v_{27} Fum (½ abcd + ½ dcba) ↔ Mal (abcd)

v_{28} Mal (abcd) ↔ OAC (abcd) + NADH

Glyoxylate Shunt

v_{29} ICit (abcdef) ↔ Glyox (ab) + Suc (½ edcf + ½ fcde)

v_{30} Glyox (ab) + AcCoA (cd) → Mal (abdc)

Amphibolic Reactions

v_{31} Mal (abcd) → Pyr (abc) + CO2 (d) + NADPH

v_{32} Mal (abcd) → Pyr (abc) + CO2 (d) + NADH

v_{33} PEP (abc) + CO2 (d) → OAC (abcd)

v_{34} OAC (abcd) + ATP → PEP (abc) + CO2 (d)

Acetic Acid Formation

v_{35} AcCoA (ab) ↔ Ac (ab) + ATP

Amino Acid Biosynthesis

v_{36} AKG (abcde) + NADPH + NH3 → Glu (abcde)

v_{37} Glu (abcde) + ATP + NH3 → Gln (abcde)

v_{38} Glu (abcde) + ATP + 2 NADPH → Pro (abcde)

Table D.1 continued

v_{39} Glu (abcde) + CO2 (f) + Gln (ghijk) + Asp (lmno) + AcCoA (pq) + 5 ATP + NADPH →

Arg (abcdef) + AKG (ghijk) + Fum (lmno) + Ac (pq)

v_{40} OAC (abcd) + Glu (efghi) → Asp (abcd) + AKG (efghi)

v_{41} Asp (abcd) + 2 ATP + NH3 → Asn (abcd)

v_{42} Pyr (abc) + Glu (defgh) → Ala (abc) + AKG (defgh)

v_{43} 3PG (abc) + Glu (defgh) → Ser (abc) + AKG (defgh) + NADH

v_{44} Ser (abc) ↔ Gly (ab) + MEETHF (c)

v_{45} Gly (ab) ↔ CO2 (a) + MEETHF (b) + NADH + NH3

v_{46} Thr (abcd) → Gly (ab) + AcCoA (cd) + NADH

v_{47} Ser (abc) + AcCoA (de) + 3 ATP + 4 NADPH + SO4 → Cys (abc) + Ac (de)

v_{48} Asp (abcd) + Pyr (efg) + Glu (hijkl) + SucCoA (mnop) + ATP + 2 NADPH →

LL-DAP (½ abcdgfe + ½ efgdcba) + AKG (hijkl) + Suc (½ mnop + ½ ponm)

v_{49} LL-DAP (½ abcdefg + ½ gfedcba) → Lys (abcdef) + CO2 (g)

v_{50} Asp (abcd) + 2 ATP + 2 NADPH → Thr (abcd)

v_{51} Asp (abcd) + METHF (e) + Cys (fgh) + SucCoA (ijkl) + ATP + 2 NADPH →

Met (abcde) + Pyr (fgh) + Suc (½ ijkl + ½ lkji) + NH3

Table D.1 continued

v_{52} Pyr (abc) + Pyr (def) + Glu (ghijk) + NADPH → Val (abcef) + CO2 (d) + AKG (ghijk)

v_{53} AcCoA (ab) + Pyr (cde) + Pyr (fgh) + Glu (ijklm) + NADPH →
Leu (abdghe) + CO2 (c) + CO2 (f) + AKG (ijklm) + NADH

v_{54} Thr (abcd) + Pyr (efg) + Glu (hijkl) + NADPH → Ile (abfcdg) + CO2 (e) + AKG (hijkl) + NH3

v_{55} PEP (abc) + PEP (def) + E4P (ghij) + Glu (klmno) + ATP + NADPH →
Phe (abcefghij) + CO2 (d) + AKG (klmno)

v_{56} PEP (abc) + PEP (def) + E4P (ghij) + Glu (klmno) + ATP + NADPH →
Tyr (abcefghij) + CO2 (d) + AKG (klmno) + NADH

v_{57} Ser (abc) + R5P (defgh) + PEP (ijk) + E4P (lmno) + PEP (pqr) + Gln (stuvw) + 3 ATP + NADPH →
Trp (abcedklmnoj) + CO2 (i) + GAP (fgh) + Pyr (pqr) + Glu (stuvw)

v_{58} R5P (abcde) + FTHF (f) + Gln (ghijk) + Asp (lmno) + 5 ATP →
His (edcbaf) + AKG (ghijk) + Fum (lmno) + 2 NADH

One-Carbon Metabolism

v_{59} MEETHF (a) + NADH → METHF (a)

v_{60} MEETHF (a) → FTHF (a) + NADPH

Table D.1 continued

Oxidative Phosphorylation

v_{61} NADH + ½ O2 → 2 ATP

v_{62} FADH2 + ½ O2 → 1 ATP

Transhydrogenation

v_{63} NADH ↔ NADPH

ATP Hydrolysis

v_{64} ATP → ATP:ext

Transport

v_{65} Ac (ab) → Ac.ext (ab)

v_{66} CO2 (a) → CO2.ext (a)

v_{67} O2.ext → O2

v_{68} NH3.ext → NH3

v_{69} SO4.ext → SO4

Table D.1 continued

Biomass Formation

v_{70} 0.470 Ala + 0.281 Arg + 0.236 Asn + 0.236 Asp + 0.087 Cys + 0.280 Glu + 0.280 Gln + 0.432 Gly + 0.082 His + 0.215 Ile + 0.377 Leu + 0.279 Lys + 0.107 Met + 0.153 Phe + 0.178 Pro + 0.23 Ser + 0.244 Thr + 0.054 Trp + 0.131 Tyr + 0.315 Val + 0.270 G6P + 0.071 F6P + 0.851 R5P + 0.081 GAP + 0.628 3PG + 0.051 PEP + 0.083 Pyr + 1.690 AcCoA + 0.087 AKG + 0.380 OAC + 0.500 MEETHF + 33.601 ATP + 3.948 NADPH $\rightarrow$ 37.12 Biomass + 1.578 NADH

CO_2 Exchange

v_{71} CO_2.unlabeled (a) + CO_2 (b) $\rightarrow$ CO_2 (a) + CO_2.out (b)

Table D.2: Metabolic network model for ^{13}C-MFA of *E. coli* (upper metabolism)

Glycolysis

v_1 Gluc.ext (abcdef) + PEP (ghi) → G6P (abcdef) + Pyr (ghi)

v_2 G6P (abcdef) ↔ F6P (abcdef)

v_3 F6P (abcdef) → FBP (abcdef)

v_4 FBP (abcdef) ↔ DHAP (cba) + GAP (def)

v_5 DHAP (abc) ↔ GAP (abc)

v_6 GAP (abc) ↔ 3PG (abc)

v_7 3PG (abc) ↔ PEP (abc)

v_8 PEP (abc) → Pyr (abc)

Pentose Phosphate Pathway

v_9 G6P (abcdef) → 6PG (abcdef)

v_{10} 6PG (abcdef) → Ru5P (bcdef) + CO2 (a)

v_{11} Ru5P (abcde) ↔ X5P (abcde)

v_{12} Ru5P (abcde) ↔ R5P (abcde)

v_{13} X5P (abcde) ↔ TK-C2 (ab) + GAP (cde)

v_{14} F6P (abcdef) ↔ TK-C2 (ab) + E4P (cdef)

v_{15} S7P (abcdefg) ↔ TK-C2 (ab) + R5P (cdefg)

Table D.2 continued

v_{16} F6P (abcdef) ↔ TA-C3 (abc) + GAP (def)

v_{17} S7P (abcdefg) ↔ TA-C3 (abc) + E4P (defg)

Entner-Doudoroff Pathway

v_{18} 6PG (abcdef) → KDPG (abcdef)

v_{19} KDPG (abcdef) → Pyr (abc) + GAP (def)

Out-fluxes

v_{20} PEP (abc) + PEP (def) + E4P (ghij) → Phe (abcefghij) + CO2 (d)

v_{21} Pyr → Lower Metabolism

v_{22} 2.040 G6P + 0.536 F6P + 7.463 R5P + 0.612 GAP + 1.400 E4P + 1.156 Phe → Biomass

Table D.3: Metabolic network model for ^{13}C-MFA of *E. coli* (upper metabolism with xylose)

Glycolysis

v_1 Gluc.ext (abcdef) + PEP (ghi) → G6P (abcdef) + Pyr (ghi)

v_2 G6P (abcdef) ↔ F6P (abcdef)

v_3 F6P (abcdef) → FBP (abcdef)

v_4 FBP (abcdef) ↔ DHAP (cba) + GAP (def)

v_5 DHAP (abc) ↔ GAP (abc)

v_6 GAP (abc) ↔ 3PG (abc)

v_7 3PG (abc) ↔ PEP (abc)

v_8 PEP (abc) → Pyr (abc)

Pentose Phosphate Pathway

v_9 G6P (abcdef) → 6PG (abcdef)

v_{10} 6PG (abcdef) → Ru5P (bcdef) + CO2 (a)

v_{11} Ru5P (abcde) ↔ X5P (abcde)

v_{12} Ru5P (abcde) ↔ R5P (abcde)

v_{13} X5P (abcde) ↔ TK-C2 (ab) + GAP (cde)

v_{14} F6P (abcdef) ↔ TK-C2 (ab) + E4P (cdef)

v_{15} S7P (abcdefg) ↔ TK-C2 (ab) + R5P (cdefg)

v_{16} F6P (abcdef) ↔ TA-C3 (abc) + GAP (def)

Table D.3 continued

v_{17} S7P (abcdefg) ↔ TA-C3 (abc) + E4P (defg)

Entner-Doudoroff Pathway

v_{18} 6PG (abcdef) → KDPG (abcdef)

v_{19} KDPG (abcdef) → Pyr (abc) + GAP (def)

Xylose Metabolism

v_{20} Xyl.ext (abcde) → Xyl (abcde)

v_{21} Xyl (abcde) → X5P (abcde)

Out-fluxes

v_{22} PEP (abc) + PEP (def) + E4P (ghij) → Phe (abcefghij) + CO2 (d)

v_{23} Pyr → Lower Metabolism

v_{24} 2.040 G6P + 0.536 F6P + 7.463 R5P + 0.612 GAP + 1.400 E4P + 1.156 Phe → Biomass

Table D.4: Metabolic network model for ^{13}C-MFA of CHO cells (upper metabolism)

Glycolysis

v_1 Gluc.ext (abcdef) + PEP (ghi) → G6P (abcdef) + Pyr (ghi)

v_2 G6P (abcdef) ↔ F6P (abcdef)

v_3 F6P (abcdef) → FBP (abcdef)

v_4 FBP (abcdef) ↔ DHAP (cba) + GAP (def)

v_5 DHAP (abc) ↔ GAP (abc)

v_6 GAP (abc) ↔ 3PG (abc)

v_7 3PG (abc) ↔ PEP (abc)

Pentose Phosphate Pathway

v_8 G6P (abcdef) → 6PG (abcdef)

v_9 6PG (abcdef) → Ru5P (bcdef) + CO2 (a)

v_{10} Ru5P (abcde) ↔ X5P (abcde)

v_{11} Ru5P (abcde) ↔ R5P (abcde)

v_{12} X5P (abcde) ↔ TK-C2 (ab) + GAP (cde)

v_{13} F6P (abcdef) ↔ TK-C2 (ab) + E4P (cdef)

v_{14} S7P (abcdefg) ↔ TK-C2 (ab) + R5P (cdefg)

v_{15} F6P (abcdef) ↔ TA-C3 (abc) + GAP (def)

v_{16} S7P (abcdefg) ↔ TA-C3 (abc) + E4P (defg)

Table D.4 continued

Out-fluxes

v_{17} PEP $\rightarrow$ Lower Metabolism

v_{18} 1.21 G6P + 1.01 R5P + 0.47 DHAP $\rightarrow$ Biomass

Appendix E

REPRINT PERMISSION LETTERS

ELSEVIER LICENSE
TERMS AND CONDITIONS
Aug 03, 2016

This Agreement between Jennifer Au ("You") and Elsevier ("Elsevier") consists of your license details and the terms and conditions provided by Elsevier and Copyright Clearance Center.

License Number	3916611134226
License date	Jul 26, 2016
Licensed Content Publisher	Elsevier
Licensed Content Publication	Metabolic Engineering
Licensed Content Title	Parallel labeling experiments validate Clostridium acetobutylicum metabolic network model for 13C metabolic flux analysis
Licensed Content Author	Jennifer Au,Jungik Choi,Shawn W. Jones,Keerthi P. Venkataramanan,Maciek R. Antoniewicz
Licensed Content Date	November 2014
Licensed Content Volume Number	26
Licensed Content Issue Number	n/a
Licensed Content Pages	11
Start Page	23
End Page	33
Type of Use	reuse in a thesis/dissertation
Portion	full article
Format	both print and electronic
Are you the author of this	Yes

Elsevier article?	
Will you be translating?	No
Order reference number	
Title of your thesis/dissertation	Novel Strategies for Validating Metabolic Network Models using Stable Isotope Tracers
Expected completion date	Aug 2016
Estimated size (number of pages)	200
Elsevier VAT number	GB 494 6272 12
Requestor Location	Jennifer Au 3900 Fairfax Dr Apt. 1410 ARLINGTON, VA 22203 United States Attn: Jennifer Au
Total	0.00 USD

Terms and Conditions

INTRODUCTION

1. The publisher for this copyrighted material is Elsevier. By clicking "accept" in connection with completing this licensing transaction, you agree that the following terms and conditions apply to this transaction (along with the Billing and Payment terms and conditions established by Copyright Clearance Center, Inc. ("CCC"), at the time that you opened your Rightslink account and that are available at any time at http://myaccount.copyright.com).

GENERAL TERMS

2. Elsevier hereby grants you permission to reproduce the aforementioned material subject to the terms and conditions indicated.

3. Acknowledgement: If any part of the material to be used (for example, figures) has appeared in our publication with credit or acknowledgement to another source, permission must also be sought from that source. If such permission is not obtained then that material may not be included in your publication/copies. Suitable acknowledgement to the source must be made, either as a footnote or in a reference list at the end of your publication, as follows:

"Reprinted from Publication title, Vol /edition number, Author(s), Title of article / title

of chapter, Pages No., Copyright (Year), with permission from Elsevier [OR APPLICABLE SOCIETY COPYRIGHT OWNER]." Also Lancet special credit - "Reprinted from The Lancet, Vol. number, Author(s), Title of article, Pages No., Copyright (Year), with permission from Elsevier."

4. Reproduction of this material is confined to the purpose and/or media for which permission is hereby given.

5. Altering/Modifying Material: Not Permitted. However figures and illustrations may be altered/adapted minimally to serve your work. Any other abbreviations, additions, deletions and/or any other alterations shall be made only with prior written authorization of Elsevier Ltd. (Please contact Elsevier at permissions@elsevier.com)

6. If the permission fee for the requested use of our material is waived in this instance, please be advised that your future requests for Elsevier materials may attract a fee.

7. Reservation of Rights: Publisher reserves all rights not specifically granted in the combination of (i) the license details provided by you and accepted in the course of this licensing transaction, (ii) these terms and conditions and (iii) CCC's Billing and Payment terms and conditions.

8. License Contingent Upon Payment: While you may exercise the rights licensed immediately upon issuance of the license at the end of the licensing process for the transaction, provided that you have disclosed complete and accurate details of your proposed use, no license is finally effective unless and until full payment is received from you (either by publisher or by CCC) as provided in CCC's Billing and Payment terms and conditions. If full payment is not received on a timely basis, then any license preliminarily granted shall be deemed automatically revoked and shall be void as if never granted. Further, in the event that you breach any of these terms and conditions or any of CCC's Billing and Payment terms and conditions, the license is automatically revoked and shall be void as if never granted. Use of materials as described in a revoked license, as well as any use of the materials beyond the scope of an unrevoked license, may constitute copyright infringement and publisher reserves the right to take any and all action to protect its copyright in the materials.

9. Warranties: Publisher makes no representations or warranties with respect to the licensed material.

10. Indemnity: You hereby indemnify and agree to hold harmless publisher and CCC, and their respective officers, directors, employees and agents, from and against any and all claims arising out of your use of the licensed material other than as specifically authorized pursuant to this license.

11. No Transfer of License: This license is personal to you and may not be sublicensed, assigned, or transferred by you to any other person without publisher's written permission.

12. No Amendment Except in Writing: This license may not be amended except in a writing signed by both parties (or, in the case of publisher, by CCC on publisher's behalf).

13. Objection to Contrary Terms: Publisher hereby objects to any terms contained in any purchase order, acknowledgment, check endorsement or other writing prepared by you, which terms are inconsistent with these terms and conditions or CCC's Billing and Payment terms and conditions. These terms and conditions, together with CCC's Billing and Payment terms and conditions (which are incorporated herein), comprise the entire agreement between you and publisher (and CCC) concerning this licensing transaction. In the event of any conflict between your obligations established by these terms and conditions and those established by CCC's Billing and Payment terms and conditions, these terms and conditions shall control.

14. Revocation: Elsevier or Copyright Clearance Center may deny the permissions described in this License at their sole discretion, for any reason or no reason, with a full refund payable to you. Notice of such denial will be made using the contact information provided by you. Failure to receive such notice will not alter or invalidate the denial. In no event will Elsevier or Copyright Clearance Center be responsible or liable for any costs, expenses or damage incurred by you as a result of a denial of your permission request, other than a refund of the amount(s) paid by you to Elsevier and/or Copyright Clearance Center for denied permissions.

LIMITED LICENSE

The following terms and conditions apply only to specific license types:

15. **Translation**: This permission is granted for non-exclusive world **English** rights only unless your license was granted for translation rights. If you licensed translation rights you may only translate this content into the languages you requested. A professional translator must perform all translations and reproduce the content word for word preserving the integrity of the article.

16. **Posting licensed content on any Website**: The following terms and conditions apply as follows: Licensing material from an Elsevier journal: All content posted to the web site must maintain the copyright information line on the bottom of each image; A hyper-text must be included to the Homepage of the journal from which you are licensing at http://www.sciencedirect.com/science/journal/xxxxx or the Elsevier homepage for books at http://www.elsevier.com; Central Storage: This license does

not include permission for a scanned version of the material to be stored in a central repository such as that provided by Heron/XanEdu.

Licensing material from an Elsevier book: A hyper-text link must be included to the Elsevier homepage at http://www.elsevier.com . All content posted to the web site must maintain the copyright information line on the bottom of each image.

Posting licensed content on Electronic reserve: In addition to the above the following clauses are applicable: The web site must be password-protected and made available only to bona fide students registered on a relevant course. This permission is granted for 1 year only. You may obtain a new license for future website posting.

17. **For journal authors:** the following clauses are applicable in addition to the above:

Preprints:

A preprint is an author's own write-up of research results and analysis, it has not been peer-reviewed, nor has it had any other value added to it by a publisher (such as formatting, copyright, technical enhancement etc.).

Authors can share their preprints anywhere at any time. Preprints should not be added to or enhanced in any way in order to appear more like, or to substitute for, the final versions of articles however authors can update their preprints on arXiv or RePEc with their Accepted Author Manuscript (see below).

If accepted for publication, we encourage authors to link from the preprint to their formal publication via its DOI. Millions of researchers have access to the formal publications on ScienceDirect, and so links will help users to find, access, cite and use the best available version. Please note that Cell Press, The Lancet and some society-owned have different preprint policies. Information on these policies is available on the journal homepage.

Accepted Author Manuscripts: An accepted author manuscript is the manuscript of an article that has been accepted for publication and which typically includes author-incorporated changes suggested during submission, peer review and editor-author communications.

Authors can share their accepted author manuscript:

- – immediately

    - via their non-commercial person homepage or blog
    - by updating a preprint in arXiv or RePEc with the accepted manuscript
    - via their research institute or institutional repository for internal institutional uses or as part of an invitation-only research collaboration work-group
    - directly by providing copies to their students or to research collaborators for their personal use
    - for private scholarly sharing as part of an invitation-only work group on commercial sites with which Elsevier has an agreement
- – after the embargo period
    - via non-commercial hosting platforms such as their institutional repository
    - via commercial sites with which Elsevier has an agreement

In all cases accepted manuscripts should:

- – link to the formal publication via its DOI
- – bear a CC-BY-NC-ND license - this is easy to do
- – if aggregated with other manuscripts, for example in a repository or other site, be shared in alignment with our hosting policy not be added to or enhanced in any way to appear more like, or to substitute for, the published journal article.

Published journal article (JPA): A published journal article (PJA) is the definitive final record of published research that appears or will appear in the journal and embodies all value-adding publishing activities including peer review co-ordination, copy-editing, formatting, (if relevant) pagination and online enrichment.

Policies for sharing publishing journal articles differ for subscription and gold open access articles:

Subscription Articles: If you are an author, please share a link to your article rather than the full-text. Millions of researchers have access to the formal publications on ScienceDirect, and so links will help your users to find, access, cite, and use the best available version.

Theses and dissertations which contain embedded PJAs as part of the formal submission can be posted publicly by the awarding institution with DOI links back to the formal publications on ScienceDirect.

If you are affiliated with a library that subscribes to ScienceDirect you have additional private sharing rights for others' research accessed under that agreement. This includes use for classroom teaching and internal training at the institution (including use in course packs and courseware programs), and inclusion of the article for grant funding purposes.

Gold Open Access Articles: May be shared according to the author-selected end-user license and should contain a CrossMark logo, the end user license, and a DOI link to the formal publication on ScienceDirect.

Please refer to Elsevier's posting policy for further information.

18. **For book authors** the following clauses are applicable in addition to the above: Authors are permitted to place a brief summary of their work online only. You are not allowed to download and post the published electronic version of your chapter, nor may you scan the printed edition to create an electronic version. **Posting to a repository:** Authors are permitted to post a summary of their chapter only in their institution's repository.

19. **Thesis/Dissertation**: If your license is for use in a thesis/dissertation your thesis may be submitted to your institution in either print or electronic form. Should your thesis be published commercially, please reapply for permission. These requirements include permission for the Library and Archives of Canada to supply single copies, on demand, of the complete thesis and include permission for Proquest/UMI to supply single copies, on demand, of the complete thesis. Should your thesis be published commercially, please reapply for permission. Theses and dissertations which contain embedded PJAs as part of the formal submission can be posted publicly by the awarding institution with DOI links back to the formal publications on ScienceDirect.

Elsevier Open Access Terms and Conditions

You can publish open access with Elsevier in hundreds of open access journals or in nearly 2000 established subscription journals that support open access publishing. Permitted third party re-use of these open access articles is defined by the author's choice of Creative Commons user license. See our open access license policy for more information.

Terms & Conditions applicable to all Open Access articles published with Elsevier:

Any reuse of the article must not represent the author as endorsing the adaptation of

ELSEVIER LICENSE
TERMS AND CONDITIONS
Aug 03, 2016

This Agreement between Jennifer Au ("You") and Elsevier ("Elsevier") consists of your license details and the terms and conditions provided by Elsevier and Copyright Clearance Center.

License Number	3916620043704
License date	Jul 26, 2016
Licensed Content Publisher	Elsevier
Licensed Content Publication	Metabolic Engineering
Licensed Content Title	13C metabolic flux analysis of microbial and mammalian systems is enhanced with GC–MS measurements of glycogen and RNA labeling
Licensed Content Author	Christopher P. Long,Jennifer Au,Jacqueline E. Gonzalez,Maciek R. Antoniewicz
Licensed Content Date	November 2016
Licensed Content Volume Number	38
Licensed Content Issue Number	n/a
Licensed Content Pages	8
Start Page	65
End Page	72
Type of Use	reuse in a thesis/dissertation
Intended publisher of new work	other
Portion	full article
Format	both print and electronic
Are you the author of this Elsevier article?	Yes
Will you be translating?	No
Order reference number	
Title of your thesis/dissertation	Novel Strategies for Validating Metabolic Network Models using Stable Isotope Tracers
Expected completion date	Aug 2016
Estimated size (number of	200

pages)

Elsevier VAT number	GB 494 6272 12
Requestor Location	Jennifer Au 3900 Fairfax Dr Apt. 1410 ARLINGTON, VA 22203 United States Attn: Jennifer Au
Total	0.00 USD

Terms and Conditions

INTRODUCTION

1. The publisher for this copyrighted material is Elsevier. By clicking "accept" in connection with completing this licensing transaction, you agree that the following terms and conditions apply to this transaction (along with the Billing and Payment terms and conditions established by Copyright Clearance Center, Inc. ("CCC"), at the time that you opened your Rightslink account and that are available at any time at http://myaccount.copyright.com).

GENERAL TERMS

2. Elsevier hereby grants you permission to reproduce the aforementioned material subject to the terms and conditions indicated.

3. Acknowledgement: If any part of the material to be used (for example, figures) has appeared in our publication with credit or acknowledgement to another source, permission must also be sought from that source. If such permission is not obtained then that material may not be included in your publication/copies. Suitable acknowledgement to the source must be made, either as a footnote or in a reference list at the end of your publication, as follows:

"Reprinted from Publication title, Vol /edition number, Author(s), Title of article / title of chapter, Pages No., Copyright (Year), with permission from Elsevier [OR APPLICABLE SOCIETY COPYRIGHT OWNER]." Also Lancet special credit - "Reprinted from The Lancet, Vol. number, Author(s), Title of article, Pages No., Copyright (Year), with permission from Elsevier."

4. Reproduction of this material is confined to the purpose and/or media for which permission is hereby given.

13. Objection to Contrary Terms: Publisher hereby objects to any terms contained in any purchase order, acknowledgment, check endorsement or other writing prepared by you, which terms are inconsistent with these terms and conditions or CCC's Billing and Payment terms and conditions. These terms and conditions, together with CCC's Billing and Payment terms and conditions (which are incorporated herein), comprise the entire agreement between you and publisher (and CCC) concerning this licensing transaction. In the event of any conflict between your obligations established by these terms and conditions and those established by CCC's Billing and Payment terms and conditions, these terms and conditions shall control.

14. Revocation: Elsevier or Copyright Clearance Center may deny the permissions described in this License at their sole discretion, for any reason or no reason, with a full refund payable to you. Notice of such denial will be made using the contact information provided by you. Failure to receive such notice will not alter or invalidate the denial. In no event will Elsevier or Copyright Clearance Center be responsible or liable for any costs, expenses or damage incurred by you as a result of a denial of your permission request, other than a refund of the amount(s) paid by you to Elsevier and/or Copyright Clearance Center for denied permissions.

LIMITED LICENSE

The following terms and conditions apply only to specific license types:

15. **Translation**: This permission is granted for non-exclusive world **English** rights only unless your license was granted for translation rights. If you licensed translation rights you may only translate this content into the languages you requested. A professional translator must perform all translations and reproduce the content word for word preserving the integrity of the article.

16. **Posting licensed content on any Website**: The following terms and conditions apply as follows: Licensing material from an Elsevier journal: All content posted to the web site must maintain the copyright information line on the bottom of each image; A hyper-text must be included to the Homepage of the journal from which you are licensing at http://www.sciencedirect.com/science/journal/xxxxx or the Elsevier homepage for books at http://www.elsevier.com; Central Storage: This license does not include permission for a scanned version of the material to be stored in a central repository such as that provided by Heron/XanEdu.

Licensing material from an Elsevier book: A hyper-text link must be included to the Elsevier homepage at http://www.elsevier.com . All content posted to the web site must maintain the copyright information line on the bottom of each image.

Posting licensed content on Electronic reserve: In addition to the above the following clauses are applicable: The web site must be password-protected and made available only to bona fide students registered on a relevant course. This permission is granted for 1 year only. You may obtain a new license for future website posting.

17. **For journal authors:** the following clauses are applicable in addition to the above:

Preprints:

A preprint is an author's own write-up of research results and analysis, it has not been peer-reviewed, nor has it had any other value added to it by a publisher (such as formatting, copyright, technical enhancement etc.).

Authors can share their preprints anywhere at any time. Preprints should not be added to or enhanced in any way in order to appear more like, or to substitute for, the final versions of articles however authors can update their preprints on arXiv or RePEc with their Accepted Author Manuscript (see below).

If accepted for publication, we encourage authors to link from the preprint to their formal publication via its DOI. Millions of researchers have access to the formal publications on ScienceDirect, and so links will help users to find, access, cite and use the best available version. Please note that Cell Press, The Lancet and some society-owned have different preprint policies. Information on these policies is available on the journal homepage.

Accepted Author Manuscripts: An accepted author manuscript is the manuscript of an article that has been accepted for publication and which typically includes author-incorporated changes suggested during submission, peer review and editor-author communications.

Authors can share their accepted author manuscript:

- – immediately
    - via their non-commercial person homepage or blog
    - by updating a preprint in arXiv or RePEc with the accepted manuscript
    - via their research institute or institutional repository for internal institutional uses or as part of an invitation-only research collaboration work-group
    - directly by providing copies to their students or to research collaborators for their personal use

    - for private scholarly sharing as part of an invitation-only work group on commercial sites with which Elsevier has an agreement
- – after the embargo period
    - via non-commercial hosting platforms such as their institutional repository
    - via commercial sites with which Elsevier has an agreement

In all cases accepted manuscripts should:

- – link to the formal publication via its DOI
- – bear a CC-BY-NC-ND license - this is easy to do
- – if aggregated with other manuscripts, for example in a repository or other site, be shared in alignment with our hosting policy not be added to or enhanced in any way to appear more like, or to substitute for, the published journal article.

Published journal article (JPA): A published journal article (PJA) is the definitive final record of published research that appears or will appear in the journal and embodies all value-adding publishing activities including peer review co-ordination, copy-editing, formatting, (if relevant) pagination and online enrichment.

Policies for sharing publishing journal articles differ for subscription and gold open access articles:

Subscription Articles: If you are an author, please share a link to your article rather than the full-text. Millions of researchers have access to the formal publications on ScienceDirect, and so links will help your users to find, access, cite, and use the best available version.

Theses and dissertations which contain embedded PJAs as part of the formal submission can be posted publicly by the awarding institution with DOI links back to the formal publications on ScienceDirect.

If you are affiliated with a library that subscribes to ScienceDirect you have additional private sharing rights for others' research accessed under that agreement. This includes use for classroom teaching and internal training at the institution (including use in course packs and courseware programs), and inclusion of the article for grant funding purposes.

Gold Open Access Articles: May be shared according to the author-selected end-user license and should contain a CrossMark logo, the end user license, and a DOI link to

the formal publication on ScienceDirect.

Please refer to Elsevier's posting policy for further information.

18. **For book authors** the following clauses are applicable in addition to the above: Authors are permitted to place a brief summary of their work online only. You are not allowed to download and post the published electronic version of your chapter, nor may you scan the printed edition to create an electronic version. **Posting to a repository:** Authors are permitted to post a summary of their chapter only in their institution's repository.

19. **Thesis/Dissertation**: If your license is for use in a thesis/dissertation your thesis may be submitted to your institution in either print or electronic form. Should your thesis be published commercially, please reapply for permission. These requirements include permission for the Library and Archives of Canada to supply single copies, on demand, of the complete thesis and include permission for Proquest/UMI to supply single copies, on demand, of the complete thesis. Should your thesis be published commercially, please reapply for permission. Theses and dissertations which contain embedded PJAs as part of the formal submission can be posted publicly by the awarding institution with DOI links back to the formal publications on ScienceDirect.

Elsevier Open Access Terms and Conditions

You can publish open access with Elsevier in hundreds of open access journals or in nearly 2000 established subscription journals that support open access publishing. Permitted third party re-use of these open access articles is defined by the author's choice of Creative Commons user license. See our open access license policy for more information.

Terms & Conditions applicable to all Open Access articles published with Elsevier:

Any reuse of the article must not represent the author as endorsing the adaptation of the article nor should the article be modified in such a way as to damage the author's honour or reputation. If any changes have been made, such changes must be clearly indicated.

The author(s) must be appropriately credited and we ask that you include the end user license and a DOI link to the formal publication on ScienceDirect.

Posting or linking by commercial companies for use by customers of those companies.

20. **Other Conditions**:

v1.8